

AD-A151 841

AN ANALYSIS AND COMPARISON OF LIGHTNING RETURN STROKE
MODELS AT ALTITUDE(U) AIR FORCE INST OF TECH
WRIGHT-PATTERSON AFB OH SCHOOL OF ENGINEERING J M CUKR

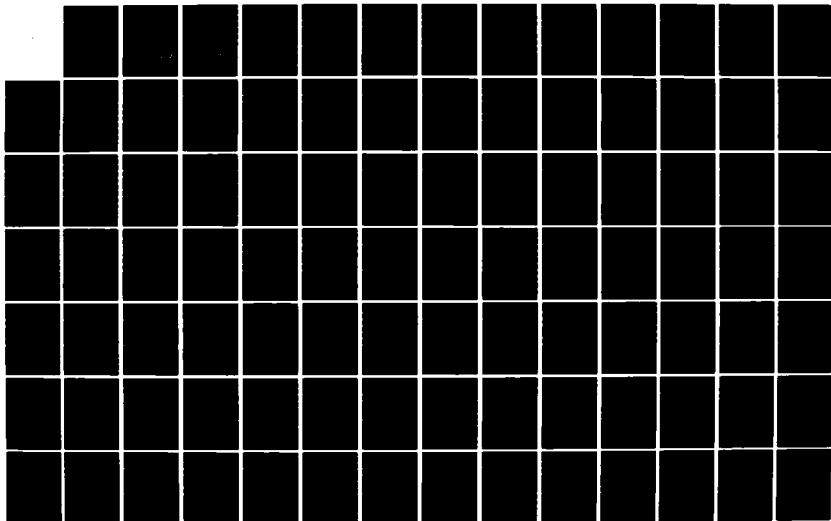
1/2

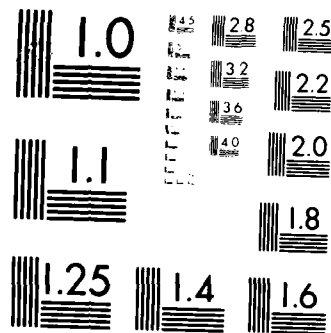
UNCLASSIFIED

DEC 81 AFIT/GE/EE/81D-15

F/G 4/2

NL





MICROCOPY RESOLUTION TEST CHART
 NATIONAL BUREAU OF STANDARDS-1963-A

①

AD-A151 841

AN ANALYSIS AND COMPARISON OF
LIGHTNING RETURN STROKE
MODELS AT ALTITUDE

THESIS

AFIT/GE/EE/81D-15

Jeffrey M. Cukr
1st Lt USAF

DTIC
ELECTE
MAR 29 1985
S B D

Approved for public release; distribution unlimited

DTIC FILE COPY

AN ANALYSIS AND COMPARISON OF LIGHTNING
RETURN STROKE MODELS AT ALTITUDE

THESIS

Presented to the Faculty of the School of Engineering
of the Air Force Institute of Technology
Air University
in Partial Fulfillment of the
Requirements for the Degree of
Master of Science

by

Jeffrey M. Cukr, B.S.E.E.
1st Lt USAF

Graduate Electrical Engineering

December 1981

Approved for public release; distribution unlimited



Acknowledgements

I would like to thank my typist, Phyllis Reynolds. Her typing of this thesis and her thorough knowledge of and guidance in the "non-text" or format portions (prefatory material, headings, titles, lists, etc.) saved me innumerable frustrating hours of work.

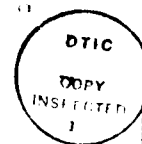
I would also like to thank the computer personnel at the remote terminal site in building 1250, specifically, Dean Anderson, Debbie Schaeff, Beth Vore, Yolanda Ward, and Anne Ware. Without the support of these people, my thesis would still be a collection of thoughts in my mind.

My greatest thanks go to Dr. Rustan. His help in finding and selecting this topic and then ensuring I complete it by acting as my task master (i.e., advisor) gently forced me to complete this project. His recognition of when I was frustrated and feeling low and then cheering me up deserves my gratitude. Finally, his fairness throughout the last nine months deserves my admiration.

Lastly, I'd like to thank Anita Rowley for being there.

— Jeffrey M. Cukr

ii



Accession War

UNITED STATES
DEPARTMENT OF THE ARMY
HEADQUARTERS
JAN 1961

Inventory Codes
Serial Number

A-1

Contents

	Page
Acknowledgements	ii
List of Figures	iv
List of Tables	xv
Abstract	xvi
I. Introduction	1
Problem	3
Scope	3
Presentation	3
II. Background	5
Lightning Process	5
Assumption	10
III. Theory	15
EM on the Ground	15
EM Everywhere	30
IV. Models	36
V. Analysis	44
Theoretical	44
Experimental	122
VI. Conclusions and Recommendations	127
Conclusions	127
Recommendations	127
Bibliography	129
Vita	130

List of Figures

Figure	Page
2.1. Typical Charge Distribution in a South African Thundercloud According to Malan (1952, 1963). Electric Field Measurements Show Typically $P=+40$ coul, $N=-40$ coul, and $p=+10$ coul (Uman, 1969:3)	6
2.2 (a) The Luminous Features of a Lightning Flash as They Would be Recorded by a Camera with a Fixed Lens and Moving Film. Time Scale Increases to the Right; Time Scale is Distorted for Clarity. (b) The Same Lightning Flash as it Would be Recorded by a Camera with Stationary Film (Uman, 1969:6).	6
3.1 Definition of Geometrical and Physical Parameters Used in Return Stroke Modeling for Points on the Ground (Lin, 1978:27)	16
3.2 The Geometry for General Solutions of the Time-Dependent Maxwell Equations (Uman, et al., 1969)	18
3.3 Definition of Geometrical and Physical Parameters Used in Return Stroke Modeling for Points Anywhere (Master et al., 1981)	31
4.1 Illustration of the Current Distribution of the Bruce-Golde Model (Model 1) (Lin, 1978:106)	37
4.2 Illustration of the Current Distribution of the Transmission Line Model (Model 2) (Lin, 1978:106)	39
4.3 Illustration of the Current Distribution of the Lin Model (Master et al., 1981)	42
5.1 Computer Solutions to Equation (39), the Electric Field, According to Model 1 at a Distance of 1 km, 500 nsec Rise Time, and 10 μ sec Fall Time, for the Ground and at Five Altitudes	50

5.2	Computer Solutions to Equation (39), the Electric Field, According to Model 1 at a Distance of 5 km, 500 nsec Rise Time, and 10 μ sec Fall Time, for the Ground and at Five Altitudes	51
5.3	Computer Solutions to Equation (39), the Electric Field, According to Model 1 at a Distance of 10 km, 500 nsec Rise Time, and 10 μ sec Fall Time for the Ground and at Five Altitudes	52
5.4	Computer Solutions to Equation (39), the Electric Field, According to Model 1 at a Distance of 100 km, 500 nsec Rise Time, and 10 μ sec Fall Time, for the Ground and at Five Altitudes	53
5.5	Computer Solutions to Equation (39), the Electric Field, According to Model 1 at a Distance of 1 km, 1 μ sec Rise Time, and 25 μ sec Fall Time, for the Ground and at Five Altitudes	54
5.6	Computer Solutions to Equation (39), the Electric Field, According to Model 1 at a Distance of 5 km, 1 μ sec Rise Time, and 25 μ sec Fall Time, for the Ground and at Five Altitudes	55
5.7	Computer Solutions to Equation (39), the Electric Field, According to Model 1 at a Distance of 10 km, 1 μ sec Rise Time, and 25 μ sec Fall Time, for the Ground and at Five Altitudes	56
5.8	Computer Solutions to Equation (39), the Electric Field, According to Model 1 at a Distance of 100 km, 1 μ sec Rise Time, and 25 μ sec Fall Time, for the Ground and at Five Altitudes	57
5.9	Computer Solutions to Equation (39), the Electric Field, According to Model 1 at a Distance of 1 km, 2 μ sec Rise Time, and 50 μ sec Fall Time, for the Ground and at Five Altitudes	58

Figure		Page
5.10	Computer Solutions to Equation (39), the Electric Field, According to Model 1 at a Distance of 5 km, 2 μ sec Rise Time, and 50 μ sec Fall Time, for the Ground and at Five Altitudes	59
5.11	Computer Solutions to Equation (39), the Electric Field, According to Model 1 at a Distance of 10 km, 2 μ sec Rise Time, and 50 μ sec Fall Time, for the Ground and at Five Altitudes	60
5.12	Computer Solutions to Equation (39), the Electric Field, According to Model 1 at a Distance of 100 km, 2 μ sec Rise Time, and 50 μ sec Fall Time, for the Ground and at Five Altitudes	61
5.13	Computer Solutions to Equation (39), the Electric Field, According to Model 2 at a Distance of 1 km, 500 nsec Rise Time, and 10 μ sec Fall Time, for the Ground and at Five Altitudes	62
5.14	Computer Solutions to Equation (39), the Electric Field, According to Model 2 at a Distance of 5 km, 500 nsec Rise Time, and 10 μ sec Fall Time, for the Ground and at Five Altitudes	63
5.15	Computer Solutions to Equation (39), the Electric Field, According to Model 2 at a Distance of 10 km, 500 nsec Rise Time, and 10 μ sec Fall Time, for the Ground and at Five Altitudes	64
5.16	Computer Solutions to Equation (39), the Electric Field, According to Model 2 at a Distance of 100 km, 500 nsec Rise Time, and 10 μ sec Fall Time, for the Ground and at Five Altitudes	65
5.17	Computer Solutions to Equation (39), the Electric Field, According to Model 2 at a Distance of 1 km, 1 μ sec Rise Time, and 25 μ sec Fall Time, for the Ground and at Five Altitudes	66

Figure		Page
5.18	Computer Solutions to Equation (39), the Electric Field, According to Model 2 at a Distance of 5 km, 1 μ sec Rise Time, and 25 μ sec Fall Time, for the Ground and at Five Altitudes	67
5.19	Computer Solutions to Equation (39), the Electric Field, According to Model 2 at a Distance of 10 km, 1 μ sec Rise Time, and 25 μ sec Fall Time, for the Ground and at Five Altitudes	68
5.20	Computer Solutions to Equation (39), the Electric Field, According to Model 2 at a Distance of 100 km, 1 μ sec Rise Time, and 25 μ sec Fall Time, for the Ground and at Five Altitudes	69
5.21	Computer Solutions to Equation (39), the Electric Field, According to Model 2 at a Distance of 1 km, 2 μ sec Rise Time, and 50 μ sec Fall Time, for the Ground and at Five Altitudes	70
5.22	Computer Solutions to Equation (39), the Electric Field, According to Model 2 at a Distance of 5 km, 2 μ sec Rise Time, and 50 μ sec Fall Time, for the Ground and at Five Altitudes	71
5.23	Computer Solutions to Equation (39), the Electric Field, According to Model 2 at a Distance of 10 km, 2 μ sec Rise Time, and 50 μ sec Fall Time, for the Ground and at Five Altitudes	72
5.24	Computer Solutions to Equation (39), the Electric Field, According to Model 2 at a Distance of 100 km, 2 μ sec Rise Time, and 50 μ sec Fall Time, for the Ground and at Five Altitudes	73
5.25	Computer Solutions to Equation (39), the Electric Field, According to Model 3 at a Distance of 1 km, 500 nsec Rise Time, and 10 μ sec Fall Time, for the Ground and at Five Altitudes	74

Figure		Page
5.26	Computer Solutions to Equation (39), the Electric Field, According to Model 3 at a Distance of 5 km, 500 nsec Rise Time, and 10 μ sec Fall Time, for the Ground and at Five Altitudes	75
5.27	Computer Solutions to Equation (39), the Electric Field, According to Model 3 at a Distance of 10 km, 500 nsec Rise Time, and 10 μ sec Fall Time, for the Ground and at Five Altitudes	76
5.28	Computer Solutions to Equation (39), the Electric Field, According to Model 3 at a Distance of 100 km, 500 nsec Rise Time, and 10 μ sec Fall Time, for the Ground and at Five Altitudes	77
5.29	Computer Solutions to Equation (39), the Electric Field, According to Model 3 at a Distance of 1 km, 1 μ sec Rise Time, and 25 μ sec Fall Time, for the Ground and at Five Altitudes	78
5.30	Computer Solutions to Equation (39), the Electric Field, According to Model 3 at a Distance of 5 km, 1 μ sec Rise Time, and 25 μ sec Fall Time, for the Ground and at Five Altitudes	79
5.31	Computer Solutions to Equation (39), the Electric Field, According to Model 3 at a Distance of 10 km, 1 μ sec Rise Time, and 25 μ sec Fall Time, for the Ground and at Five Altitudes	80
5.32	Computer Solutions to Equation (39), the Electric Field, According to Model 3 at a Distance of 100 km, 1 μ sec Rise Time, and 25 μ sec Fall Time, for the Ground and at Five Altitudes	81
5.33	Computer Solutions to Equation (39), the Electric Field, According to Model 3 at a Distance of 1 km, 2 μ sec Rise Time, and 25 μ sec Fall Time for the Ground and at Five Altitudes	82

Figure		Page
5.34	Computer Solutions to Equation (39), the Electric Field, According to Model 3 at a Distance of 5 km, 2 μ sec Rise Time, and 25 μ sec Fall Time for the Ground and at Five Altitudes	83
5.35	Computer Solutions to Equation (39), the Electric Field, According to Model 3 at a Distance of 10 km, 2 μ sec Rise Time, and 25 μ sec Fall Time for the Ground and at Five Altitudes	84
5.36	Computer Solutions to Equation (39), the Electric Field, According to Model 3 at a Distance of 100 km, 2 μ sec Rise Time, and 25 μ sec Fall Time for the Ground and at Five Altitudes	85
5.37	Computer Solutions to Equation (40), the Magnetic Field, According to Model 1 at a Distance of 1 km, 500 μ sec Rise Time, and 10 μ sec Fall Time for the Ground and at Five Altitudes	86
5.38	Computer Solutions to Equation (40), the Magnetic Field, According to Model 1 at a Distance of 5 km, 500 μ sec Rise Time, and 10 μ sec Fall Time for the Ground and at Five Altitudes	87
5.39	Computer Solutions to Equation (40), the Magnetic Field, According to Model 1 at a Distance of 10 km, 500 μ sec Rise Time, and 10 μ sec Fall Time for the Ground and at Five Altitudes	88
5.40	Computer Solutions to Equation (40), the Magnetic Field, According to Model 1 at a Distance of 100 km, 500 μ sec Rise Time, and 10 μ sec Fall Time for the Ground and at Five Altitudes	89
5.41	Computer Solutions to Equation (40), the Magnetic Field, According to Model 1 at a Distance of 1 km, 1 μ sec Rise Time, and 25 μ sec Fall Time for the Ground and at Five Altitudes	90

5.42	Computer Solutions to Equation (40), the Magnetic Field, According to Model 1 at a Distance of 5 km, 1 μ sec Rise Time, and 25 μ sec Fall Time for the Ground and at Five Altitudes	91
5.43	Computer Solutions to Equation (40), the Magnetic Field, According to Model 1 at a Distance of 10 km, 1 μ sec Rise Time, and 25 μ sec Fall Time for the Ground and at Five Altitudes	92
5.44	Computer Solutions to Equation (40), the Magnetic Field, According to Model 1 at a Distance of 100 km, 1 μ sec Rise Time, and 25 μ sec Fall Time for the Ground and at Five Altitudes	93
5.45	Computer Solutions to Equation (40), the Magnetic Field, According to Model 1 at a Distance of 1 km, 2 μ sec Rise Time, and 50 μ sec Fall Time for the Ground and at Five Altitudes	94
5.46	Computer Solutions to Equation (40), the Magnetic Field, According to Model 1 at a Distance of 5 km, 2 μ sec Rise Time, and 50 μ sec Fall Time for the Ground and at Five Altitudes	95
5.47	Computer Solutions to Equation (40), the Magnetic Field, According to Model 1 at a Distance of 10 km, 2 μ sec Rise Time, and 50 μ sec Fall Time for the Ground and at Five Altitudes	96
5.48	Computer Solutions to Equation (40), the Magnetic Field, According to Model 1 at a Distance of 100 km, 2 μ sec Rise Time, and 50 μ sec Fall Time for the Ground and at Five Altitudes	97
5.49	Computer Solutions to Equation (40), the Magnetic Field, According to Model 2 at a Distance of 1 km, 500 nsec Rise Time, and 10 μ sec Fall Time for the Ground and at Five Altitudes	98

Figure		Page
5.50	Computer Solutions to Equation (40), the Magnetic Field, According to Model 2 at a Distance of 5 km, 500 nsec Rise Time, and 10 μ sec Fall Time for the Ground and at Five Altitudes	99
5.51	Computer Solutions to Equation (40), the Magnetic Field, According to Model 2 at a Distance of 10 km, 500 nsec Rise Time, and 10 μ sec Fall Time for the Ground and at Five Altitudes	100
5.52	Computer Solutions to Equation (40), the Magnetic Field, According to Model 2 at a Distance of 100 km, 500 nsec Rise Time, and 10 μ sec Fall Time for the Ground and at Five Altitudes	101
5.53	Computer Solutions to Equation (40), the Magnetic Field, According to Model 2 at a Distance of 1 km, 1 μ sec Rise Time, and 25 μ sec Fall Time for the Ground and at Five Altitudes	102
5.54	Computer Solutions to Equation (40), the Magnetic Field, According to Model 2 at a Distance of 5 km, 1 μ sec Rise Time, and 25 μ sec Fall Time for the Ground and at Five Altitudes	103
5.55	Computer Solutions to Equation (40), the Magnetic Field, According to Model 2 at a Distance of 10 km, 1 μ sec Rise Time, and 25 μ sec Fall Time for the Ground and at Five Altitudes	104
5.56	Computer Solutions to Equation (40), the Magnetic Field, According to Model 2 at a Distance of 100 km, 1 μ sec Rise Time, and 25 μ sec Fall Time for the Ground and at Five Altitudes	105
5.57	Computer Solutions to Equation (40), the Magnetic Field, According to Model 2 at a Distance of 1 km, 2 μ sec Rise Time, and 50 μ sec Fall Time for the Ground and at Five Altitudes	106

Figure		Page
5.58	Computer Solutions to Equation (40), the Magnetic Field, According to Model 2 at a Distance of 5 km, 2 μ sec Rise Time, and 50 μ sec Fall Time for the Ground and at Five Altitudes	107
5.59	Computer Solutions to Equation (40), the Magnetic Field, According to Model 2 at a Distance of 10 km, 2 μ sec Rise Time, and 50 μ sec Fall Time for the Ground and at Five Altitudes	108
5.60	Computer Solutions to Equation (40), the Magnetic Field, According to Model 2 at a Distance of 100 km, 2 μ sec Rise Time, and 50 μ sec Fall Time for the Ground and at Five Altitudes	109
5.61	Computer Solutions to Equation (40), the Magnetic Field, According to Model 3 at a Distance of 1 km, 500 nsec Rise Time, and 10 μ sec Fall Time for the Ground and at Five Altitudes	110
5.62	Computer Solutions to Equation (40), the Magnetic Field, According to Model 3 at a Distance of 5 km, 500 nsec Rise Time, and 10 μ sec Fall Time for the Ground and at Five Altitudes	111
5.63	Computer Solutions to Equation (40), the Magnetic Field, According to Model 3 at a Distance of 10 km, 500 nsec Rise Time, and 10 μ sec Fall Time for the Ground and at Five Altitudes	112
5.64	Computer Solutions to Equation (40), the Magnetic Field, According to Model 3 at a Distance of 100 km, 500 nsec Rise Time, and 10 μ sec Fall Time for the Ground and at Five Altitudes	113
5.65	Computer Solutions to Equation (40), the Magnetic Field, According to Model 3 at a Distance of 1 km, 1 μ sec Rise Time, and 25 μ sec Fall Time for the Ground and at Five Altitudes	114

Figure		Page
5.66	Computer Solutions to Equation (40), the Magnetic Field, According to Model 3 at a Distance of 5 km, 1 μ sec Rise Time, and 25 μ sec Fall Time for the Ground and at Five Altitudes	115
5.67	Computer Solutions to Equation (40), the Magnetic Field, According to Model 3 at a Distance of 10 km, 1 μ sec Rise Time, and 25 μ sec Fall Time for the Ground and at Five Altitudes	116
5.68	Computer Solutions to Equation (40), the Magnetic Field, According to Model 3 at a Distance of 100 km, 1 μ sec Rise Time, and 25 μ sec Fall Time for the Ground and at Five Altitudes	117
5.69	Computer Solutions to Equation (40), the Magnetic Field, According to Model 3 at a Distance of 1 km, 2 μ sec Rise Time, and 50 μ sec Fall Time for the Ground and at Five Altitudes	118
5.70	Computer Solutions to Equation (40), the Magnetic Field, According to Model 3 at a Distance of 5 km, 2 μ sec Rise Time, and 50 μ sec Fall Time for the Ground and at Five Altitudes	119
5.71	Computer Solutions to Equation (40), the Magnetic Field, According to Model 3 at a Distance of 10 km, 2 μ sec Rise Time, and 50 μ sec Fall Time for the Ground and at Five Altitudes	120
5.72	Computer Solutions to Equation (40), the Magnetic Field, According to Model 3 at a Distance of 100 km, 2 μ sec Rise Time, and 50 μ sec Fall Time for the Ground and at Five Altitudes	121
5.73	Comparison of the Electric Field Predicted by the Three Models and Lin's Modified Model (Master et al., 1981) with Experimental Data Taken on the Ground at a Distance of 10 kilometers. Estimated Rise Time of 2 μ sec	124

Figure		Page
5.74	Comparison of the Electric Field Predicted by the Three Models and Lin's Modified Model (Master et al., 1981) with Experimental Data Taken at 1500 Feet at a Distance of 10 kilometers. Estimated Rise Time of 2 μ sec . .	125
5.75	Comparison of the Electric Field Predicted by the Three Models and Lin's Modified Model (Master et al., 1981) with Experimental Data Taken at 8300 Feet at a Distance of 10 kilometers. Estimated Rise Time of 2 μ sec . .	126

List of Tables

Table		Page
2.1	Lightning Flash Components and Parameters . . .	11
5.1	Location of the Electric and Magnetic Field Figures for the Various Parameters	46

Abstract

A comprehensive analysis and comparison of lightning return stroke models is presented. A brief description of the lightning process and deviations of the equations for calculating the electric and magnetic fields at points on the ground and at points at altitude for an arbitrary current waveform are also presented. The models analyzed are the Bruce-Golde model, Uman's transmission line model (the breakdown pulse current not attenuated), and Uman's model using an attenuating breakdown pulse current. Plots of the electric and magnetic fields that these three models predict for various distances and altitudes and different parameters (rise and fall time of the current) are included. The above three models along with a recently modified version of Lin's model (where the breakdown pulse is attenuated) are then compared with recently acquired lightning return stroke electromagnetic data. The data was obtained simultaneously on the ground and at various altitudes in a WC-130 aircraft in South Florida.

AN ANALYSIS AND COMPARISON OF LIGHTNING RETURN STROKE MODELS AT ALTITUDE

I. Introduction

A study of how much energy from a lightning-sourced electromagnetic (EM) field couples into and affects modern aircraft is necessary to insure continued flight safety. Modern aircraft are more susceptible to lightning phenomena because of the increased use of smaller (and therefore faster, lower capacitance, and lower voltage) electronics and new carbon composite structural materials in their design (Baum, 1980a; Master, 1981).

Due to their higher operating speeds and lower capacities, modern electronic devices are more responsive or "resonate" at higher frequencies and can be destroyed at lower voltages than their predecessors.

The use of composite is highly desirable because of its lower cost, lighter weight (and therefore lower fuel costs), and its lower radar return signature (e.g., stealth aircraft) as compared to the more conventional use of aluminum. The lower radar return these composite materials offer is due to their ability to absorb electromagnetic energy as opposed to reflecting it as aluminum does. This,

however, also results in a very major disadvantage in using composite materials, that of allowing any undesirable external EM energy into the aircraft. Therefore, these composite materials provide less protection or "shielding" of the aircraft interior to external EM radiation. This means that more energy from the high-frequency, high-voltage lightning can transfer or "couple" into the interior of an aircraft and jeopardize flight safety by destroying electronic components or causing data and software errors in the on-board computers (Baum, 1980).

In order to be able to accurately calculate the amount of energy due to lightning that couples into an aircraft, one must first have an accurate model of the lightning process. Lightning has been studied and modeled for many years; however, it has always been done from a surface of the Earth standpoint. Not until recently (Master, 1981; Pitts and Thomas, 1980; Baum, 1980b) have researchers been studying lightning at altitudes and trying to write equations to predict the EM fields at those altitudes. The only such modeling of the EM fields published at this time is one done by Uman, et al. which uses a slightly modified version of the most recent model of ground data put forth by Lin, et al. (Master, 1981).

Problem

The problem of this thesis is to investigate the results of applying other models for analysis and comparison with data taken at altitudes and determining how well those previous models predict the data. Also, one new model which utilizes the modification Uman has made to Lin's model (Master, 1981) is investigated.

Scope

This paper briefly describes the lightning process, presents the theory for calculating the electric and magnetic fields, presents two past models of lightning and one new model, presents the results of those three models (predicted values), and then compares the three models with actual data.

The three models are:

1. The Bruce-Golde model
2. Uman's transmission line model
3. Uman's transmission line model with a height-dependent attenuation

Each of these models has advantages and disadvantages for use over the other models.

Presentation

Chapter II gives a brief description of how the lightning process occurs and defines pertinent terminology. Chapter III derives equations for calculating the electric

and magnetic fields at points on the surface of the Earth. Then the more general equations for calculating the EM fields at altitude are presented. Chapter IV discusses the advantages and disadvantages of each of the three models relative to each other and relative to Master's recent study (Master, 1981) which uses a slightly modified form of Lin's model. Chapter V presents the graphical results of the three models and a discussion of how each of the models varies as a function of distance, height, and lightning parameters and compares each with actual data. Chapter VI discusses the results of this research and makes some conclusions and recommendations.

II. Background

Lightning Process (Uman, 1969)

Lightning is defined as a "transient, high-current electric discharge whose path length is generally measured in kilometers [Uman, 1969:1]." The discharge occurs when one region of space contains enough charge or voltage potential relative to another region. When the charge differential is sufficient to cause electrical breakdown of the air between the two regions, the discharge or lightning occurs.

The build-up of electrical charge occurs most often in thunderclouds; although, lightning also can be produced by snowstorms, sandstorms, and the clouds over erupting volcanoes. Sufficient charge regions to produce lightning have been reported to exist even in clear air (Uman, 1969:1).

As shown in Figure 2.1, the major region of positive charge build-up occurs at the top of the cloud (P). Moving down from the top of the cloud, it becomes less densely positive, eventually becoming weakly negative and then becoming strongly negative (N). At the very bottom tip of the cloud, there is a weak positive region (p).

The lightning flash can be of several types. The most common is called intracloud lightning. As the name

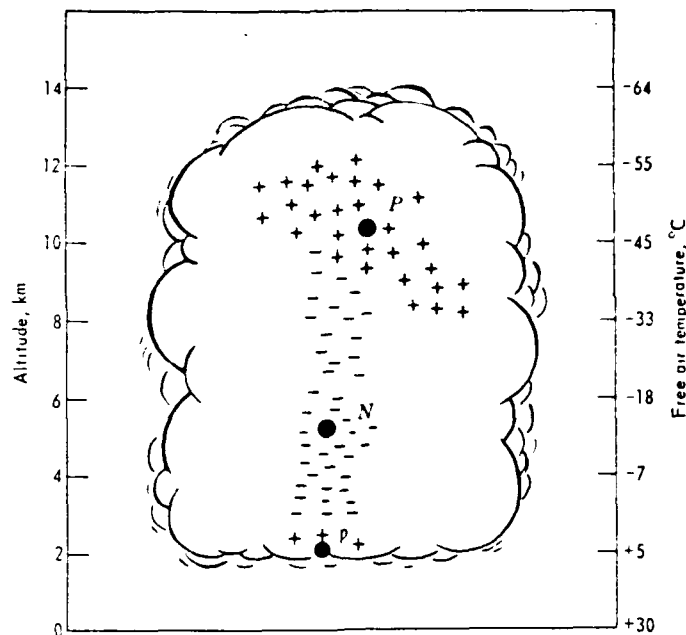


Fig. 2.1. Typical Charge Distribution in a South African Thundercloud According to Malan (1952, 1963). Electric Field Measurements Show Typically $P=+40$ coul, $N=-40$ coul, and $p=+10$ coul (Uman, 1969:3).

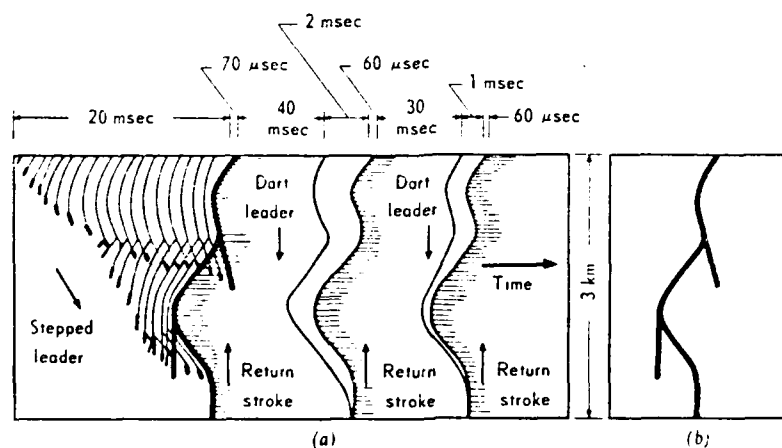


Fig. 2.2. (a) The Luminous Features of a Lightning Flash as They Would be Recorded by a Camera with a Fixed Lens and Moving Film. Time Scale Increases to the Right; Time Scale is Distorted for Clarity. (b) The Same Lightning Flash as it Would be Recorded by a Camera with Stationary Film (Uman, 1969:6).

indicates, intracloud lightning takes place within the cloud itself. Another category of lightning is called cloud-to-cloud lightning. Other types of lightning are heat, sheet, ribbon, ball, rocket, and bead lightning (Uman, 1969:13).

The type of lightning one usually thinks of at the mention of lightning and is the most commonly studied and written about is called cloud-to-ground (CG) lightning, sometimes referred to as streaked or forked lightning. This is the type of lightning that this thesis will investigate.

The CG lightning flash is made up of individual discharges called strokes. There is always at least one stroke per flash, typically there are three or four. As many as 26 strokes have been reported in one flash (Uman, 1969:10). Each stroke, in turn, is made up of two parts: the leader and the return stroke. The leader generally propagates from the cloud to the ground and is usually negatively charged. Relative to the return stroke, the leader transfers less charge.

The first leader in a flash is called the stepped leader. The reason for this terminology is that moving film, fixed lens cameras (e.g., a boy's camera) show that this leader propagates in segments or steps (typically 50 meter lengths) with pauses of approximately 50 μ sec between steps (Uman, 1969:5). A stepped leader would show

up on a streak film as a luminous step, a dark period, a new luminous step with a faint channel above the new step to the cloud, a dark period, a new step and faint channel, a dark period, and so forth. The stepped leader is usually strongly branched downward and is thought to originate due to electrical breakdown between the N and p regions of the cloud (Uman, 1969:5) shown in Figure 2.1.

Once the stepped leader propagates to within a few hundred meters of the Earth (ground or zero potential), electrical breakdown between the high potential (usually negative (Uman, 1969:10)) of the leader and the ground occurs. When the upward moving ground potential contacts with the leader, a short-circuit-like situation exists. At this point, an upward moving wavefront of ground potential starts (the return stroke). The wavefront travels up the same channel that the leader came down (including any "branches"), eventually grounding-out all negative charges that were in the leader. The return stroke is the main discharge in a flash and carries the larger currents.

The first return stroke in a flash (i.e., the return stroke following the stepped leader) will travel up the channel at a constant velocity until it reaches the first branch point. At this point, the channel luminosity increases (called a branch point), then the return stroke will continue at a slightly slower velocity until the next branch point, and so on. An increase in the luminosity

of the entire cloud-to-ground channel is known as an M component.

If the return stroke channel is allowed to decay for more than approximately 100 msec after it reaches the cloud, the lightning flash is ended. If, however, more negative charge is made available to the channel (apparently from higher in the N region of the cloud) and the channel is still sufficiently ionized (typically less than 100 msec after the return stroke ends), then a secondary leader can start. This new leader is called a dart leader. It will follow the same main channel that the stepped leader and return stroke used (i.e., no "branching"). The dart leader appears to propagate an order of magnitude faster than the stepped leader, but carries less charge.

Unlike the stepped leader, the dart leader will tend to get closer to the ground because the channel is still ionized. Then a new return stroke occurs; however, these secondary return strokes travel at a constant velocity, presumably due to the lack of "branching" in the dart leader. Also, these return strokes tend to have higher velocities and transfer less charge than initial return strokes. This leader-return-stroke sequence will repeat until the charges in the cloud are sufficiently depleted.

Strokes carrying positive charge to Earth have been observed via direct measurements during discharges to

instrumented towers (Uman, 1969:10) in addition to upward propagating leaders carrying both negative and positive charges with no apparent return stroke (Uman, 1969:11). These types of lighting flashes will not be investigated in this thesis.

Table 2.1 from the book Lightning (Uman, 1969:4) shows some of the pertinent parameters for the stepped leader, the dart leader, the return stroke, and the lightning flash.

Assumption

As stated earlier, this thesis is concerned with investigating cloud-to-ground lightning flashes; specifically, we will calculate the EM fields at various points in space under various conditions for each of four models. These calculated values will be compared to experimentally obtained values. From this comparison a qualitative judgment of the "goodness" of each model performs. Since the EM fields are of concern here, only the return stroke is of interest due to its much larger peak current relative to the leader (thereby producing larger EM field values).

Other assumptions used in this study are the following:

1. Free space permittivity ($\epsilon_0 = 1/36\pi \times 10^{-9}$) and permeability ($\mu_0 = 4\pi \times 10^{-7}$).

TABLE 2.1
LIGHTNING FLASH COMPONENTS AND PARAMETERS

	Minimum (Observed)	Typical	Maximum (Observed)
- Stepped Leader			
- Length of step, m	3	50	200
- Time interval between steps, μsec	30	50	125
- Average velocity of propagation of stepped leader, m/sec	1.0×10^5	1.5×10^5	2.6×10^6
- Charge deposited on channel, coul	3	5	20
- Dart Leader			
- Velocity of propagation, m/sec	1.0×10^6	2.0×10^6	2.1×10^7
- Charge deposited on channel, coul	0.2	1	6
- Return Stroke			
- Velocity of propagation, m/sec	2.0×10^7	6.0×10^7	1.4×10^8
- Current rate of increase, Ka/ μsec	<1	10	>80
- Time to peak current, μsec	<1	2	30
- Peak current, Ka		10-20	110
- Time to half of peak current, μsec	10	40	250

TABLE 2.1--Continued

	Minimum (Observed)	Typical	Maximum (Observed)
- Charge transferred excluding continuing current, coul	.02	2.5	20
- Channel length, Km	2	5	14
- Lightning Flash			
- Number of strokes per flash	1	3-4	26
- Time interval between strokes in absence of continuing current, msec	3	40	100
- Time duration of flash, sec	0.01	0.2	15-20
- Charge transferred including con- tinuing current, coul	3	25	90

2. The Earth is a flat, perfectly conducting, infinite ground plane.
3. Constant velocity of propagation.
4. Only secondary return strokes are investigated.
5. The channel is straight and vertical.
6. The channel will be modeled as a transmission line.

The third and fourth assumptions are interrelated in that a constant velocity is only a valid assumption on analyzing secondary return strokes. The choice of secondary return strokes prevents the difficulty introduced when trying to functionally describe the velocity of a return stroke that changes at every branch point as is the case for first return strokes.

Another reason for studying only secondary return strokes comes from the lack of definitive knowledge of the EM fields due to the stepped leader/initial return stroke process. Measurements of the first stroke show that the fields have a slower initial rise time than secondary strokes. Many researchers believe the slower rise time of first strokes is due to the interaction of the slow, downward propagating stepped leader and the simultaneous upward moving ground leader before it contacts the stepped leader. Whereas dart leader, traveling an order of magnitude faster than the stepped leader, down an already ionized channel, tend to get closer to the ground before the return stroke

begins, resulting in a faster initial rise time of the EM fields. All this, however, is not clearly understood and therefore most return stroke studies deal only with secondary return strokes as will be the case in this thesis.

The channel will be assumed to be straight and vertical. Some studies show that path tortuosity does not affect the induced EM fields (Pearlman, 1979), whereas other studies show that path tortuosity does have an effect (Levine, 1979). The matter of path tortuosity is as yet in dispute and this thesis is not concerned with resolving the issue; therefore, because it is easier to model the lightning channel as straight and vertical, it will be so modeled in this thesis as it is in most other studies not concerned with investigating path tortuosity effects.

Lastly, the channel will also be modeled as a transmission line or antenna of finite length. Initially, in the first two models, the line will be lossless. For the second two models a more realistic loss factor (attenuation) is introduced. Throughout this thesis the transmission line will have matched impedance loads at both ends. Naturally, the lightning channel, as can any transmission line, could be modeled as a lumped parameter circuit (e.g., an LRC network) as is done in a study by Little (Little, 1978). This thesis will use more conventional transmission line analysis methods.

III. Theory

EM on the Ground

Since it is assumed to be straight, the lightning channel can be looked upon as a vertical antenna with a finite length. The analysis is done using the same methods as used by Uman (Uman, 1975). Figure 3.1 shows the lightning model and the parameters of concern for determining \bar{E} and \bar{B} at point P on the ground.

Beginning with the time-dependent Maxwell's equation in free-space,

$$\nabla \cdot \bar{E} = \rho/\epsilon_0 \quad (1)$$

$$\nabla \cdot \bar{B} = 0 \quad (2)$$

$$\nabla \times \bar{E} = -\partial\bar{B}/\partial t \quad (3)$$

$$\nabla \times \bar{B} = \mu_0 \bar{J} + \frac{1}{c^2} \frac{\partial\bar{E}}{\partial t} \quad (4)$$

and their general solutions in terms of retarded scalar and vector potentials,

$$\bar{E} = -\nabla\phi - \frac{\partial\bar{A}}{\partial t} \quad (5)$$

$$\bar{B} = \nabla \times \bar{A} \quad (6)$$

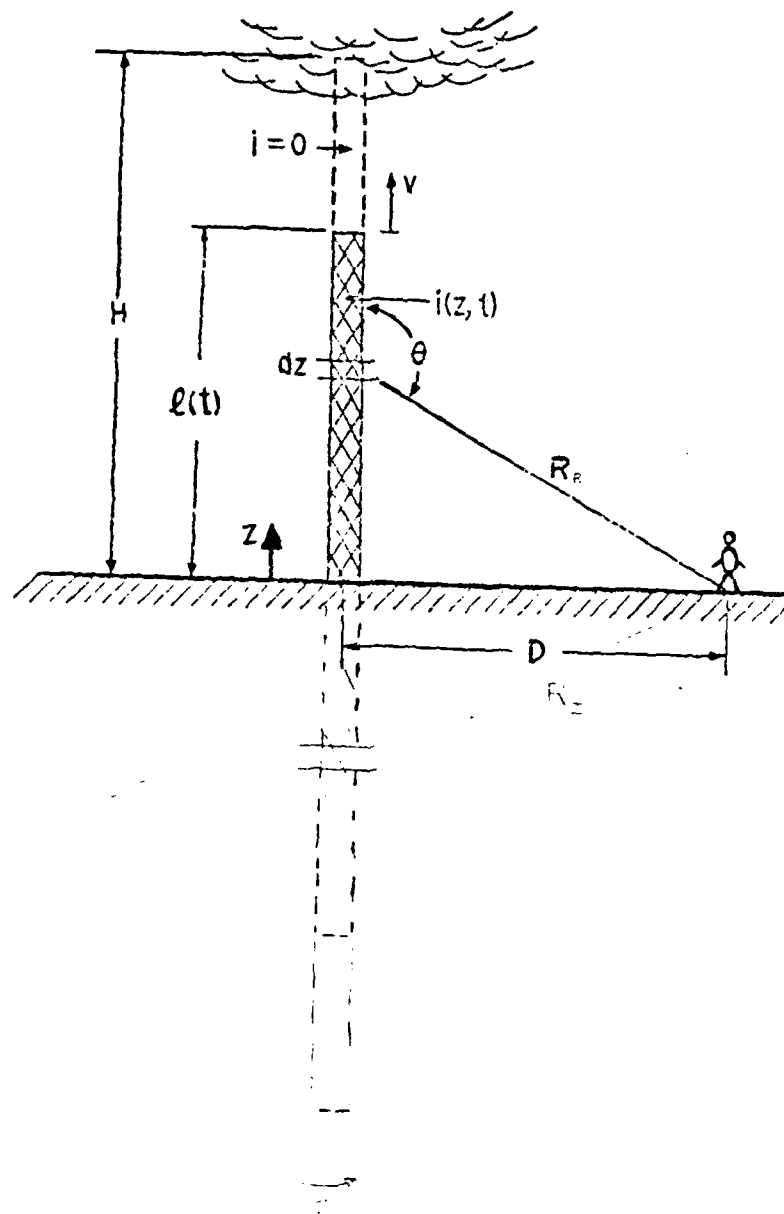


Fig. 3.1. Definition of Geometrical and Physical Parameters Used in Return Stroke Modeling for Points on the Ground (Lin, 1978:27).

where

$$\phi(\bar{r}, t) = \frac{1}{4\pi\epsilon_0} \int_V \frac{1}{R} \rho(\bar{r}', t-R/c) dv' \quad (7)$$

= scalar potential

$$\bar{A}(\bar{r}, t) = \frac{\mu_0}{4\pi} \int_V \frac{1}{R} \bar{J}(\bar{r}', t-R/c) dv' \quad (8)$$

= vector potential

$$\nabla \cdot \bar{A} + \frac{1}{c^2} \frac{\partial \phi}{\partial t} = 0 \quad (9)$$

The scalar and vector potentials are based on the geometry shown in Figure 3.2.

The problem is to analyze a straight vertical antenna of length H that lies perpendicular to a perfectly conducting ground plane. Boundary conditions dictate the existence of an image antenna of equal length below the ground plane as shown in Figure 3.2. The antenna cross-section is much less than the radiation wavelength. The current, $i(z, t)$, is a continuous function and is zero everywhere for $t \leq 0$.

Since $i(z, t)$ lies along the z -axis, $\bar{r}' = z\hat{a}_z$

and

$$\bar{J}(\bar{r}', t-R/c) dv' = i(z, t-R/c) dz \hat{a}_z \quad (10)$$

To derive the differential magnetic field, $d\bar{B}_R$, due to an infinitesimal current element on the real antenna,

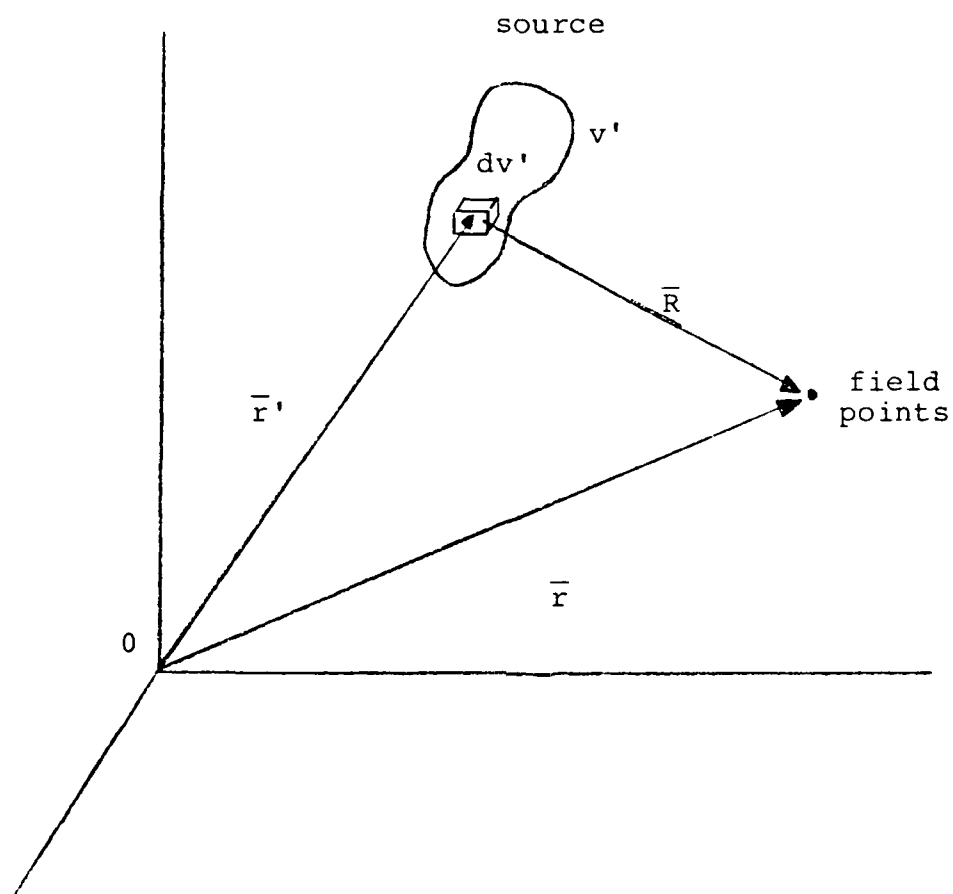


Fig. 3.2. The Geometry for General Solutions of the Time-Dependent Maxwell Equations (Uman, et al., 1969).

start with Maxwell's equations. Equation (6) becomes

$$d\bar{B}_R = \nabla \times d\bar{A}_R \quad (11)$$

To find $d\bar{A}_R$, substitute (10) into (8) to get

$$\bar{A}_R(\bar{r}, t) = \frac{\mu_0}{4\pi} \int_0^H \frac{1}{R} i(z, t-R/c) \hat{a}_z dz \quad (12)$$

which means

$$d\bar{A}_R = \frac{\mu_0}{4\pi} \frac{1}{R} i(z, t-R/c) \hat{a}_z dz \quad (13)$$

To convert Equation (13) from cylindrical to spherical coordinates, let

$$\hat{a}_z = \hat{a}_r \cos \theta - \hat{a}_\theta \sin \theta.$$

Equation (13) becomes

$$d\bar{A}_R = \frac{\mu_0}{4\pi} \frac{1}{R} i(z, t-R/c) [\hat{a}_r \cos \theta - \hat{a}_\theta \sin \theta] dz \quad (14)$$

$$= d\bar{A}_r \hat{a}_r + d\bar{A}_\theta \hat{a}_\theta + d\bar{A}_\phi \hat{a}_\phi \quad (15)$$

Substitute Equation (14) into Equation (11) to get

$$\begin{aligned}
d\bar{B}_R &= \hat{a}_r \frac{1}{R \sin \theta} \left[\frac{\partial}{\partial \theta} (dA_\phi \sin \theta) - \frac{\partial}{\partial \phi} (dA_\theta) \right] \\
&+ \hat{a}_\theta \frac{1}{R} \left[\frac{1}{\sin \theta} \frac{\partial}{\partial \phi} (dA_R) - \frac{\partial}{\partial R} (R dA_\phi) \right] \\
&+ \hat{a}_\phi \left[\frac{\partial}{\partial R} (R dA_\theta) - \frac{\partial}{\partial \theta} (dA_R) \right] \quad (16)
\end{aligned}$$

By comparing Equations (14) and (15), it is seen that $dA_\phi = 0$. Also, $d\bar{A}_R$ has no dependence on ϕ ; therefore, the derivatives with respect to ϕ are zero (i.e., $\partial/\partial\phi = 0$). Equation (15) becomes

$$\begin{aligned}
d\bar{B}_R &= \hat{a}_\phi \frac{1}{R} \left\{ \frac{\partial}{\partial R} \left[-R \frac{\mu_0}{4\pi} \frac{1}{R} i(z, t-R/c) \sin \theta dz \right] \right. \\
&\quad \left. - \frac{\partial}{\partial \theta} \left[\frac{\mu_0}{4\pi} \frac{1}{R} i(z, t-R/c) \cos \theta dz \right] \right\} \\
&= \hat{a}_\phi \frac{\mu_0}{4\pi} \left\{ -\frac{1}{R} \sin \theta \frac{\partial}{\partial R} i(z, t-R/c) \right. \\
&\quad \left. + \frac{1}{R^2} \sin \theta i(z, t-R/c) \right\} dz \quad (17)
\end{aligned}$$

Using the identity

$$\frac{\partial}{\partial R} i(z, t-R/c) = -\frac{1}{c} \frac{\partial}{\partial t} i(z, t-R/c)$$

Equation (17) becomes

$$\begin{aligned}
d\bar{E}_R &= \hat{a}_\phi \frac{\mu_0}{4\pi} \sin \theta \left[-\frac{1}{R^2} i(z, t-R/c) \right. \\
&\quad \left. + \frac{1}{cR} \frac{\partial}{\partial t} i(z, t-R/c) \right] dz \quad (18)
\end{aligned}$$

As mentioned earlier, boundary conditions require an imaginary differential current element with the same magnitude, direction, and distance below the ground plane as the real current element above the plane. Now proceed to calculate the differential magnetic field, $d\bar{B}_I$, due to an infinitesimal current element as was done for the real current element above to find

$$\begin{aligned} d\bar{B}_I &= \hat{a}_\phi \frac{\mu_0}{4\pi} \sin \theta \left[\frac{1}{R^2} i(z, t-R/c) \right. \\ &\quad \left. + \frac{1}{cR} \frac{\partial}{\partial t} i(z, t-R/c) \right] dz \\ &= d\bar{B}_R \end{aligned}$$

The total differential magnetic field is the sum of the fields due to the real and imaginary currents.

Thus

$$\begin{aligned} d\bar{B} &= d\bar{B}_R + d\bar{B}_I \\ &= \hat{a}_\phi \frac{\mu_0}{2\pi} \sin \theta \left[\frac{1}{R^2} i(z, t-R/c) \right. \\ &\quad \left. + \frac{1}{cR} \frac{\partial}{\partial t} i(z, t-R/c) \right] dz \end{aligned} \tag{19}$$

Find the electric field due to the infinitesimal real current by starting with Equation (5)

$$d\bar{E}_R = - \nabla d\bar{\phi}_R - \frac{\partial}{\partial t} d\bar{A}_R \quad (20)$$

First, $d\bar{\phi}_R$ is needed. Get it by solving Equation (9) for $\bar{\phi}$.

$$\nabla \cdot \bar{A} + \frac{1}{c^2} \frac{\partial \bar{\phi}}{\partial t} = 0$$

$$\frac{\partial \bar{\phi}}{\partial t} = -c^2 \nabla \cdot \bar{A} \quad (21)$$

Since Equation (9) involves the derivative of $\bar{\phi}$ with respect to time, integrate Equation (21) over time to undo the derivative.

$$\bar{\phi}(\bar{R}, t) = -c^2 \int_0^t \nabla \cdot \bar{A} d\tau$$

The differential scalar potential due to the real current element being

$$d\bar{\phi}_R(\bar{R}, t) = -c^2 \int_0^t \nabla \cdot d\bar{A}_R d\tau \quad (22)$$

Taking the divergence of Equation (14) results in

$$\begin{aligned} \nabla \cdot d\bar{A}_R &= \frac{\mu_0}{4\pi} \frac{1}{R^2} \cos\theta \left\{ \frac{\partial}{\partial R} [Ri(z, t-R/c)] \right. \\ &\quad \left. - 2i(z, t-R/c) \right\} \end{aligned}$$

Substituting this into Equation (22) and noting that $\mu_0 c^2 = 1/\epsilon_0$ yields

$$\begin{aligned}
 d\vec{A}_R(\vec{R}, t) = & \frac{1}{4\pi\epsilon_0} \cos\theta \left[\frac{1}{R^2} \int_0^t i(z, \tau - R/c) d\tau \right. \\
 & \left. + \frac{1}{cR} i(z, t - R/c) \right] \quad (23)
 \end{aligned}$$

Now take the negative gradient of Equation (23) to get

$$\begin{aligned}
 -\nabla d\vec{A}_R = & \hat{a}_r \frac{1}{4\pi\epsilon_0} \cos\theta \left[\frac{2}{cR^2} i(z, t - R/c) \right. \\
 & + \frac{2}{R^3} \int_0^t i(z, \tau - R/c) d\tau \\
 & + \frac{1}{c^2 R} \frac{\partial}{\partial t} i(z, t - R/c) \left. \right] dz \\
 & + \hat{a}_\theta \frac{1}{4\pi\epsilon_0} \frac{1}{R} \sin\theta \left[\frac{1}{R^2} \int_0^t i(z, \tau - R/c) d\tau \right. \\
 & \left. + \frac{1}{cR} i(z, t - R/c) \right] dz \quad (24)
 \end{aligned}$$

Using Equation (14), take the derivative with respect to time and get

$$\begin{aligned}
 \frac{\partial}{\partial t} d\vec{A}_R = & \hat{a}_r \frac{u_0}{4\pi} \left[\frac{1}{R} \cos\theta \frac{\partial}{\partial t} i(z, t - R/c) \right] dz \\
 & + \hat{a}_\theta \frac{u_0}{4\pi} \left[\frac{1}{R} \sin\theta \frac{\partial}{\partial t} i(z, t - R/c) \right] dz \quad (25)
 \end{aligned}$$

Finally, to find the differential electric field due to the real current element, add Equations (24) and (25)

$$\begin{aligned}
d\bar{E}_R = & \frac{1}{4\pi\epsilon_0} \left\{ \cos \theta \left[\frac{2}{R^3} \int_0^t i(z, \tau - R/c) d\tau \right. \right. \\
& + \frac{2}{cR^2} i(z, t - R/c) \left. \right] \hat{a}_r \\
& + \sin \theta \left[\frac{1}{R^3} \int_0^t i(z, \tau - R/c) d\tau \right. \\
& + \frac{1}{cR^2} i(z, t - R/c) + \frac{1}{c^2 R} \frac{\partial}{\partial t} i(z, t - R/c) \left. \right] \hat{a}_\theta \left. \right\} dz \quad (26)
\end{aligned}$$

The electric field due to an infinitesimal imaginary current element can be found in a similar manner with, as shown in Figure 3.1, θ replaced by $\pi - \theta$. The result is

$$\begin{aligned}
d\bar{E}_I = & \frac{1}{4\pi\epsilon_0} \left\{ -\cos \theta \left[\frac{2}{R^3} \int_0^t i(z, \tau - R/c) d\tau \right. \right. \\
& + \frac{2}{cR^2} i(z, t - R/c) \left. \right] \hat{a}_{r_I} \\
& + \sin \theta \left[\frac{1}{R^3} \int_0^t i(z, \tau - R/c) d\tau \right. \\
& + \frac{1}{cR^2} i(z, t - R/c) + \frac{1}{c^2 R} \frac{\partial}{\partial t} i(z, t - R/c) \left. \right] \hat{a}_{\theta_I} \left. \right\} dz \quad (27)
\end{aligned}$$

Before adding Equations (26) and (27) to get the total electric field, the unit vectors \hat{a}_R , \hat{a}_θ , \hat{a}_{r_I} , and \hat{a}_{θ_I} need to be converted to common terms. The four unit vectors can be broken up into two components: a vertical component (\hat{a}_z) and a horizontal component (\hat{a}_H). From Figure 3.1 it is seen that

$$\begin{aligned}
\hat{a}_r &= -a_z \hat{a}_z + a_H \hat{a}_H \\
&= -\sin\left(\theta - \frac{\pi}{2}\right) \hat{a}_z + \cos\left(\theta - \frac{\pi}{2}\right) \hat{a}_H \\
&= \cos\theta \hat{a}_z + \sin\theta \hat{a}_H
\end{aligned} \tag{28}$$

$$\begin{aligned}
\hat{a}_\theta &= -a_z \hat{a}_z - a_H \hat{a}_H \\
&= -\cos\left(\theta - \frac{\pi}{2}\right) \hat{a}_z - \sin\left(\theta - \frac{\pi}{2}\right) \hat{a}_H \\
&= -\sin\theta \hat{a}_z + \cos\theta \hat{a}_H
\end{aligned} \tag{29}$$

$$\begin{aligned}
\hat{a}_{r_I} &= a_z \hat{a}_z + a_H \hat{a}_H \\
&= \cos(\pi - \theta) \hat{a}_z + \sin(\pi - \theta) \hat{a}_H \\
&= -\cos\theta \hat{a}_z + \sin\theta \hat{a}_H
\end{aligned} \tag{30}$$

$$\begin{aligned}
\hat{a}_{\theta_I} &= -a_z \hat{a}_z + a_H \hat{a}_H \\
&= -\sin(\pi - \theta) \hat{a}_z + \cos(\pi - \theta) \hat{a}_H \\
&= -\sin\theta \hat{a}_z - \cos\theta \hat{a}_H
\end{aligned} \tag{31}$$

The total differential electric field is the sum of the fields due to the real and imaginary currents.

Thus, with appropriate substitutions of Equations (28),
(29), (30), and (31)

$$\begin{aligned}
 d\bar{E} &= d\bar{E}_R + d\bar{E}_I \\
 &= \frac{1}{4\pi\epsilon_0} \left\{ \cos\theta \left[\frac{2}{R^3} \int_0^t i(z, \tau-R/c) d\tau \right. \right. \\
 &\quad + \frac{2}{cR^2} i(z, t-R/c) \left. \right] (\cos\theta \hat{a}_z + \sin\theta \hat{a}_H) \\
 &\quad + \sin\theta \left[\frac{1}{R^3} \int_0^t i(z, \tau-R/c) d\tau + \frac{1}{cR^2} i(z, t-R/c) \right. \\
 &\quad + \frac{1}{c^2 R} \frac{\partial}{\partial t} i(z, t-R/c) \left. \right] (-\sin\theta \hat{a}_z + \cos\theta \hat{a}_H) \left. \right\} dz \\
 &\quad + \frac{1}{4\pi\epsilon_0} \left\{ -\cos\theta \left[\frac{2}{R^3} \int_0^t i(z, \tau-R/c) d\tau \right. \right. \\
 &\quad + \frac{2}{cR^2} i(z, t-R/c) \left. \right] (-\cos\theta \hat{a}_z + \sin\theta \hat{a}_H) \\
 &\quad + \sin\theta \left[\frac{1}{R^3} \int_0^t i(z, \tau-R/c) d\tau + \frac{1}{cR^2} i(z, t-R/c) \right. \\
 &\quad + \frac{1}{c^2 R} \frac{\partial}{\partial t} i(z, t-R/c) \left. \right] (-\sin\theta \hat{a}_z - \cos\theta \hat{a}_H) \left. \right\} dz \\
 &= \frac{1}{2\pi\epsilon_0} \left\{ \cos^2\theta \left[\frac{2}{R^3} \int_0^t i(z, \tau-R/c) d\tau \right. \right. \\
 &\quad + \frac{2}{cR^2} i(z, t-R/c) \left. \right] \hat{a}_z \left. \right\} dz
 \end{aligned}$$

$$\begin{aligned}
& - \frac{1}{2\pi\epsilon_0} \{ \sin^2 \theta \left[\frac{1}{R^3} \int_0^t i(z, \tau - R/c) d\tau \right. \\
& + \frac{1}{cR^2} i(z, t - R/c) + \frac{1}{c^2 R} \frac{\partial}{\partial t} i(z, t - R/c) \} \hat{a}_z \} dz \\
& = \frac{1}{2\pi\epsilon_0} \left[\frac{1}{R^3} (2 \cos^2 \theta - \sin^2 \theta) \int_0^t i(z, \tau - R/c) d\tau \right. \\
& + \frac{1}{cR^2} (2 \cos^2 \theta - \sin^2 \theta) i(z, t - R/c) \\
& \left. - \frac{1}{c^2 R} \frac{\partial}{\partial t} i(z, t - R/c) \right] \hat{a}_z dz \tag{32}
\end{aligned}$$

Using trig identities

$$\begin{aligned}
2 \cos^2 \theta - \sin^2 \theta &= 2 \times \frac{1}{2} (1 + \cos 2\theta) - \frac{1}{2} (1 - \cos 2\theta) \\
&= \frac{1}{2} + \frac{3}{2} \cos 2\theta \\
&= \frac{1}{2} (1 + 3 \cos 2\theta) \\
&= \frac{1}{2} (1 + 3(1 - 2 \sin^2 \theta)) \\
&= \frac{1}{2} (1 + 3 - 6 \sin^2 \theta) \\
&= 2 - 3 \sin^2 \theta \tag{33}
\end{aligned}$$

Substituting Equation (33) into Equation (32)

$$\begin{aligned}
d\bar{E} = & \frac{1}{2\pi\epsilon_0} \left[\frac{1}{R^3} (2-3\sin^2\theta) \int_0^t i(z, \tau-R/c) d\tau \right. \\
& + \frac{1}{cR^2} (2-3\sin^2\theta) i(z, t-R/c) \\
& \left. - \frac{1}{c^2R} \sin^2\theta \frac{\partial}{\partial t} i(z, t-R/c) \right] \hat{a}_z dz
\end{aligned} \tag{34}$$

To get the magnetic and electric fields due to the current along the entire length of the channel, integrate Equations (19) and (34), respectively, from zero to maximum height, H.

$$\begin{aligned}
B_\phi(D, t) &= \int_0^H dB_\phi(R, \theta, t) dz \\
&= \int_0^H \frac{\mu_0}{2\pi} \sin\theta \left[\frac{1}{R^2} i(z, t-R/c) \right. \\
&\quad \left. + \frac{1}{cR} \frac{\partial}{\partial t} i(z, t-R/c) \right] dz \\
&= \frac{\mu_0}{2\pi} \int_0^H \frac{1}{R^2} \sin\theta i(z, t-R/c) dz \\
&\quad + \frac{\mu_0}{2\pi} \int_0^H \frac{1}{cR} \frac{\partial}{\partial t} i(z, t-R/c) dz
\end{aligned} \tag{35}$$

$$\begin{aligned}
E_z(D, t) &= \int_0^H dE_z(R, \theta, t) dz \\
&= \int_0^H \frac{1}{2\pi\epsilon_0} \left[\frac{1}{R^3} (2-3\sin^2\theta) \int_0^t i(z, \tau-R/c) d\tau \right.
\end{aligned}$$

$$\begin{aligned}
& + \frac{1}{cR^2} (2-3 \sin^2 \theta) i(z, t-R/c) \\
& - \frac{1}{c^2 R} \frac{\partial}{\partial t} i(z, t-R/c) \} dz \\
& = \frac{1}{2\pi\epsilon_0} \int_0^H \frac{1}{R^3} (2-3 \sin^2 \theta) dz \int_0^t i(z, \tau-R/c) d\tau \\
& + \frac{1}{2\pi\epsilon_0} \int_0^H \frac{1}{cR^2} (2-3 \sin^2 \theta) i(z, t-R/c) dz \\
& - \frac{1}{2\pi\epsilon_0} \int_0^H \frac{1}{c^2 R} \sin^2 \theta \frac{\partial}{\partial t} i(z, t-R/c) dz \tag{36}
\end{aligned}$$

The first term in Equation (35) is called the induction or intermediate term. The second term is called the radiation or far-field term. The terms in Equation (36) are called the electrostatic, the induction, and the radiation terms.

Because of the integral of the current, the electrostatic term should have the longest lasting effect on the electric field. It should result in a theoretically constant value (actually it would slowly decay) in the electric field. Due to the $1/R^3$ dependence, the electrostatic term has less effect the further away the calculated point is from the return stroke.

The induction terms also have less effect on the EM fields, but do not drop off as fast as the electrostatic term since the induction term is dependent on $1/R^2$; therefore, the induction term has a longer effect on the

field (in terms of distance away from the return stroke) than does the electrostatic term. Because it is a scaled value of the current, the induction terms should produce a hump in the field.

The radiation terms have the most effect on the fields the further from the return stroke one gets. This is due to it having only a $1/R$ dependence. Also, due to its partial derivative with respect to time dependence, it will be predominate in the first few hundred nanoseconds (until the peak of the current) after the return stroke starts.

EM Everywhere

Equations (25) and (36) are good only for calculating the electric and magnetic fields at points on the ground plane. Using methods similar to deriving Equations (35) and (36), equations for determining the \bar{E} and \bar{B} at any point in space can be derived.

Looking at Figure 3.3, it is seen that the distance from the real current element to the field point, R_R , and the distance from the imaginary current element to the field point, R_I , are no longer always equal. Also, the inside angle between R_I and the vertical is no longer $\pi - \theta$. Taking these two differences into account, Equation (26) with Equations (28) and (29) substituted and noting that $\sin \theta = D/R_R$ and $\cos \theta = (HA-z)/R_R$ becomes

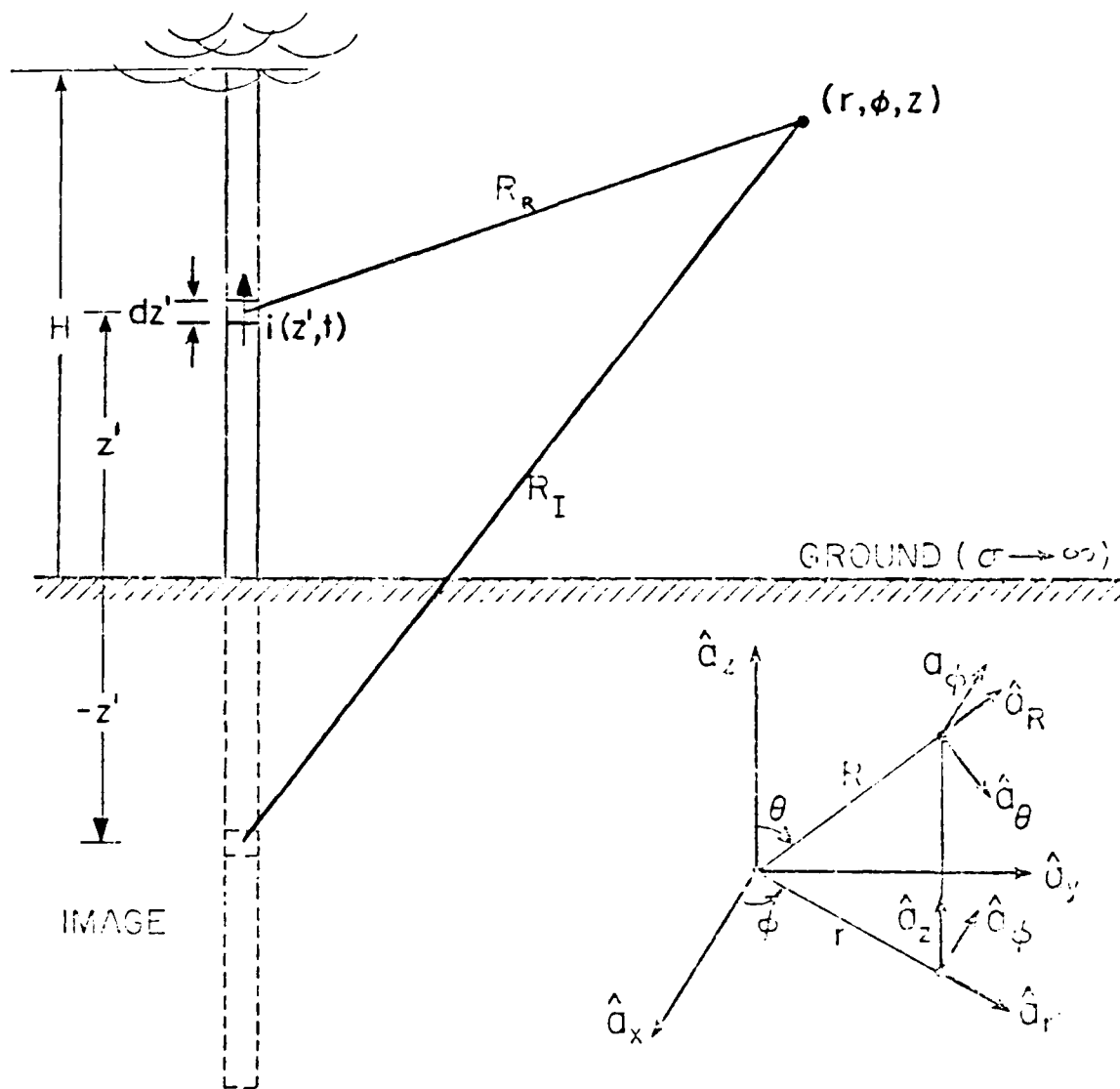


Fig. 3.3. Definition of Geometrical and Physical Parameters Used in Return Stroke Modeling for Points Anywhere (Master et al., 1981).

$$\begin{aligned}
d\bar{E}_R = & \frac{1}{4\pi\epsilon_0} \left\{ \left[\frac{2HA-z}{R_R} \right]^2 \frac{D^2}{5} \int_0^t i(z, t-R_R/c) dt \right. \\
& + \frac{2(HA-z)}{cR_R} \frac{D^2}{4} i(z, t-R_R/c) \\
& - \frac{D^2}{c^2 R_R} \frac{1}{3} \frac{\partial}{\partial t} i(z, t-R_R/c) \left. \right\} \hat{a}_z \\
& + \frac{3D(HA-z)}{R_R^5} \int_0^t i(z, t-R_R/c) dt \\
& + \frac{3D(HA-z)}{cR_R^4} i(z, t-R_R/c) \\
& + \frac{D(HA-z)}{c^2 R_R} \frac{1}{3} \frac{\partial}{\partial t} i(z, t-R_R/c) \left. \right\} \hat{a}_r dz
\end{aligned} \tag{37}$$

Comparing Equation (37) with the equations found in Master, et al. (Master, 1981), it is seen that Equation (37) is equivalent with different notation.

The differential magnetic field for all points in space is simply found by letting $\sin\theta = D/R_R$ in Equation (18) to get

$$\begin{aligned}
d\bar{B}_R = & \frac{\mu_0}{4\pi} \left\{ \frac{D}{R_R} \frac{1}{3} i(z, t-R_R/c) \right. \\
& + \frac{D}{cR_R} \frac{1}{2} \frac{\partial}{\partial t} i(z, t-R_R/c) \left. \right\} dz \hat{a}_\phi
\end{aligned} \tag{38}$$

which is equivalent to the equations found in Master, et al. (Master, 1981) with appropriate notational changes.

The electric and magnetic fields due to the differential length image current element is found by substituting R_I for R_R and $-z$ for z into Equations (37) and (38). The resulting $d\bar{E}_R$ and $d\bar{E}_I$ are added to get the total differential electric field $d\bar{E}$. Likewise, $d\bar{B}$ is obtained by adding $d\bar{B}_R$ and $d\bar{B}_I$.

The \bar{E} and \bar{B} are found by integrating $d\bar{E}$ and $d\bar{B}$ from zero to H , respectively. Finally, it is found that

$$\begin{aligned}\bar{E}(D, HA, t) = & \frac{1}{4\pi\epsilon_0} \left[\int_0^H \frac{3D(HA-z)}{R_R^5} \int_0^t i(z, \tau-R_R/c) d\tau dz \right. \\ & + \int_0^{-H} \frac{3D(HA+z_I)}{R_I^5} \int_0^t i(-z_I, \tau-R_I/c) d\tau dz_I \\ & + \int_0^H \frac{3D(HA-z)}{cR_R^4} i(z, t-R_R/c) dz \\ & + \int_0^{-H} \frac{3D(z+z_I)}{cR_I^4} i(-z_I, t-R_I/c) dz_I \\ & + \int_0^H \frac{D(HA-z)}{c^2 R_R^3} \frac{\partial}{\partial t} i(z, t-R_R/c) dz \\ & \left. + \int_0^{-H} \frac{D(HA+z_I)}{c^2 R_I^3} \frac{\partial}{\partial t} i(-z_I, t-R_I/c) dz_I \right] \hat{a}_R\end{aligned}$$

$$\begin{aligned}
& + \frac{1}{4\pi\epsilon_0} \left[\int_0^H \frac{2(HA-z)^2 - D^2}{R_R^5} \int_0^t i(z, \tau - R_R/c) d\tau dz \right. \\
& + \int_0^{-H} \frac{2(HA+z_I)^2 - D^2}{R_I^5} \int_0^t i(-z_I, \tau - R_I/c) d\tau dz_I \\
& + \int_0^H \frac{2(HA-z)^2 - D^2}{cR_R^4} i(z, t - R_R/c) dz \\
& + \int_0^{-H} \frac{2(HA+z_I)^2 - D^2}{cR_I^3} i(-z_I, t - R_I/c) dz_I \\
& - \int_0^H \frac{D^2}{c^2 R_R^3} \frac{\partial}{\partial t} i(z, t - R_R/c) dz \\
& \left. - \int_0^{-H} \frac{D^2}{c^2 R_I^3} \frac{\partial}{\partial t} i(-z_I, t - R_I/c) dz_I \right] \hat{a}_z \quad (39)
\end{aligned}$$

and

$$\begin{aligned}
\bar{B}(D, HA, t) = & \frac{\mu_0}{4\pi} \left[\int_0^H \frac{D}{R_R^3} i(z, \tau - R_R/c) dz \right. \\
& + \int_0^{-H} \frac{D}{R_I^3} i(-z_I, \tau - R_I/c) dz_I \\
& + \int_0^H \frac{D}{cR_R^2} \frac{\partial}{\partial t} i(z, t - R_R/c) dz \\
& \left. + \int_0^{-H} \frac{D}{cR_I^2} \frac{\partial}{\partial t} i(-z_I, t - R_I/c) dz_I \right] \hat{a}_\phi \quad (40)
\end{aligned}$$

$$\text{where } R_R = (D^2 + (HA - z)^2)^{1/2}$$

$$\text{and } R_I = (D^2 + (HA + z)^2)^{1/2}$$

Just as was seen in the \bar{E} and \bar{B} equations for ground point calculations, the electric field has an electrostatic term, an induction term, and a radiation term in both the vertical and horizontal directions. Obviously, since it is the same equation, the magnetic field still has an induction term and a radiation term in the ϕ -direction. The characteristics of these terms as discussed in the previous section still hold.

IV. Models

As was mentioned in Chapter I, this thesis investigates three models of the current in the lightning channel. They are:

1. $i(z,t) = I_0[\exp(-\alpha t) - \exp(-\beta t)]$
2. $i(z,t) = I_0[\exp(-\alpha(t-z/v)) - \exp(-\beta(t-z/v))]$
3. $i(z,t) = I_0[\exp(-\alpha(t-z/v)) - \exp(-\beta(t-z/v))]$
 $\exp(-z/\lambda)$

The first model is called the Bruce-Golde (BG) model. It was first proposed by Bruce and Golde in 1941. It consists of a uniform current that propagates up the channel. This uniform current has a time-dependent decay factor (in the form of a double-exponential) applied to it. The BG model can be thought of as returning charge stored in the corona envelope surrounding the lightning channel to ground (Golde, 1977:331; Lin et al., 1980). Figure 4.1 pictorially displays this model.

An advantage of the BG model is that its simplicity provides easy calculations of the EM fields. A disadvantage of the BG model is that it is physically untenable because it has a discontinuity at the leading edge of the current. Also, the time-dependent decay results in the current channel between the leading edge and the ground changing uniformly and equivalently throughout. This

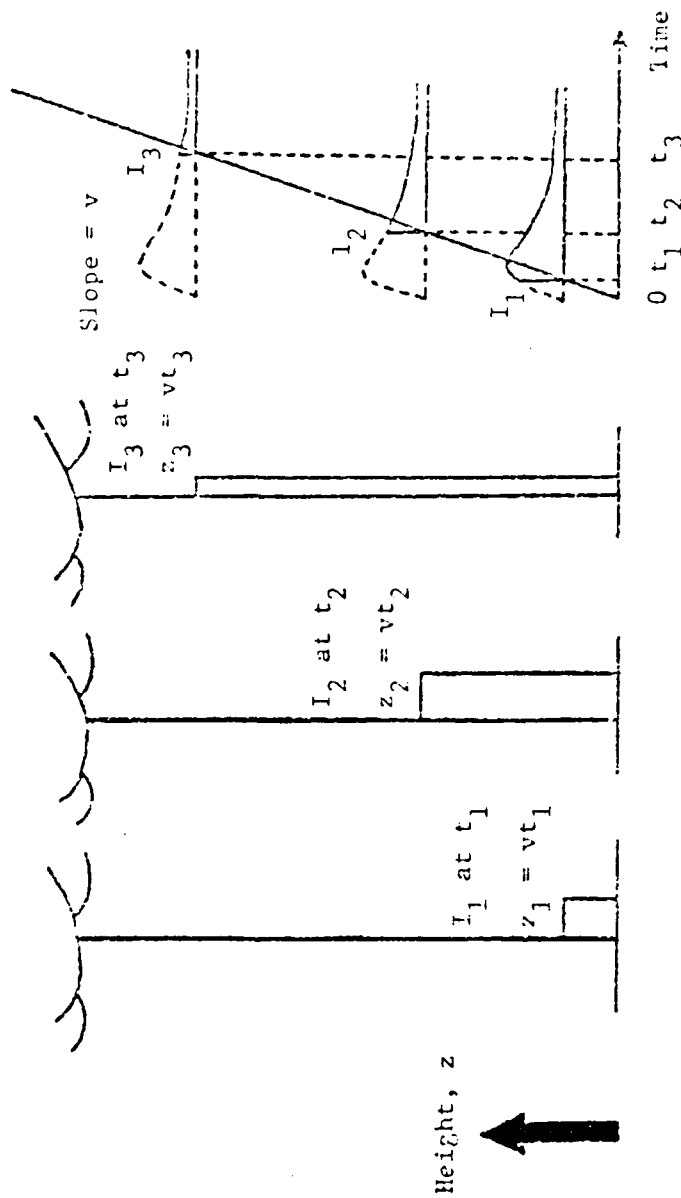


Fig. 4.1. Illustration of the Current Distribution of the Bruce-Golde Model (Model 1) (Lin, 1978:106).

means the channel must be able to instantaneously transfer charge from any point along the channel to ground.

Another disadvantage to the BG model is that the velocities and peak currents it predicts seem to be distant dependent (Lin, 1978:128; Lin et al., 1980).

The second model was first proposed by Uman and McLain in 1969. Uman and McLain's model is commonly known as the transmission line model because the negative z/v factors in the exponentials cause the pulse to propagate up the lightning channel as it would up a transmission line. (Uman and McLain used a non-exponential pulse in their model, but in this paper the pulse will be modeled as a double-exponential.) The current in this model does not represent a removal of charge from the corona; rather, it represents an impulse-like current due to the atmospheric breakdown between the end of the leader and the start of the return stroke. Figure 4.2 shows the current representation in this model.

The advantage to the transmission line model is that it is more physically reasonable than the BG model; there is not any discontinuity of the current at the leading edge nor are there any instantaneous charge transfers through the channel. Another advantage of the transmission line model is that it provides easy analytical computation of the EM fields relative to more recent models (i.e., Lin's model, 1978).

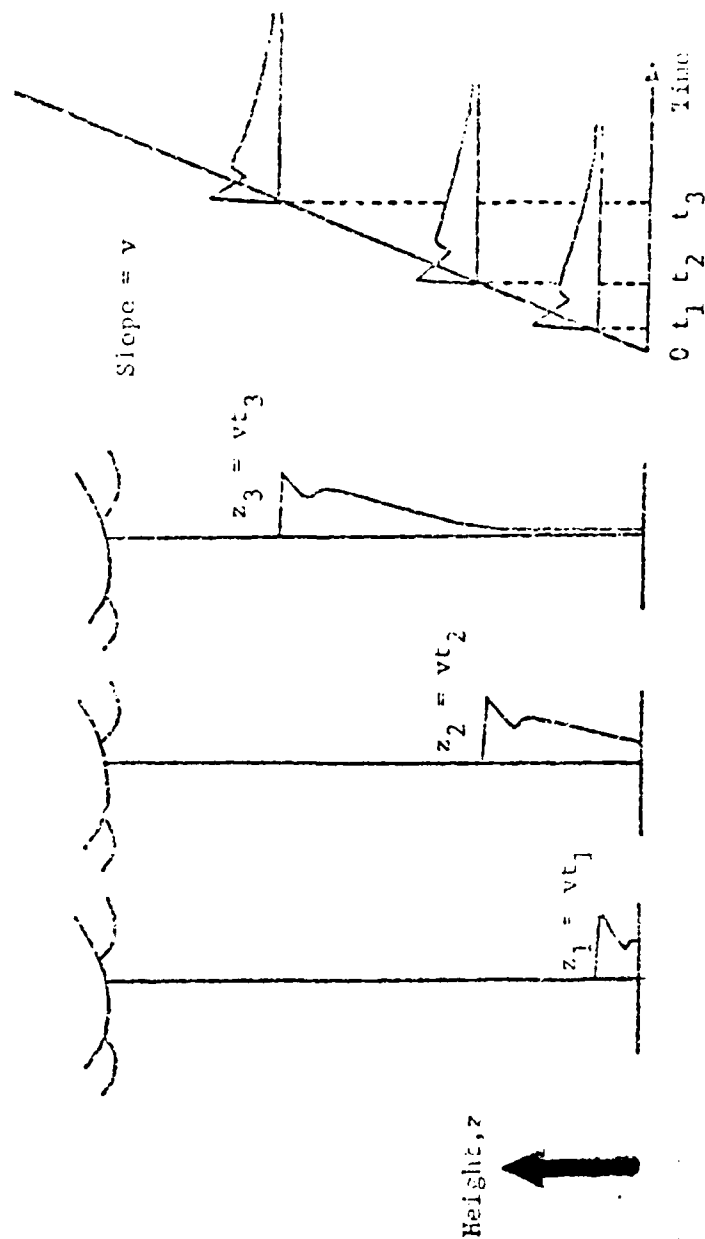


Fig. 4.2. Illustration of the Current Distribution of the Transmission Line Model (Model 2) (Lin, 1978:106).

Lin (1978) showed that a primary disadvantage to Uman and McLain's model is that it requires the propagating pulse to have a much shorter duration than direct measurements showed to be the case (Lin, 1978:128). Another disadvantage of the transmission line model is that it predicts peak currents generally greater than 30 kA and often as high as 50 to 100 kA; however, direct measurement shows the peak current to be usually on the order of 10 kA (Lin et al., 1980). Yet another disadvantage of this model is that for far-fields, it predicts the occurrence of a "mirror image" effect that rarely occurs in the data (Master et al., 1981).

The third model is the same as the second model, but the breakdown pulse undergoes attenuation as it propagates upward through the channel. The reason for adding this attenuation is twofold: (1) In 1980, Jordan and Uman showed that the channel luminosity (and hence, by implication, the current) decreased with height. (2) Allowing the breakdown pulse to attenuate to a negligible value when it reaches the top of the channel should greatly reduce the undesirable "mirror image" effect (Master et al., 1981).

Because the pulse current is modeled as a double-exponential, the current function in the third model becomes very close to the corona current that Lin uses in his model (explained below). The differences are that in the third model in their thesis the time constants in the double-

exponential (1 and 2) are such that a much faster rise and fall time occurs and that the corona current in Lin's model (and the BG model) does not propagate (no z/v factors in the exponentials).

The advantage to this model is that it is somewhat more physically realistic as outlined above; essentially, the transmission line is now no longer lossless.

As mentioned in Chapter I, one model has been analytically examined at altitude. That model is a modified form of Lin's model. Lin's model consists of three currents:

1. breakdown pulse current,
2. uniform current, and
3. corona current that "turns on" after the peak

of the breakdown pulse current has passed (Lin, 1978). Originally, the breakdown pulse current did not undergo any attenuation. In this fourth model, however, the breakdown pulse current is attenuated as it is in the third model (Master et al., 1981). Fig. 4.3 pictorially represents Lin's model.

The advantage to Lin's model is that it has been shown (Lin, 1978) to more closely predict the EM fields than the BG or transmission line models. The disadvantage is that it is much more analytically complicated to predict the EM fields with this model.

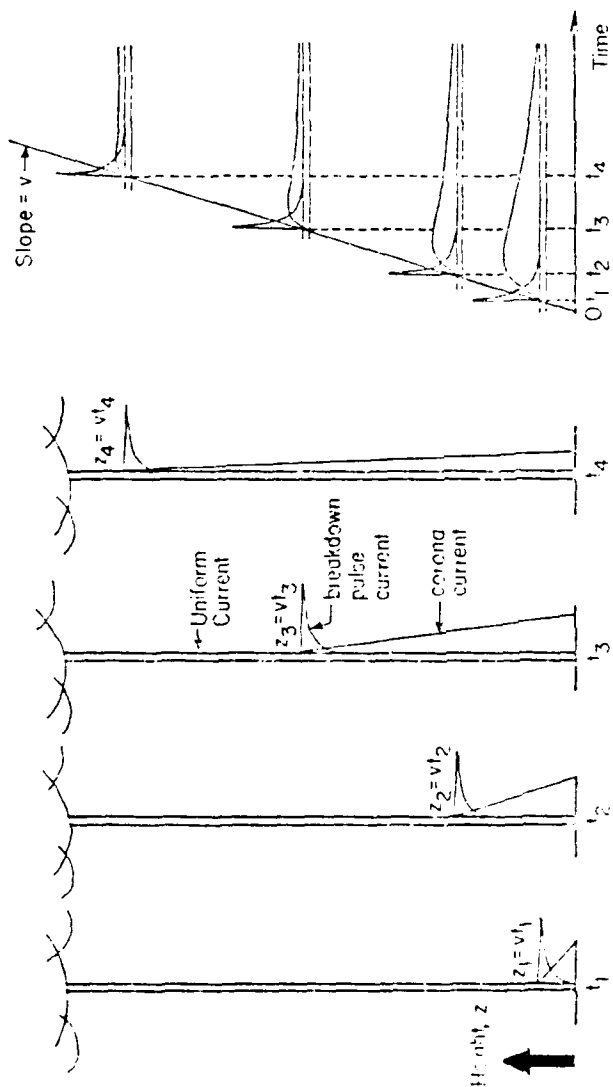


Fig. 4.3. Illustration of the Current Distribution of the Lin Model (Master et al., 1981).

Looking at the above models, one notices that there are generally three physical characteristics of the lightning being taken into account in the form of currents. These three currents are:

1. current due to the atmospheric breakdown, having an impulse-like structure, I_p ;
2. constant uniform current due to the leader, I_e ;
and
3. current due to the charges stored in the corona envelope going to ground, I_c .

Also, the currents have three types of attenuation or decay:

1. no attenuation or decay (e.g., the second model);
2. height-dependent attenuation [$\exp(-z/\lambda)$]
(e.g., the pulse current in the third and fourth models);
and
3. time-dependent decay [$\exp(-\alpha t) - \exp(-\beta t)$]
(e.g., the corona current in the first and fourth models).

The first and second models have been analyzed and compared only at ground level. The third model has never before been analyzed or compared with data. The fourth model has been analyzed at altitude (Master et al., 1981) but has yet to be compared to any real data.

V. Analysis

Theoretical

In the theoretical analysis, computer solutions to Equations (39) and (40) for each of the three models were found. Figures 5.1 through 5.36 are the electric field predictions and the units on the vertical scale for all of them is volts per meter. Figures 5.37 through 5.72 are the magnetic field predictions with units of webers per square meter on the vertical scale.

For each model, the rise and fall time for the pulse or double exponential was varied. Each model was analyzed for the following rise and fall times:

1. 500 nsec rise time, 10 μ sec fall time
2. 1 μ sec rise time, 25 μ sec fall time
3. 2 μ sec rise time, 50 μ sec fall time

For each rise and fall time, the distance was varied. The distances selected were one kilometer, five kilometers, ten kilometers, and one hundred kilometers.

Finally, at each distance, the fields were calculated at ground level, fifteen hundred feet, five thousand feet, eight thousand feet, fifteen thousand feet, and thirty thousand feet. All six altitudes for each distance are in one figure. The top left graph in each figure represents

ground level; the center left graph represents fifteen hundred feet; the bottom left graph represents five thousand feet; the top right graph represents eight thousand feet; the center right graph represents fifteen thousand feet; the bottom right graph represents thirty thousand feet.

The distances and altitudes used were chosen to correspond with both experimental data (taken in August 1981) and with the predictions by Master (Master et al., 1981).

Table 5.1 shows the breakdown of the electric and magnetic field figures for the various parameters.

In any of the plots, the radiation term predominates at the start. This is because the fast rise time of the current yields a large positive value for its derivative with respect to time.

The initial radiation effect in the first model is generally shorter in duration and magnitude than in the second and third models. This is due to the pulse not propagating in the first model. Initially, the radiation term predominates because of the fast rise time of the current; however, the derivative is at its maximum at the beginning and immediately starts dropping off, eventually going to zero. As the radiation term drops off, the induction term (and the electrostatic term in the electric field) is getting larger. In the first model, the current is represented by a propagating uniform current that

TABLE 5.1
LOCATION OF THE ELECTRIC AND MAGNETIC FIELD FIGURES
FOR THE VARIOUS PARAMETERS

Model	Rise/Fall	Distance	Electric Field Figure	Magnetic Field Figure
1	500 nsec/ 10 μ sec	1	5.1	5.37
		5	5.2	5.38
		10	5.3	5.39
		100	5.4	5.40
	1 μ sec/25 μ sec	1	5.5	5.41
		5	5.6	5.42
		10	5.7	5.43
		100	5.8	5.44
	2 μ sec/50 μ sec	1	5.9	5.45
		5	5.10	5.46
		10	5.11	5.47
		100	5.12	5.48
2	500 nsec/10 μ sec	1	5.13	5.49
		5	5.14	5.50
		10	5.15	5.51
		100	5.16	5.52
	1 μ sec/25 μ sec	1	5.17	5.53
		5	5.18	5.54
		10	5.19	5.55
		100	5.20	5.56

TABLE 5.1--Continued

Model	Rise/Fall	Distance	Electric Field Figure	Magnetic Field Figure
2	2 μ sec/50 μ sec	1	5.21	5.57
		5	5.22	5.58
		10	5.23	5.59
		100	5.24	5.60
3	500 nsec/10 μ sec	1	5.25	5.61
		5	5.26	5.62
		10	5.27	5.63
		100	5.28	5.64
	1 μ sec/25 μ sec	1	5.29	5.65
		5	5.30	5.66
		10	5.31	5.67
		100	5.32	5.68
	2 μ sec/50 μ sec	1	5.33	5.69
		5	5.34	5.70
		10	5.35	5.71
		100	5.36	5.72

changes amplitude according to a double exponential; nowhere along the channel at any instant of time can this double exponential shape be seen (and hence, the rise time). In the second and third models, however, the double exponential shape is always seen along the channel (until it reaches the top) since these two models use a propagating pulse. Consequently, integrating from the ground to the height of the return stroke at any instant of time would not include the fast rise time in the first model whereas it would be included in the second and third models.

The difference between the second and third models is that the initial peak or effect of the radiation term is slightly less in the third model because of the height dependent attenuation ($e^{-z/\lambda}$). In the first few hundred nanoseconds during which the radiation term predominates, the pulse has not propagated very far up the channel and consequently the attenuation has little although noticeable effect at this point.

In the work done by Master et al. using the fourth model (Master et al., 1981), it was seen that attenuating the breakdown pulse did not much affect the fields on the ground at all distances and the fields at all attitudes beyond ten kilometers. This was due to the radiation term predominating the initial portion of the fields while the pulse is near the ground and not having much attenuation. Latter portions of the fields are due to the uniform and

corona currents which did not change from Lin's original model (Master et al., 1981).

In comparing the second and third models, it is seen that there is quite a difference between the two models at all distances and all altitudes. This would be due to there being no uniform and corona currents to predominate later portions of the fields.

Another difference between the two models is that the third model has essentially gotten rid of the undesired "mirror image" effect. This is due to the pulse having been greatly attenuated by the time it reached the top of the channel.

Looking at Figures 5.1 through 5.72, it is seen that the positive portions of the electric field decrease while the negative portions increase. This is especially true in the second and third models. Eventually, above a certain altitude (higher with increasing distance), the field becomes essentially totally negative. This is apparently due to more of the channel lying below the local horizon of the observation point.

In the plots of the electric and magnetic fields predicted by the second and third models, it is seen that at a given distance as altitude increases, the maximum magnitude increases while at the same time the field becomes more and more impulsive. This could be due to a decrease in the effect of the radiation term due to the time

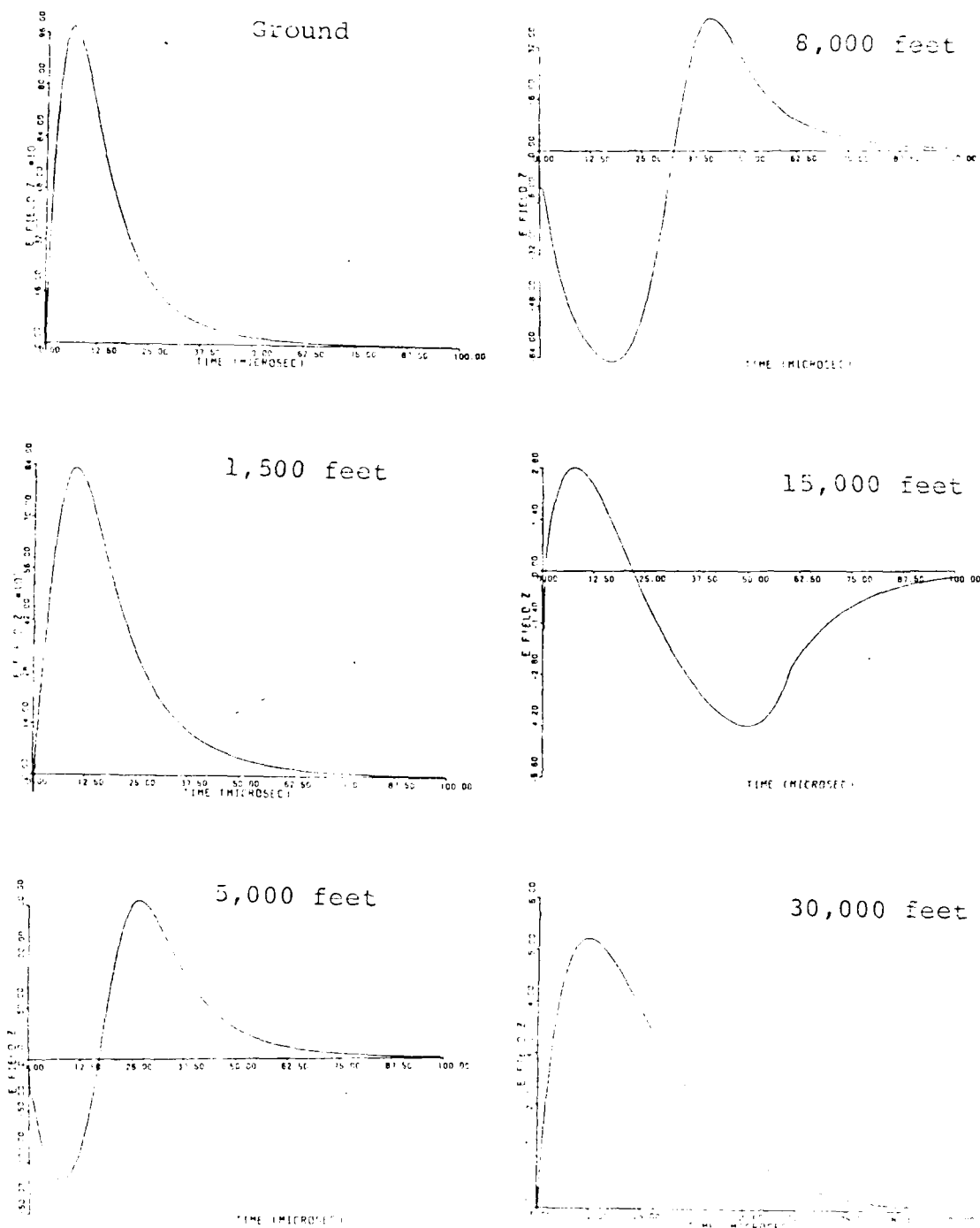


Fig. 5.1. Computer Solutions to Equation (39), the Electric Field, According to Model 1 at a Distance of 1 km, 500 nsec rise time, and 10 μ sec fall time, for the ground and at five altitudes.

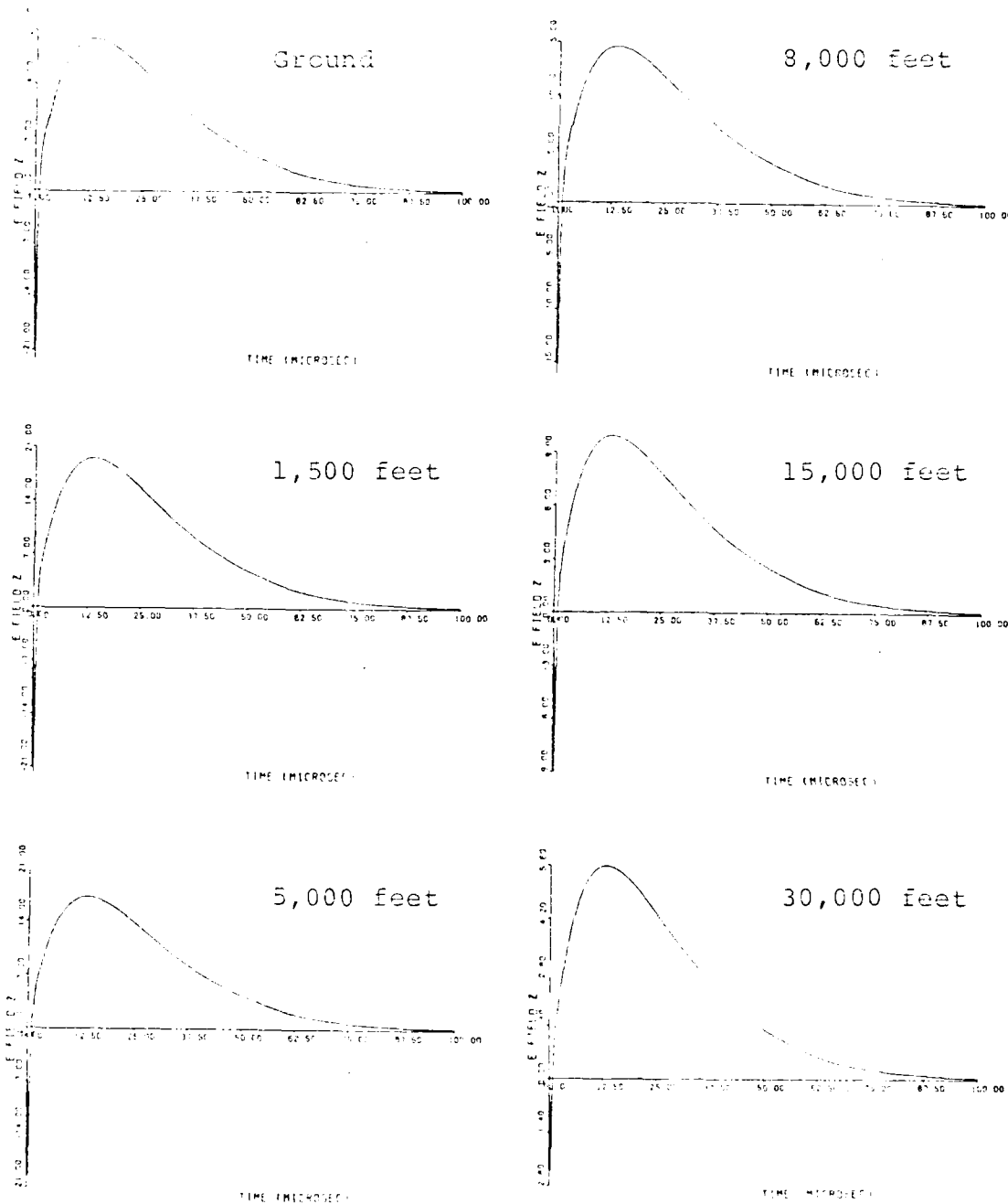


Fig. 5.2. Computer Solutions to Equation (39) the Electric Field, According to Model 1 at a Distance of 5 km, 500 nsec Rise Time, and 10 μ sec Fall Time, for the Ground and at Five Altitudes.

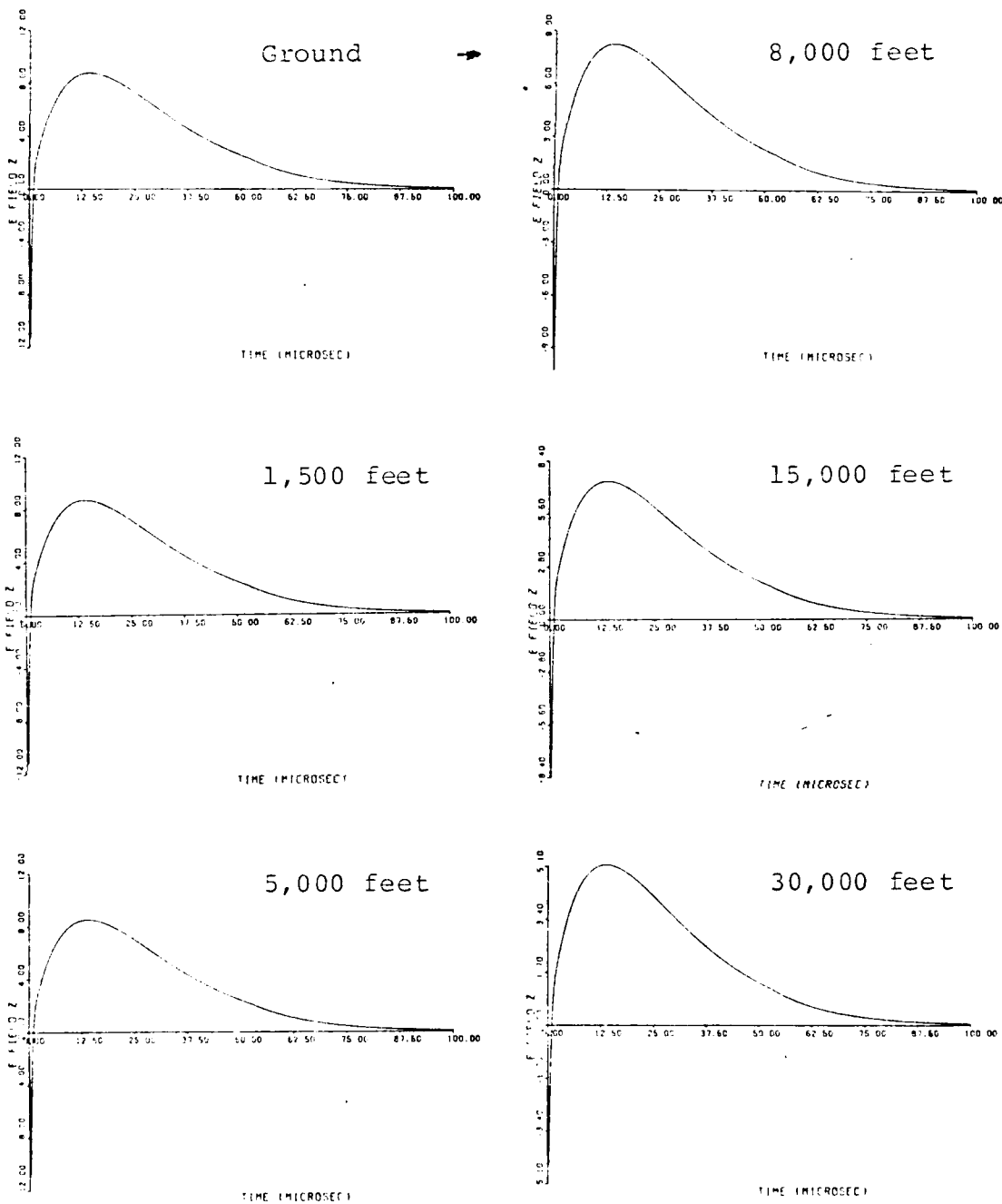


Fig. 5.3. Computer Solutions to Equation (39), the Electric Field, According to Model 1 at a Distance of 10 km, 500 nsec Rise Time, and 10 μ sec Fall Time for the Ground and at Five Altitudes.

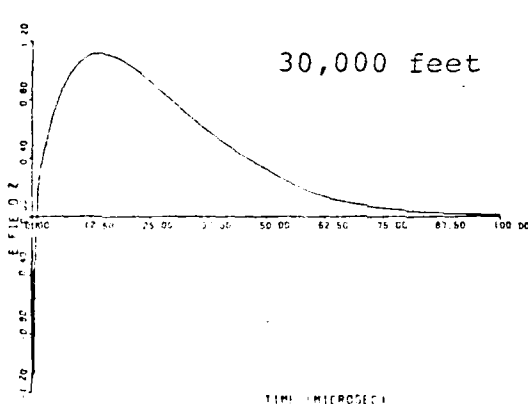
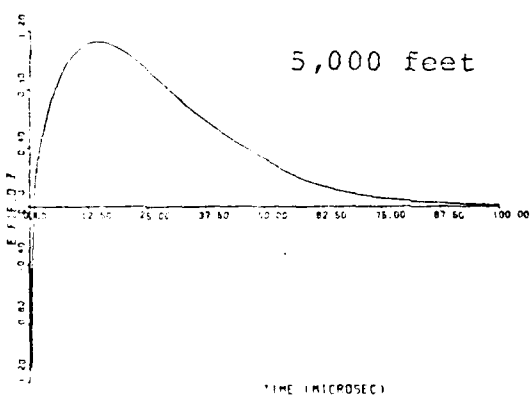
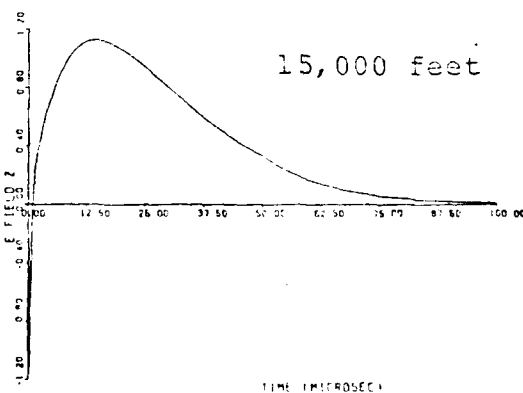
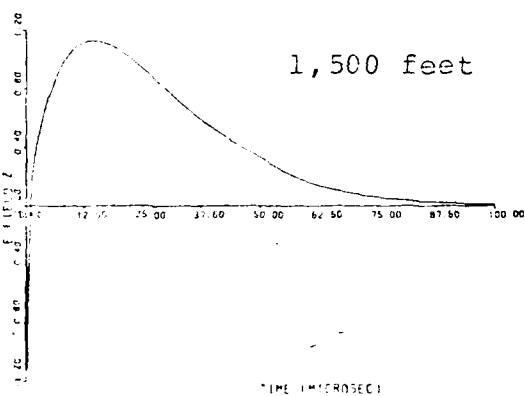
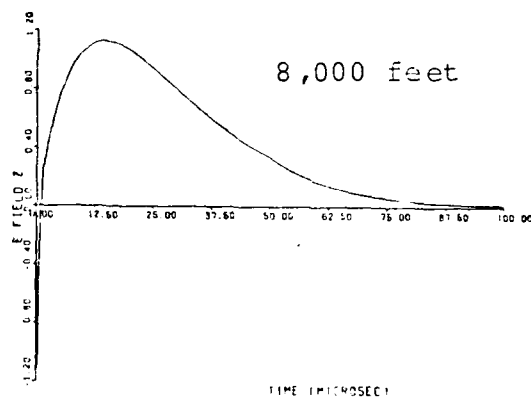
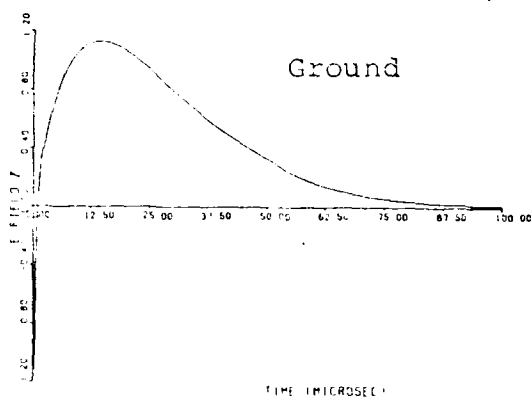


Fig. 5.4. Computer Solutions to Equation (39), the Electric Field, According to Model 1 at a Distance of 100 km, 500 nsec Rise Time, and 10 μ sec Fall Time, for the Ground and at Five Altitudes.

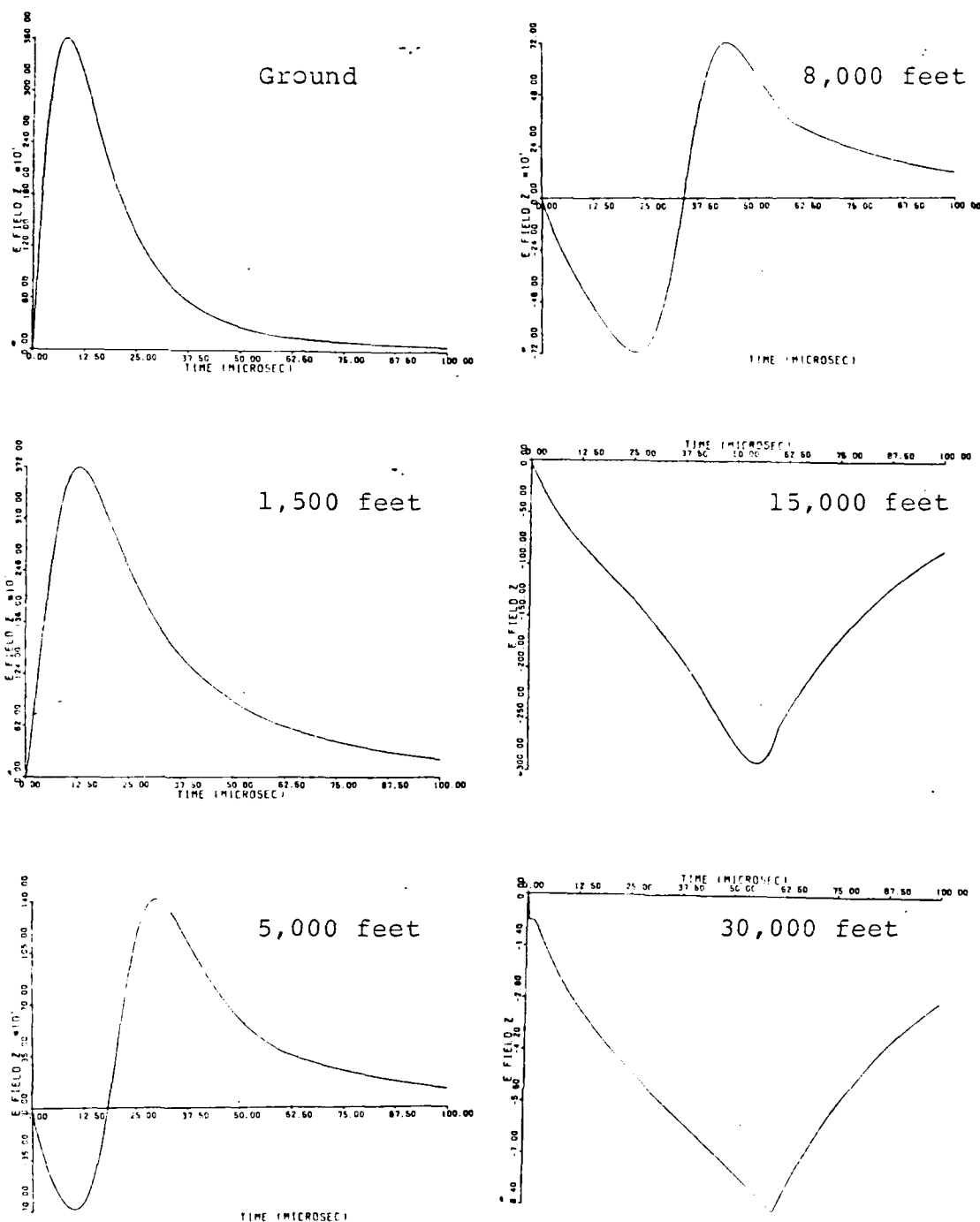


Fig. 5.5. Computer Solutions to Equation (39), the Electric Field, According to Model 1 at a Distance of 1 km, 1 usec Rise Time, and 25 usec Fall Time, for the Ground and at Five Altitudes.

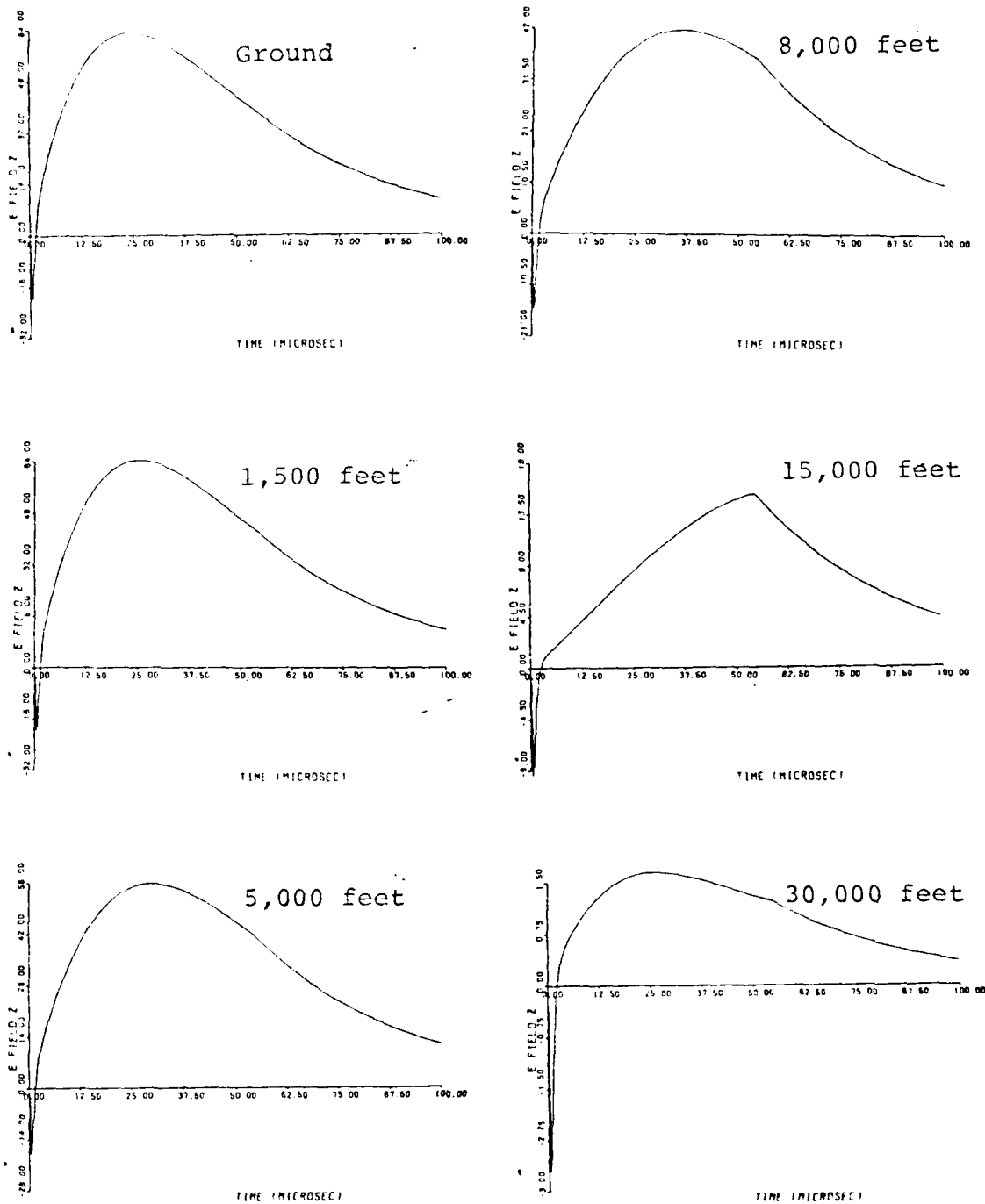


Fig. 5.6. Computer Solutions to Equation (39), the Electric Field, According to Model 1 at a Distance of 5 km, 1 μ sec Rise Time, and 25 μ sec Fall Time, for the Ground and at Five Altitudes.

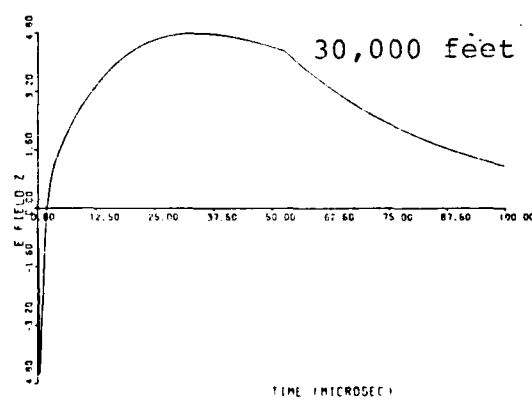
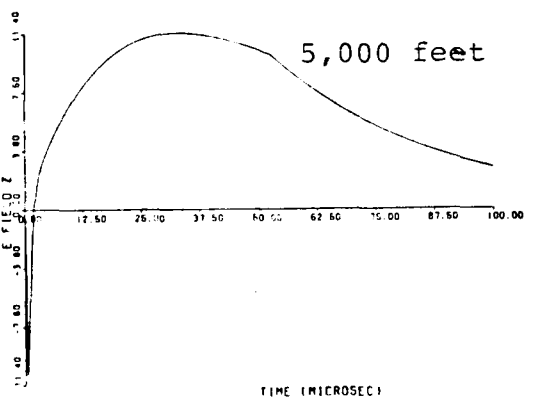
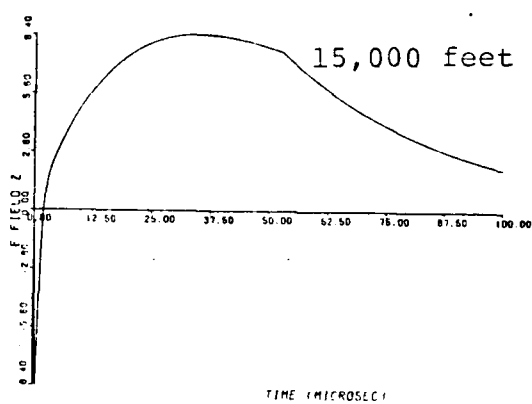
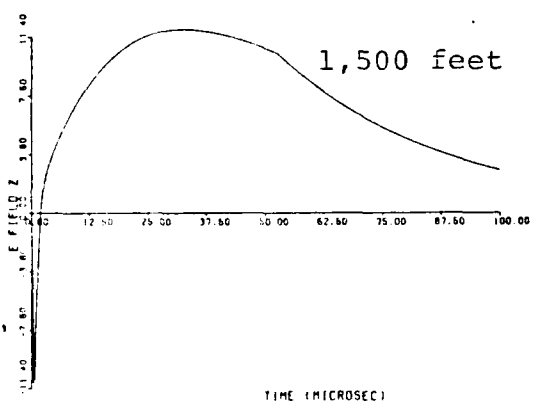
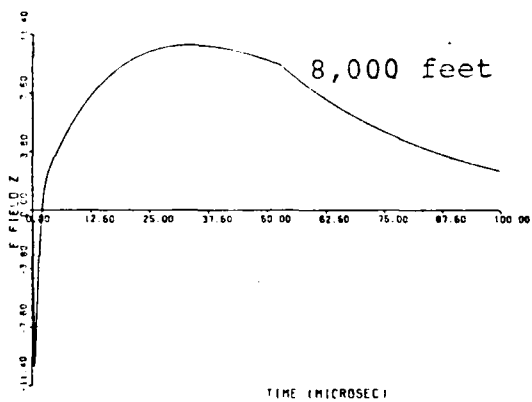
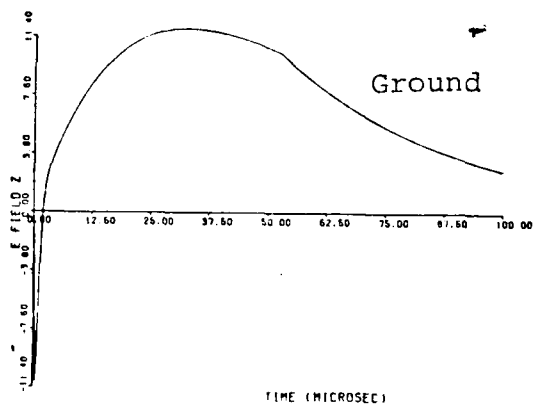


Fig. 5.7. Computer Solutions to Equation (39), the Electric Field, According to Model 1 at a Distance of 10 km, 1 μ sec Rise Time, and 25 μ sec Fall Time, for the Ground and at Five Altitudes.

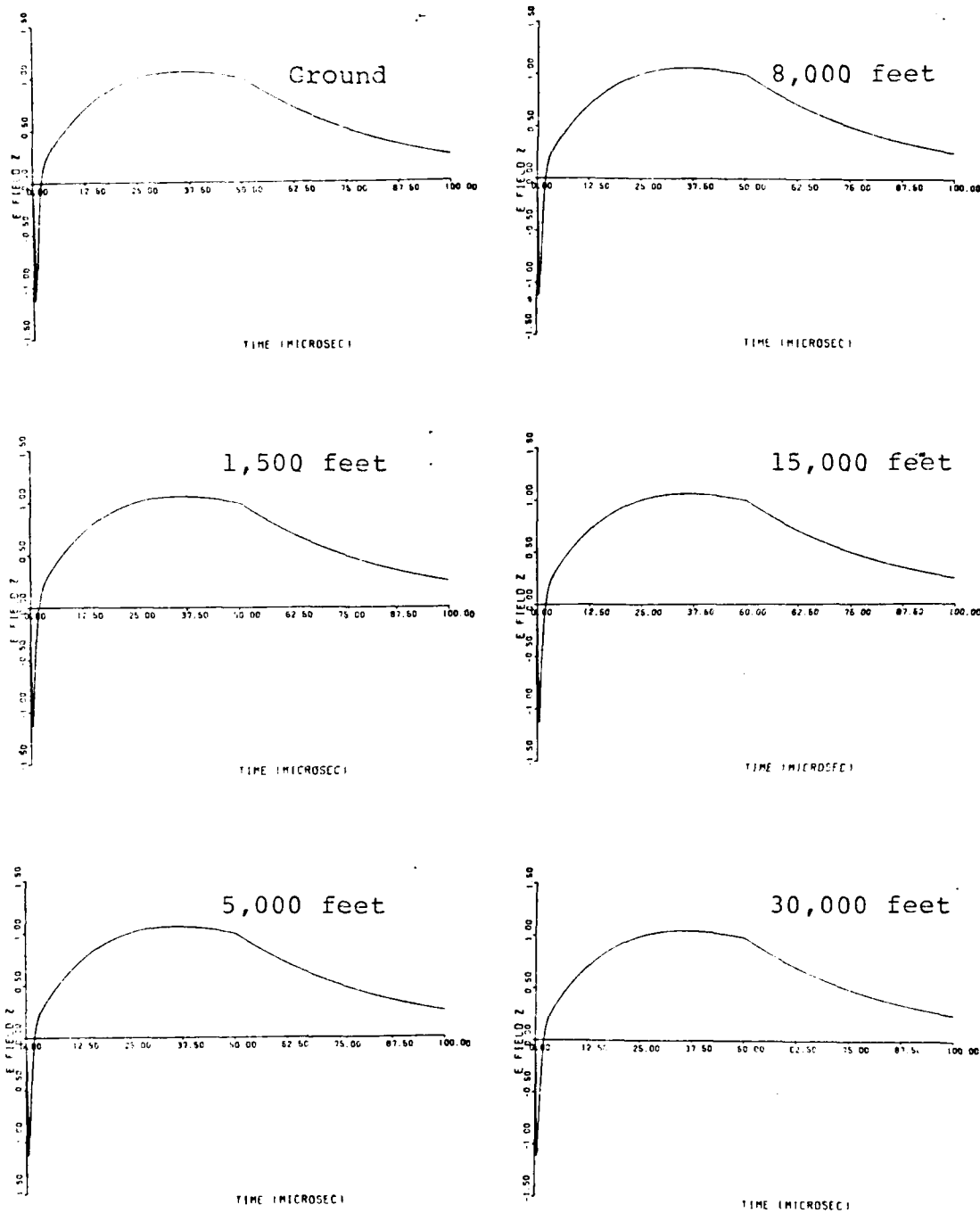


Fig. 5.8. Computer Solutions to Equation (39), the Electric Field, According to Model 1 at a Distance of 100 km, 1 μ sec Rise Time, and 25 μ sec Fall Time, for the Ground and at Five Altitudes.

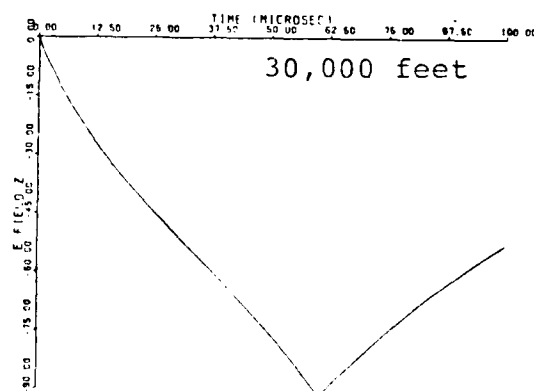
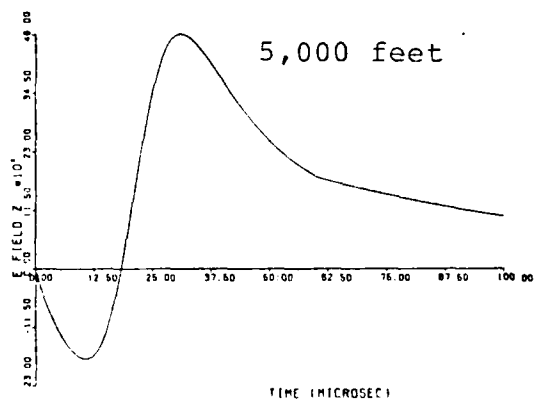
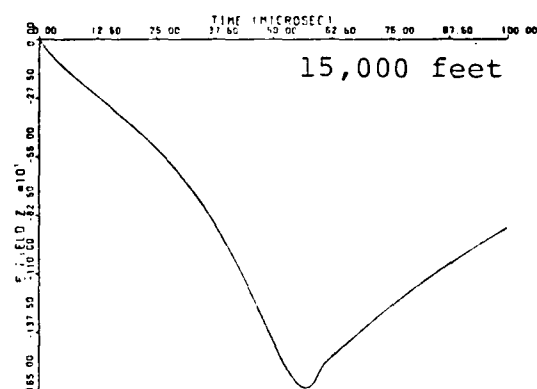
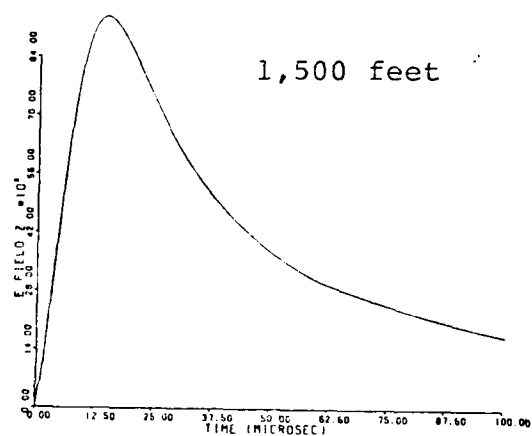
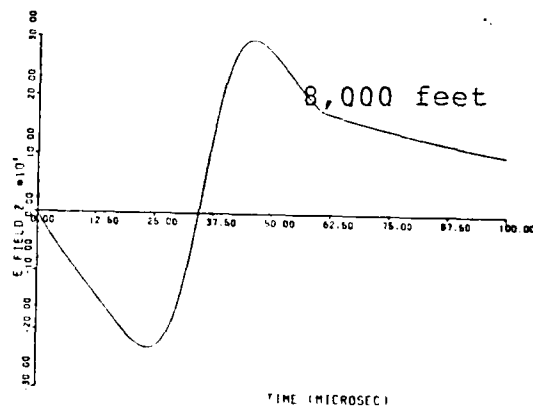
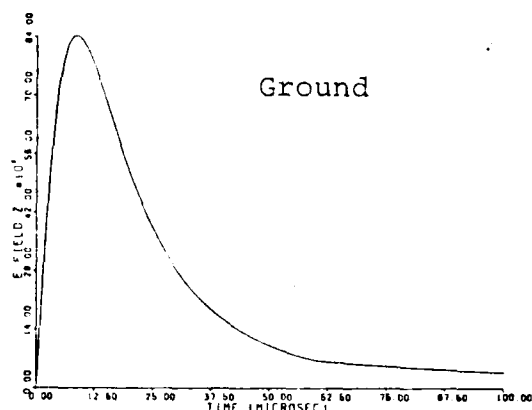


Fig. 5.9. Computer Solutions to Equation (39), the Electric Field, According to Model 1 at a Distance of 1 km, 2 μ sec Rise Time, and 50 μ sec Fall Time, for the Ground and at Five Altitudes.

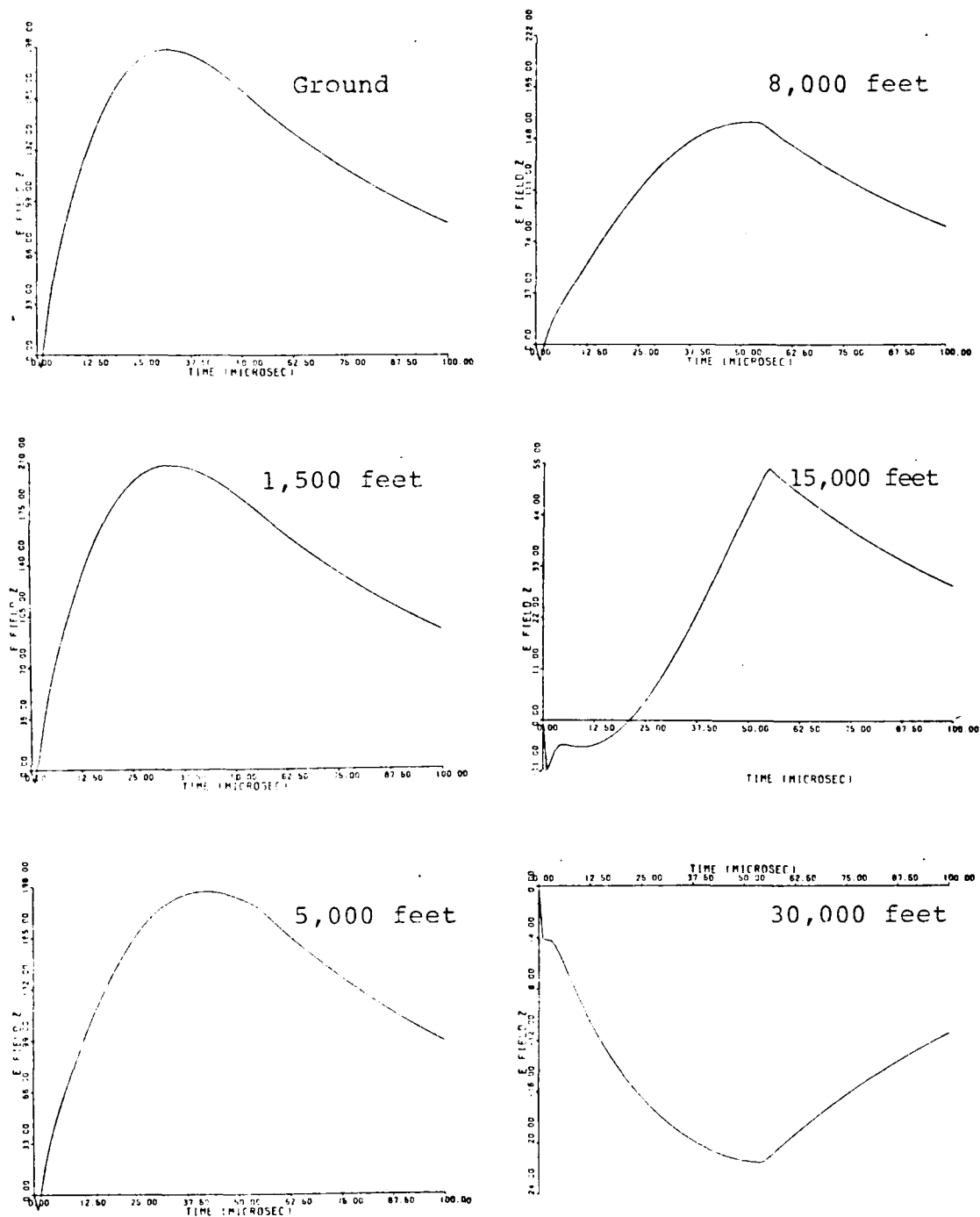


Fig. 5.10. Computer Solutions to Equation (39), the Electric Field, According to Model 1 at a Distance of 5 km, 2 μ sec Rise Time, and 50 μ sec Fall Time, for the Ground and at Five Altitudes.

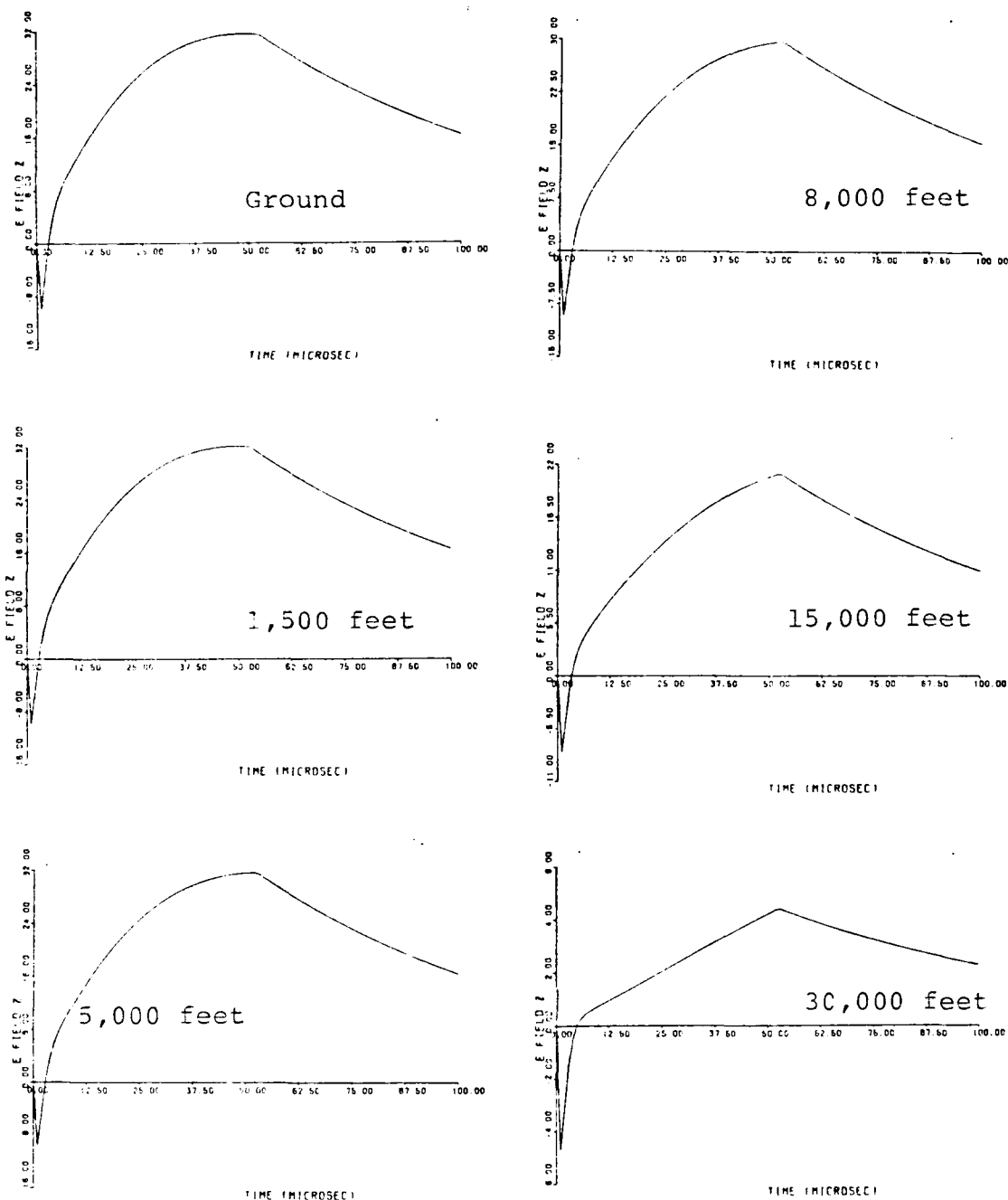


Fig. 5.11. Computer Solutions to Equation (39), the Electric Field, According to Model 1 at a Distance of 10 km, 2 μ sec Rise Time, and 50 μ sec Fall Time, for the Ground and at Five Altitudes.

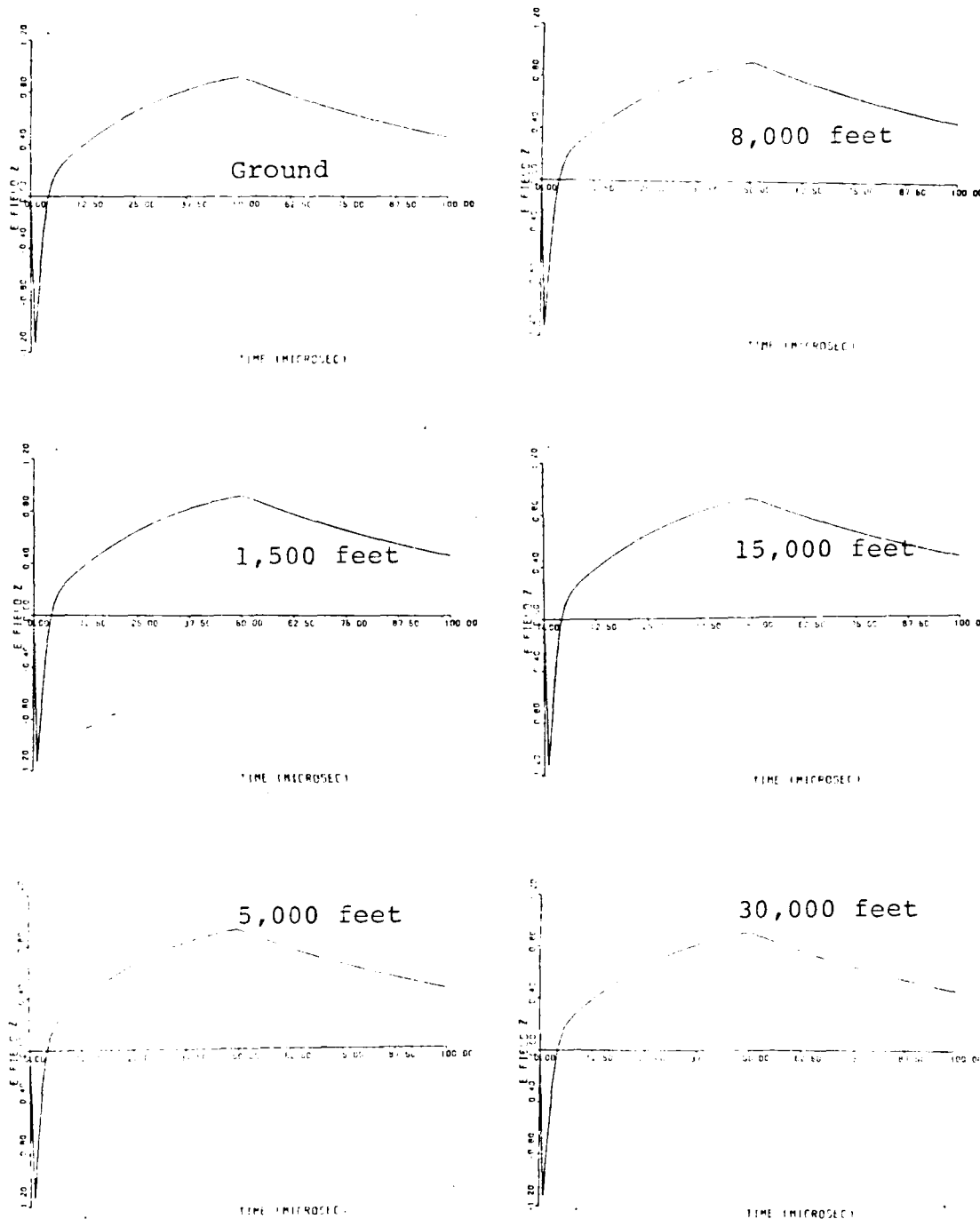


Fig. 5.12. Computer Solutions to Equation (39), the Electric Field, According to Model 1 at a Distance of 100 km, 2 μ sec Rise Time, and 50 μ sec Fall Time, for the Ground and at Five Altitudes.

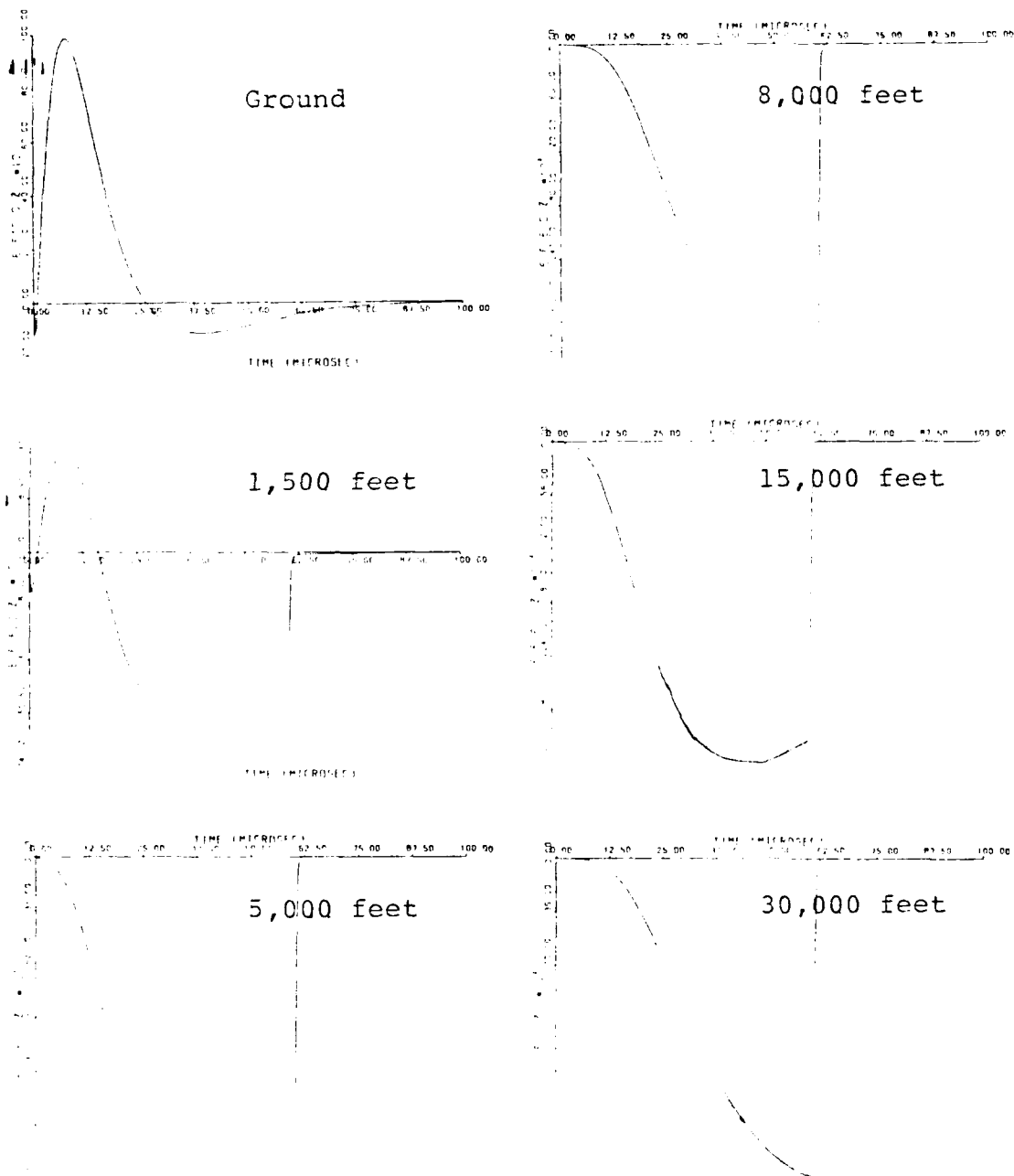


Fig. 5.13. Computer Solutions to Equation (39), the Electric Field, According to Model 2 at a Distance of 1 km, 500 nsec Rise Time, and 10 nsec Fall Time, for the Ground and at Five Altitudes.

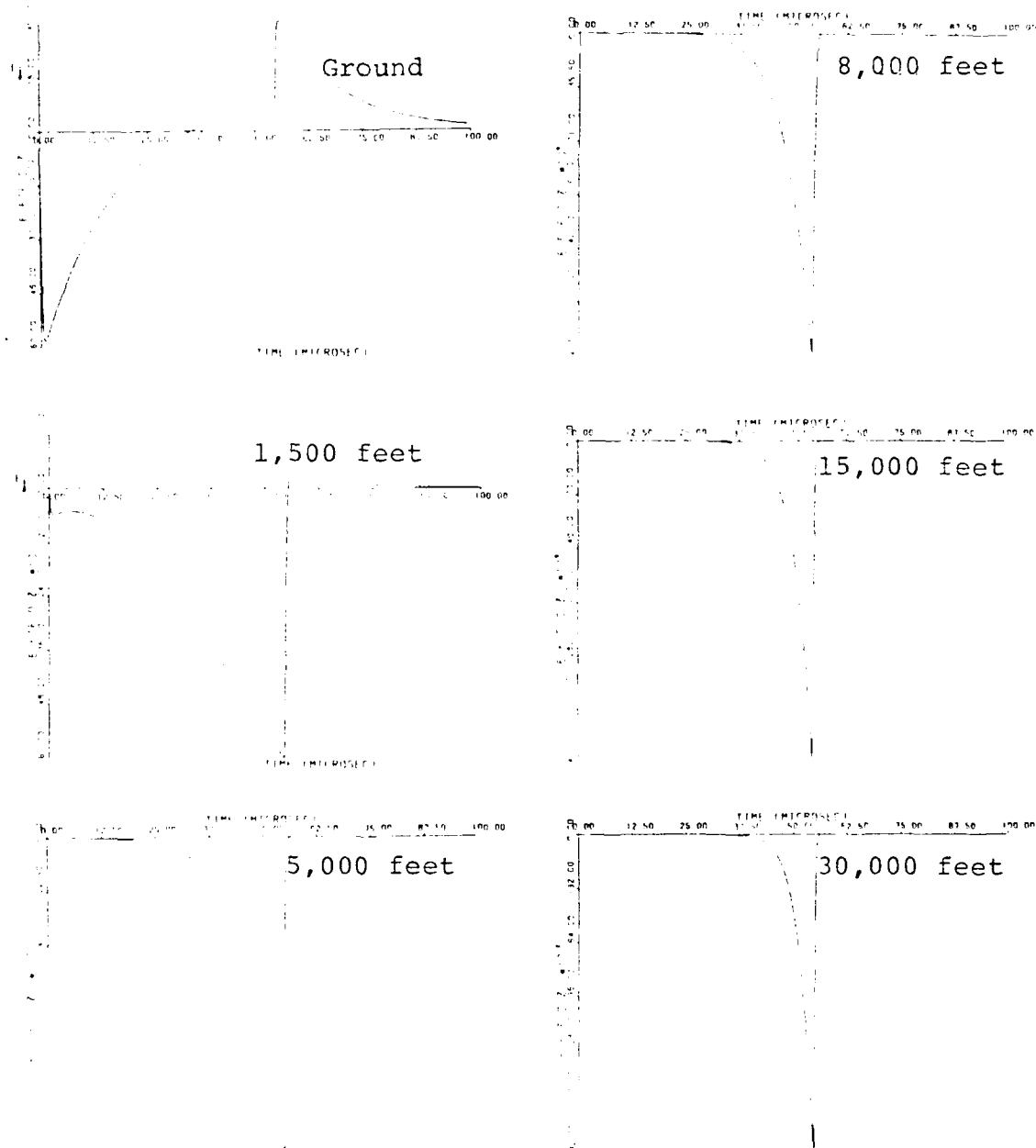


Fig. 5.14. Computer Solutions to Equation (39), the Electric Field, According to Model 2 at a Distance of 5 km, 500 nsec Rise Time, and 10 μsec Fall Time, for the Ground and at Five Altitudes.

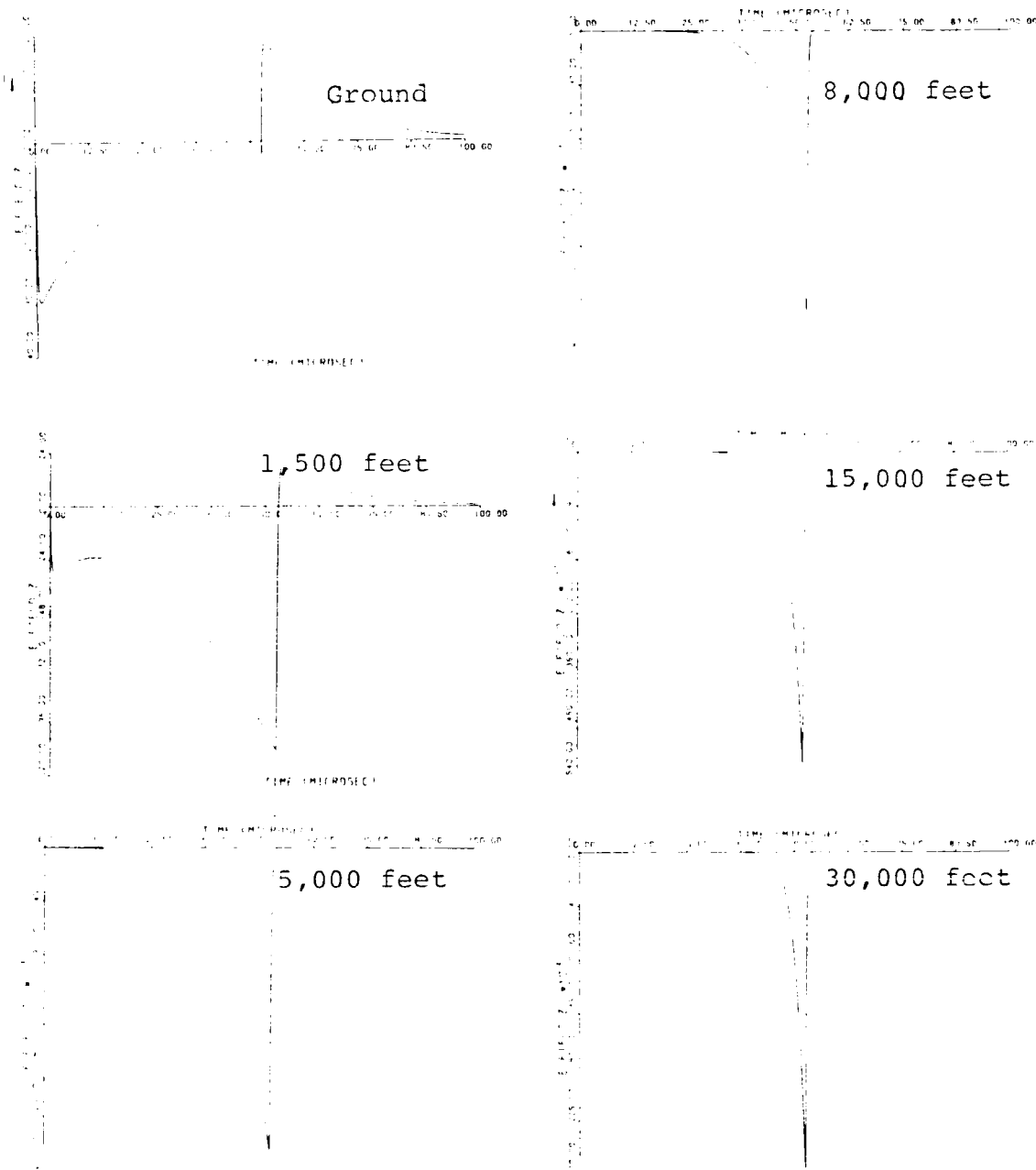


Fig. 5.15. Computer Solutions to Equation (39), the Electric Field, According to Model 2 at a Distance of 10 km, 500 nsec Rise Time, and 10 nsec Fall Time, for the Ground and at Five Altitudes.

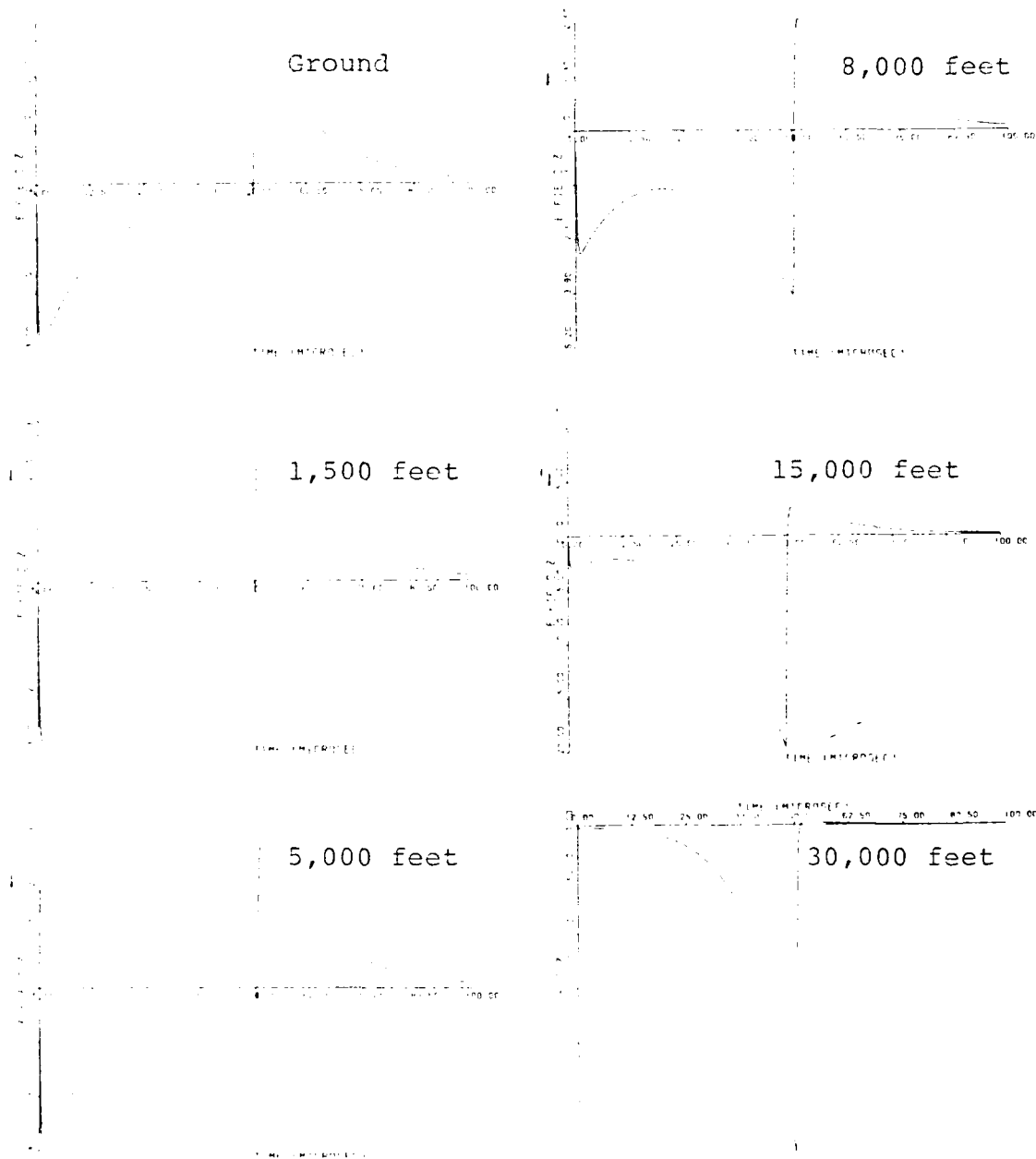


Fig. 5.16. Computer Solutions to Equation (39), the Electric Field, According to Model 2 at a Distance of 100 km, 500 nsec Rise Time, and 10 nsec Fall Time, for the Ground and at Five Altitudes.

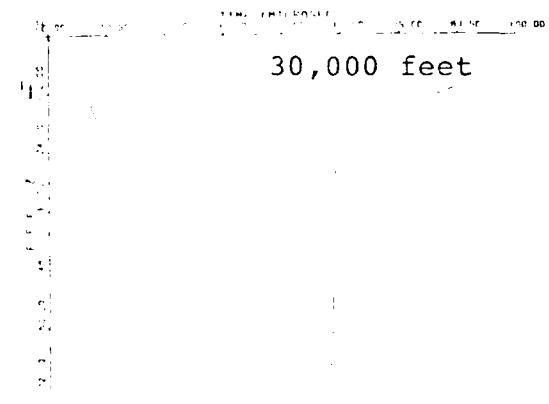
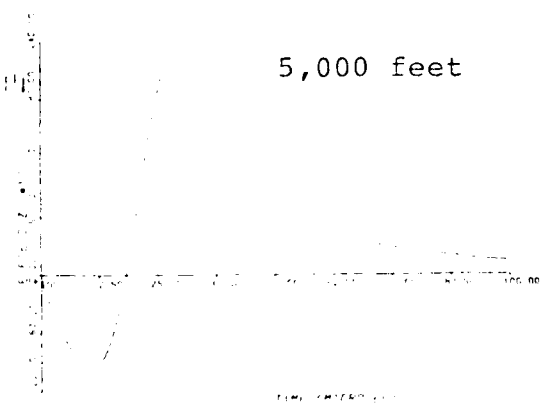
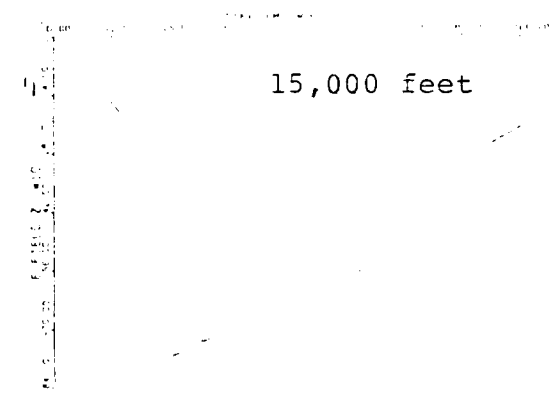
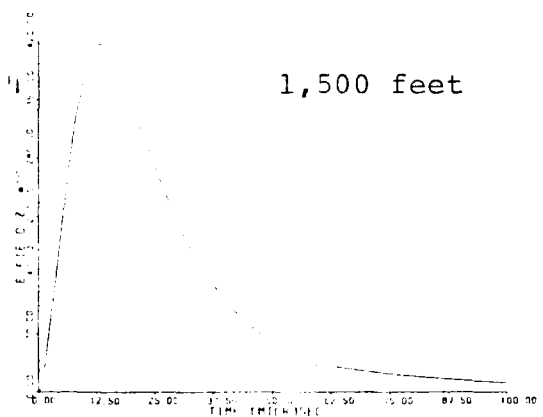
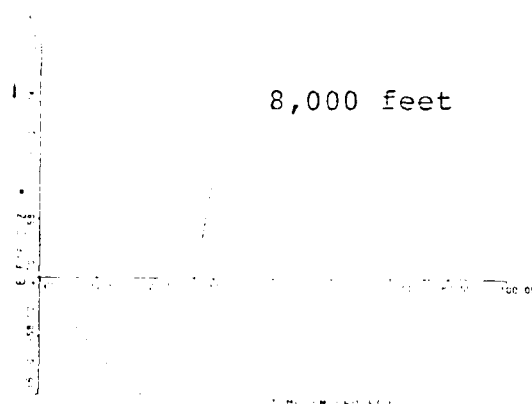
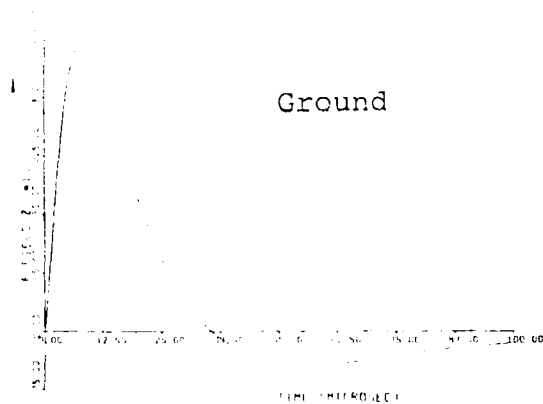


Fig. 5.17. Computer Solutions to Equation (39), the Electric Field, According to Model 2 at a Distance of 1 km, 1 μ sec Rise Time, and 25 μ sec Fall Time, for the Ground and at Five Altitudes.

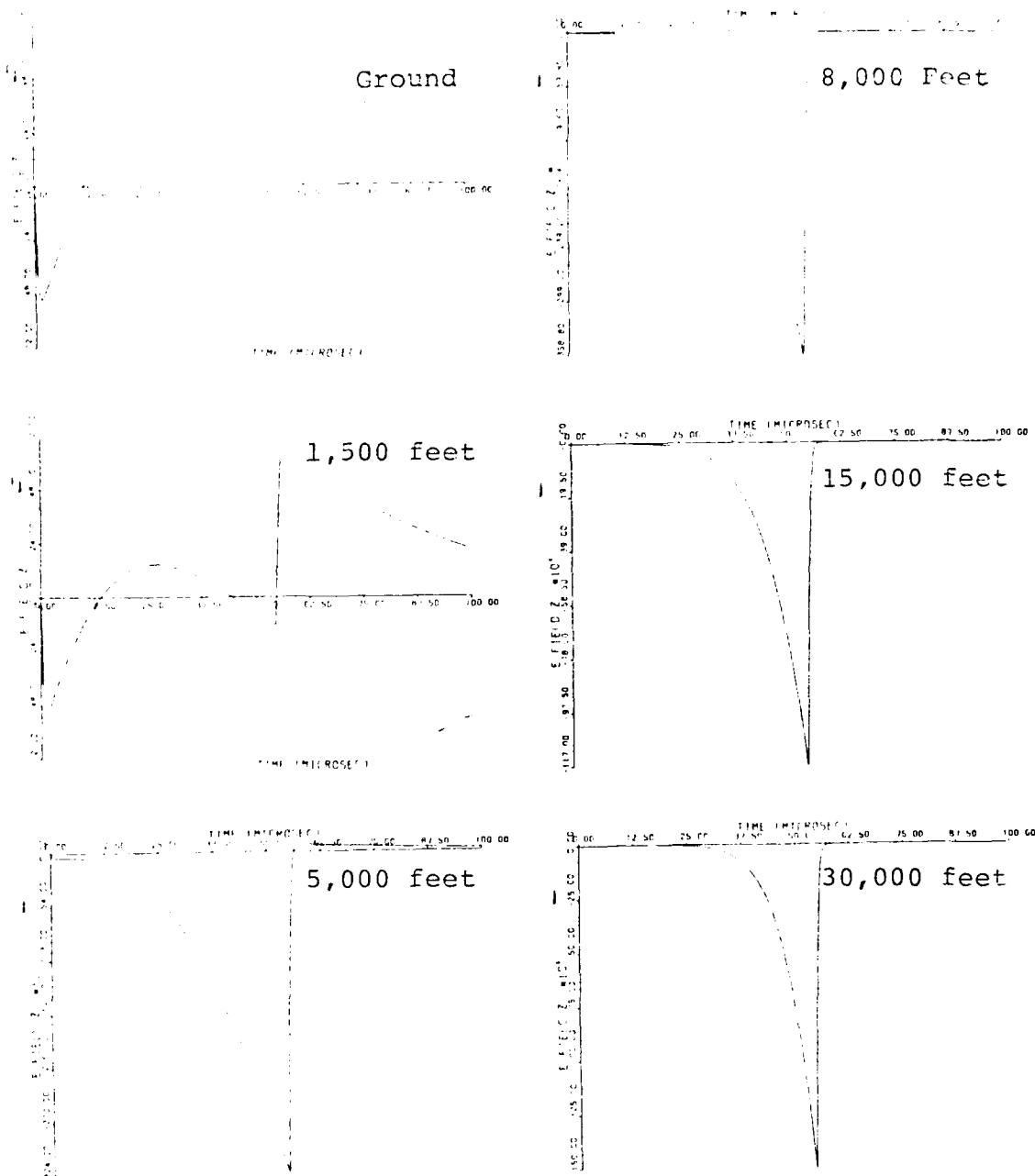


Fig. 5.18. Computer Solutions to Equation (39), the Electric Field, According to Model 2 at a Distance of 5 km, 1 μ sec Rise Time, and 25 μ sec Fall Time, for the Ground and at Five Altitudes.

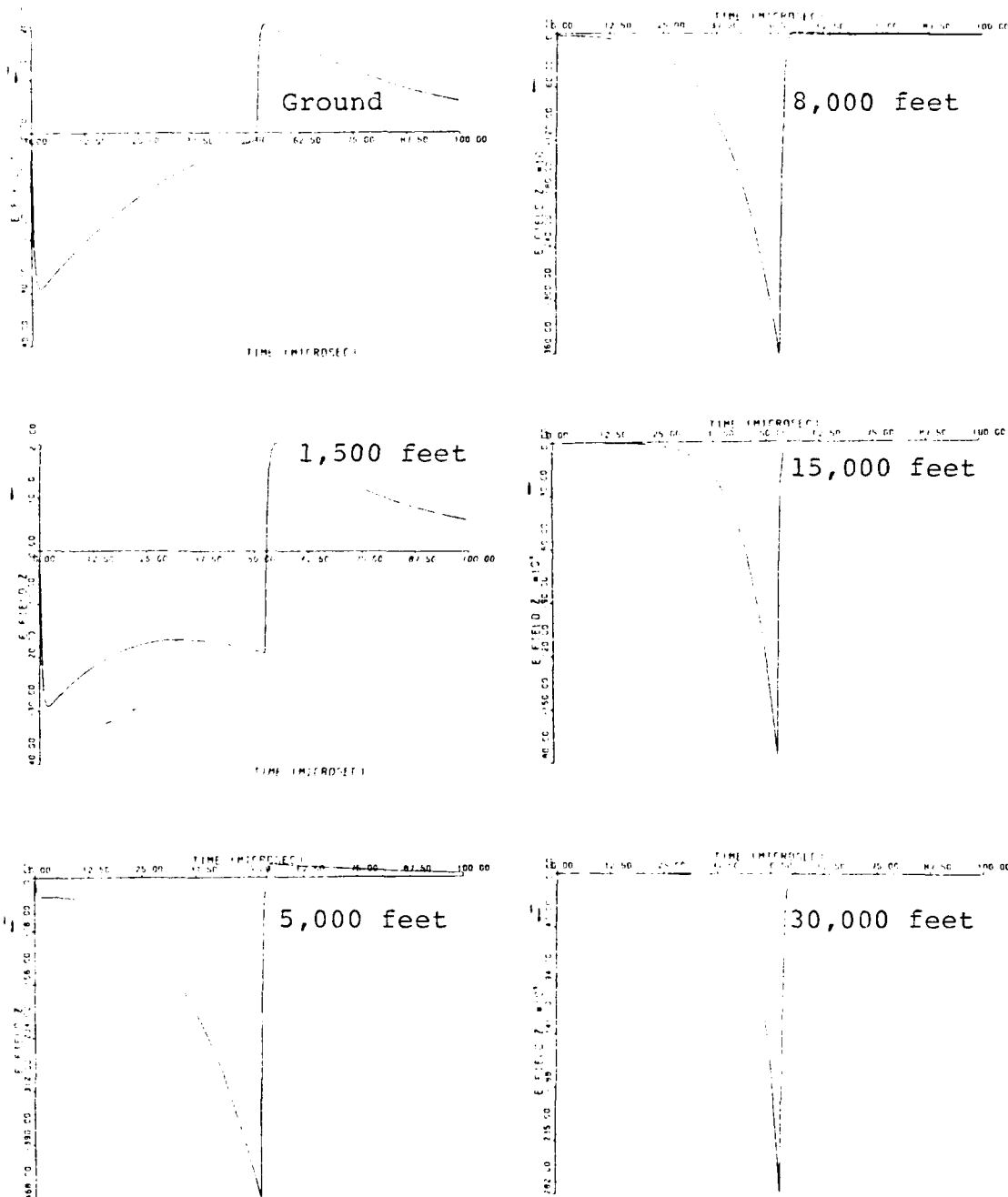


Fig. 5.19. Computer Solutions to Equation (39), the Electric Field, According to Model 2 at a Distance of 10 km, 1 μ sec Rise Time, and 25 μ sec Fall Time, for the Ground and at Five Altitudes.

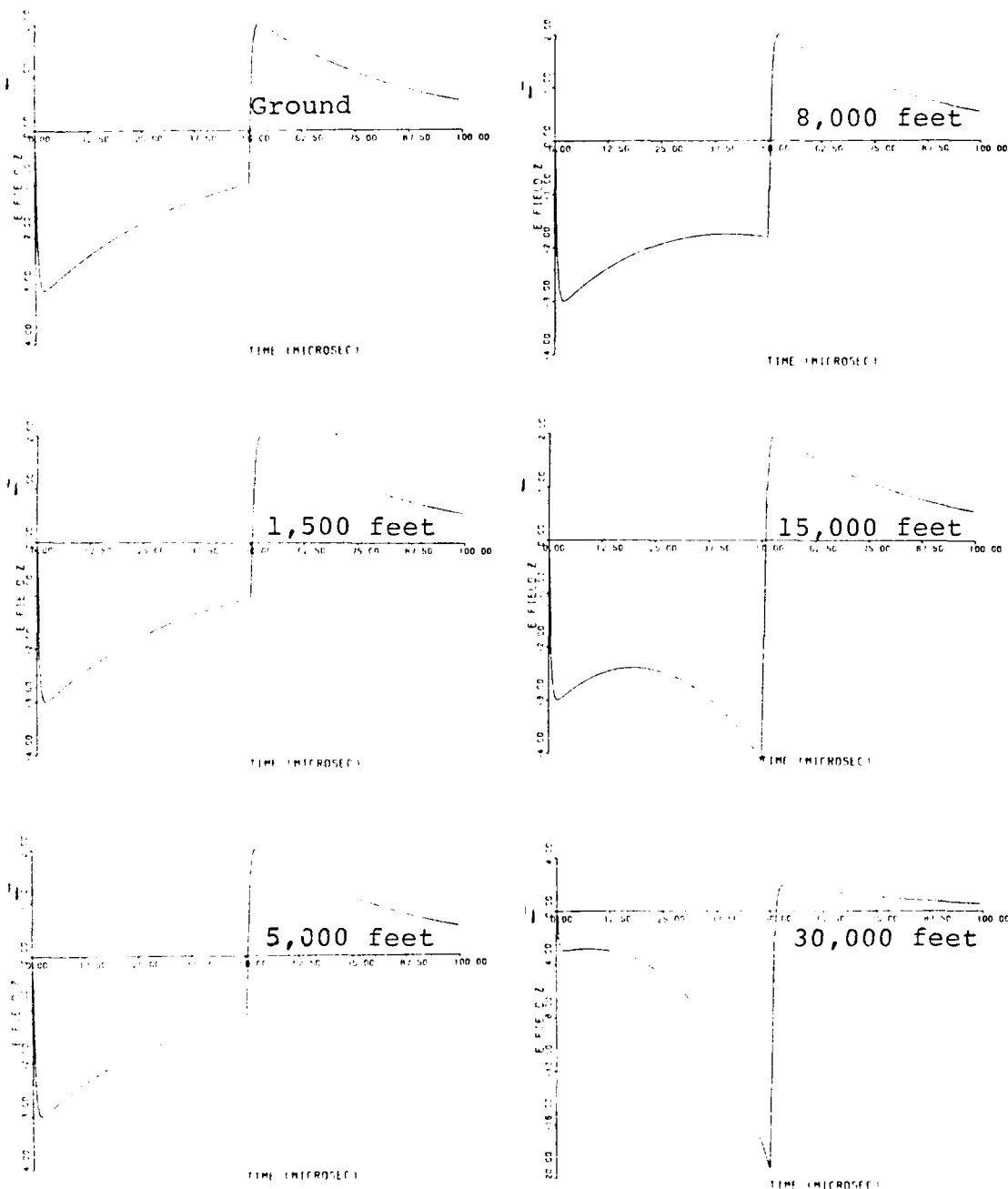


Fig. 5.20. Computer Solutions to Equation (39), the Electric Field, According to Model 2 at a Distance of 100 km, 1 μ sec Rise Time, and 25 μ sec Fall Time, for the Ground and at Five Altitudes.

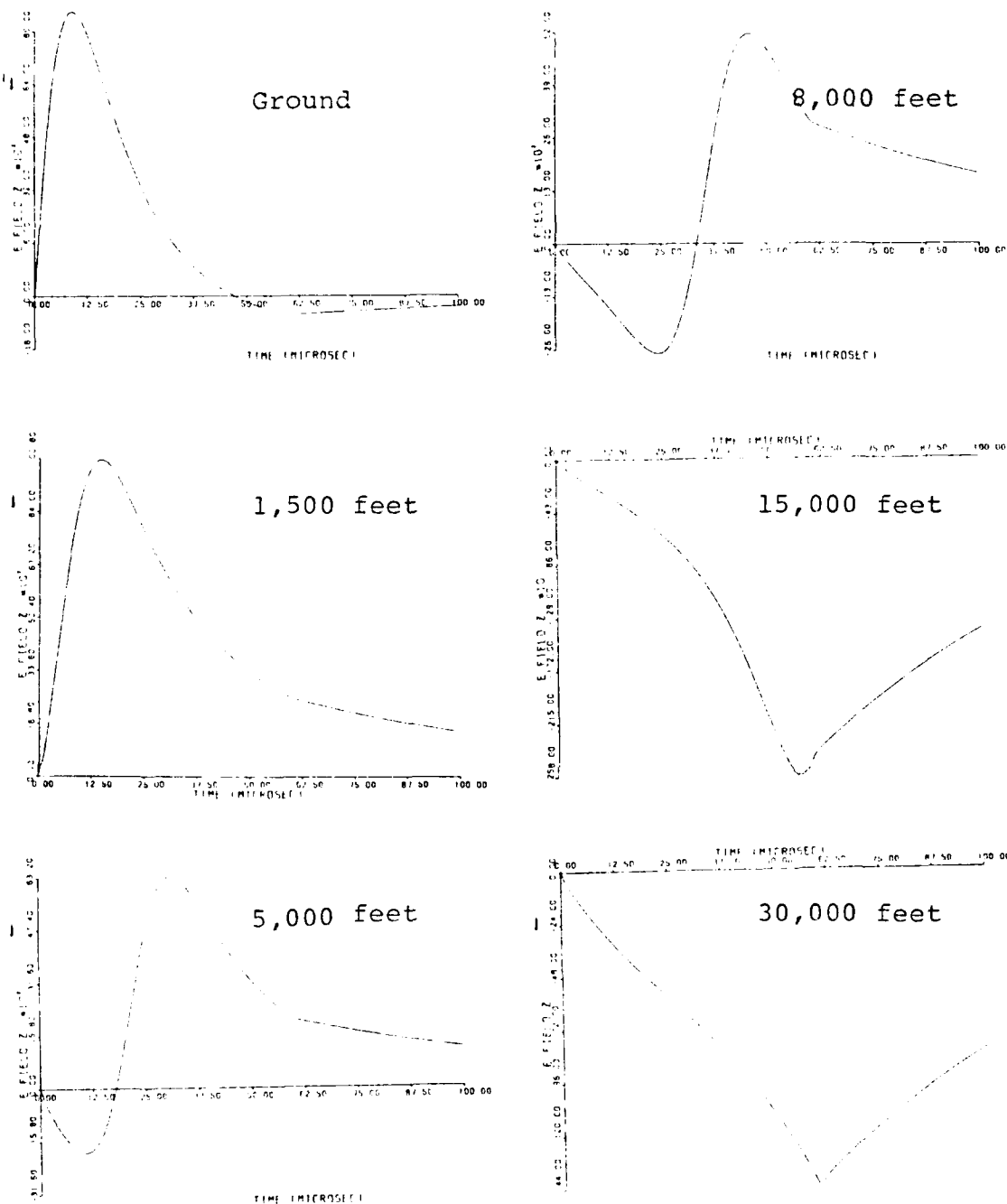


Fig. 5.21. Computer Solutions to Equation (39), the Electric Field, According to Model 2 at a Distance of 1 km, 2 μ sec Rise Time, and 50 μ sec Fall Time, for the Ground and at Five Altitudes.

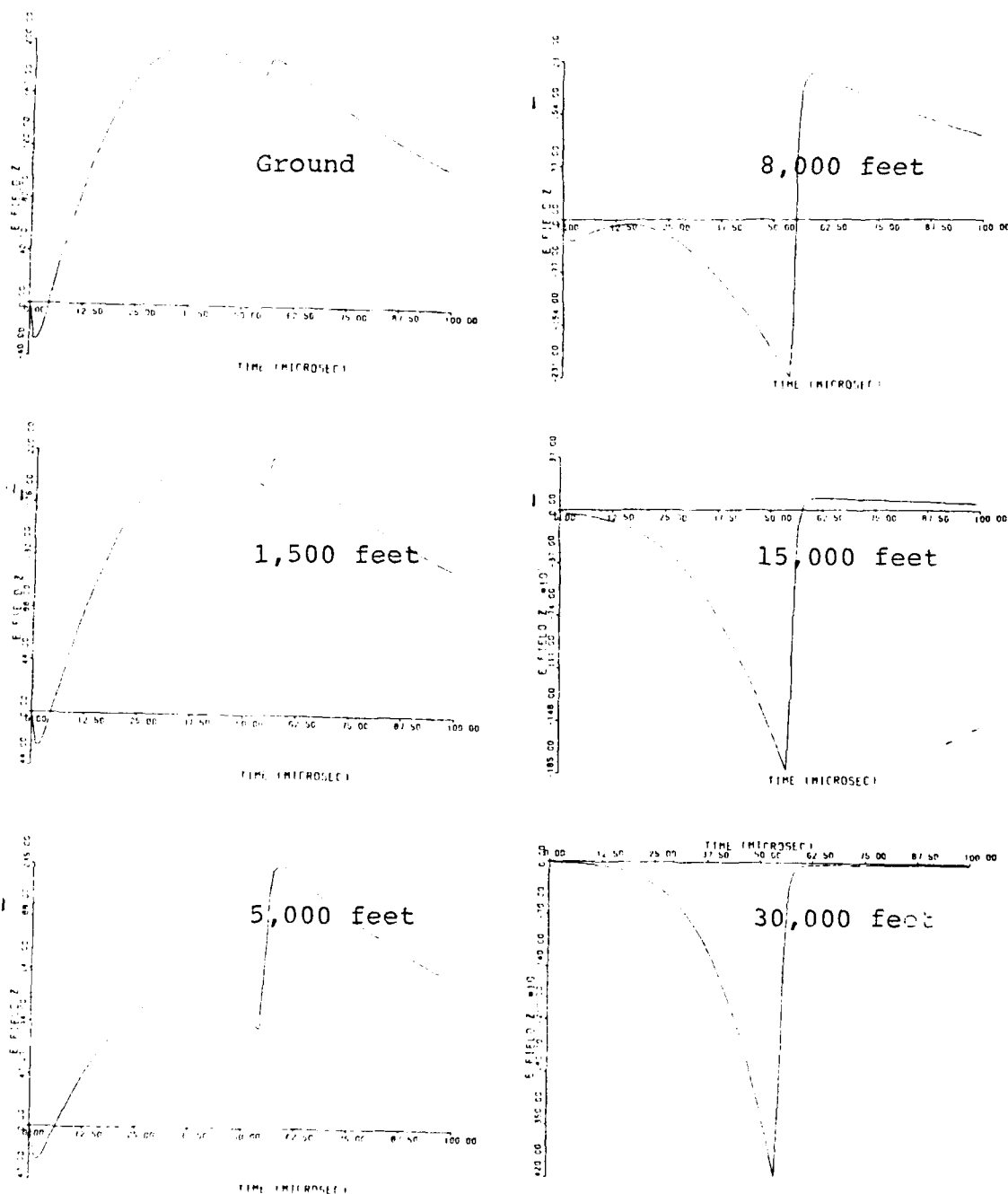


Fig. 5.22. Computer Solutions to Equation (39), the Electric Field, According to Model 2 at a Distance of 5 km, 2 μ sec Rise Time, and 50 μ sec Fall Time, for the Ground and at Five Altitudes.

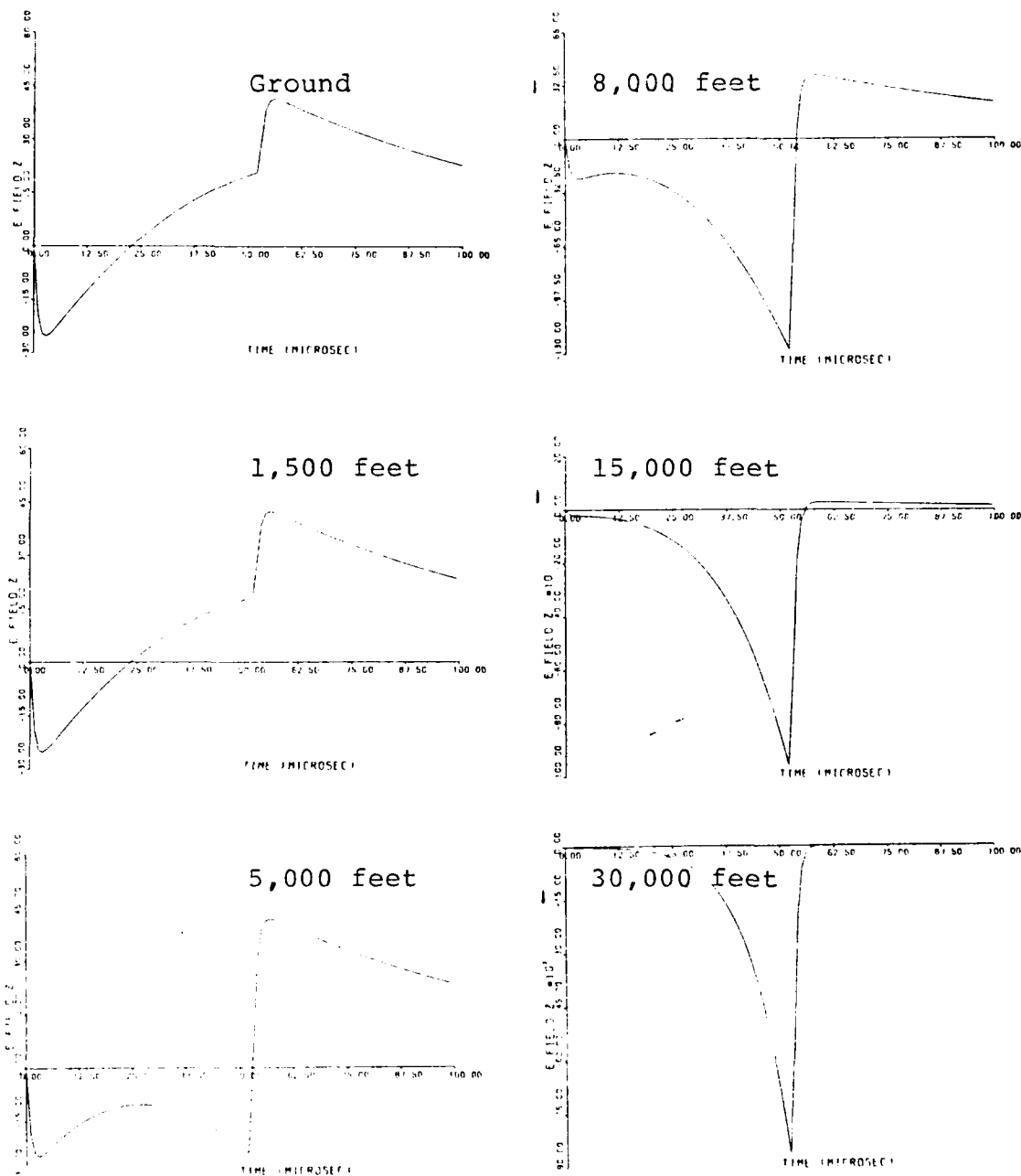


Fig. 5.23. Computer Solutions to Equation (39), the Electric Field, According to Model 2 at a Distance of 10 km, 2 μ sec Rise Time, and 50 μ sec Fall Time, for the Ground and at Five Altitudes.

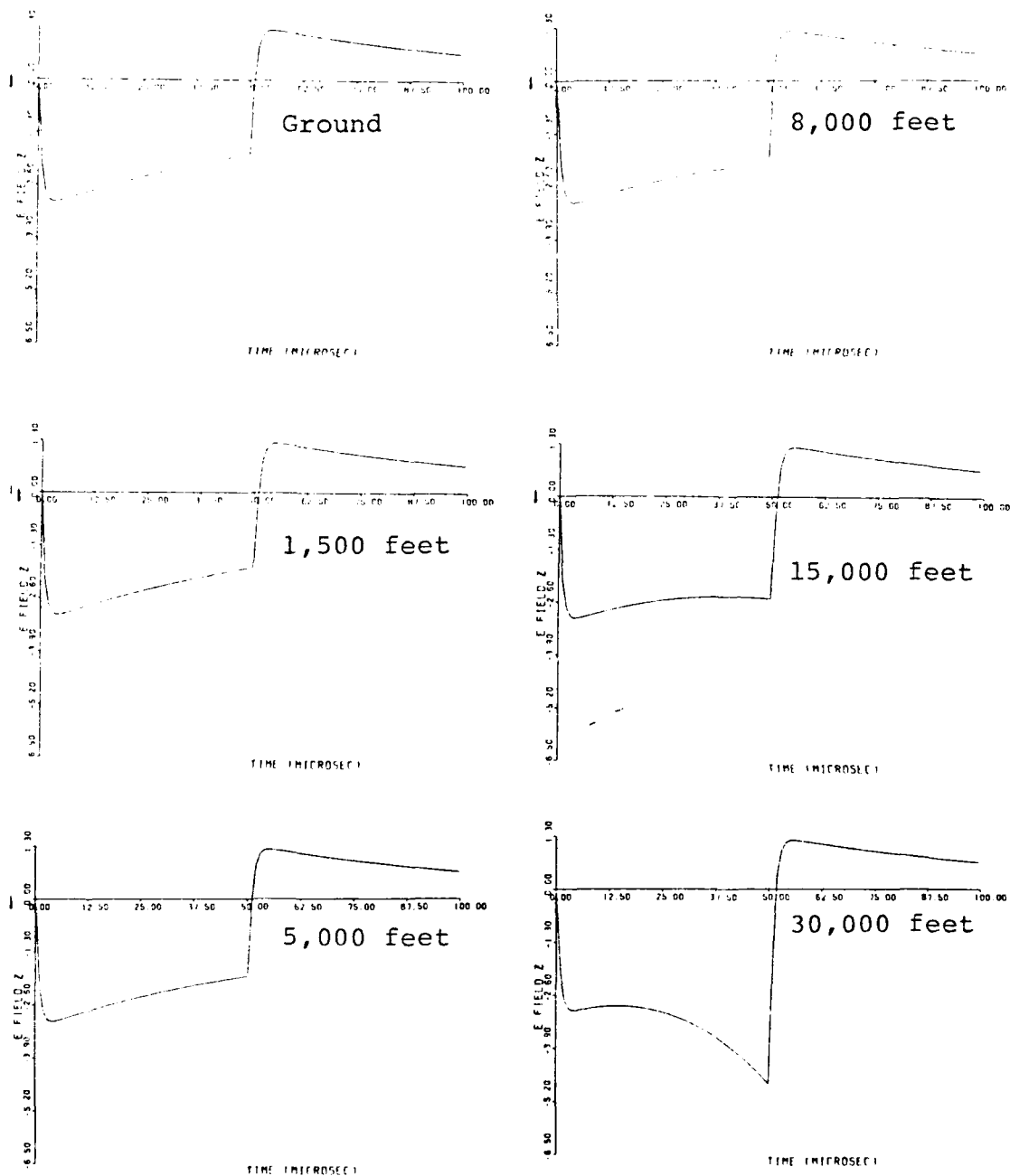


Fig. 5.24. Computer Solutions to Equation (39), the Electric Field, According to Model 2 at a Distance of 100 km, 2 μ sec Rise Time, and 50 μ sec Fall Time, for the Ground and at Five Altitudes.

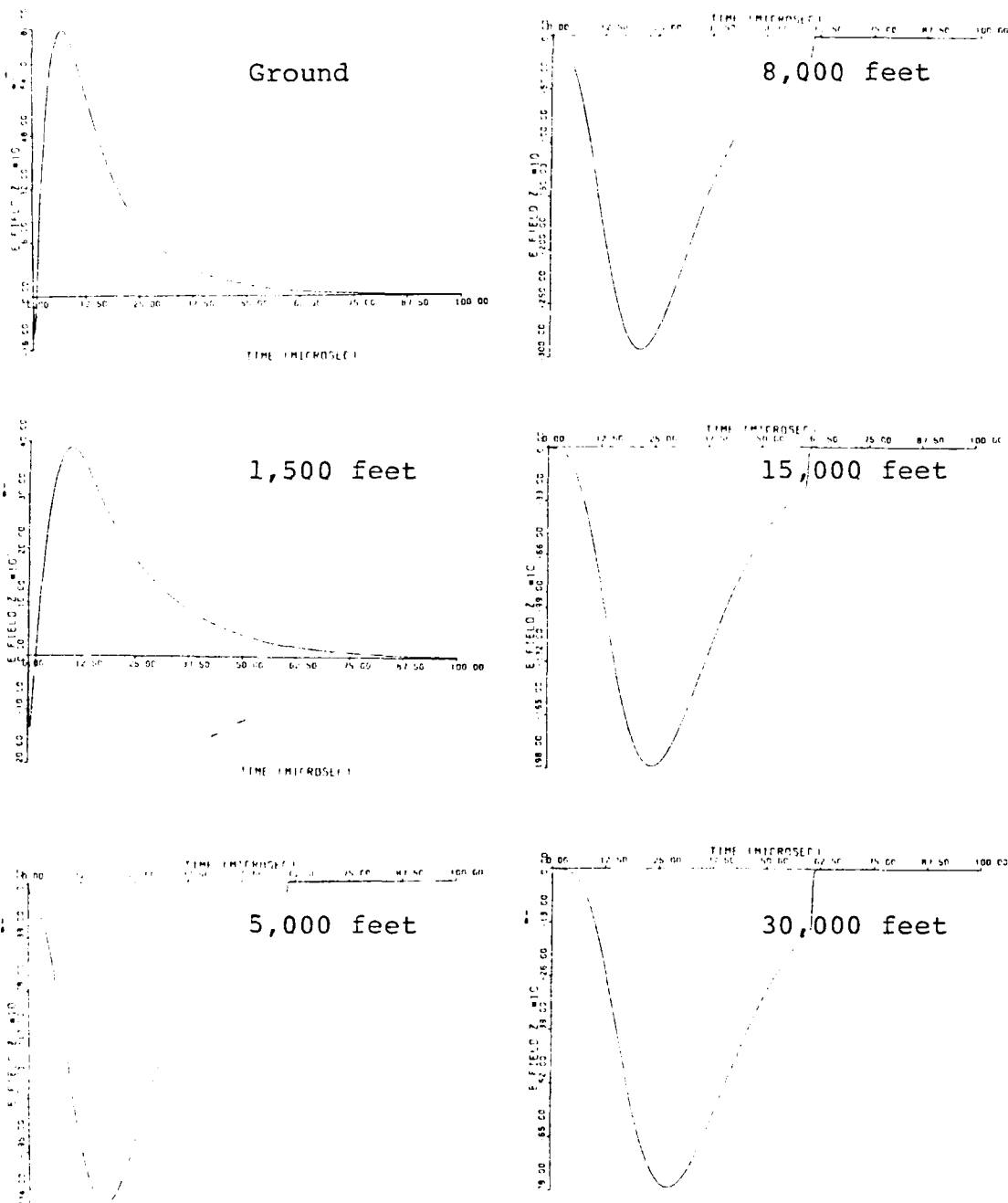


Fig. 5.25. Computer Solutions to Equation (39), The Electric Field, According to Model 3 at a Distance of 1 km, 500 nsec Rise Time, and 10 μ sec Fall Time, for the Ground and at Five Altitudes.

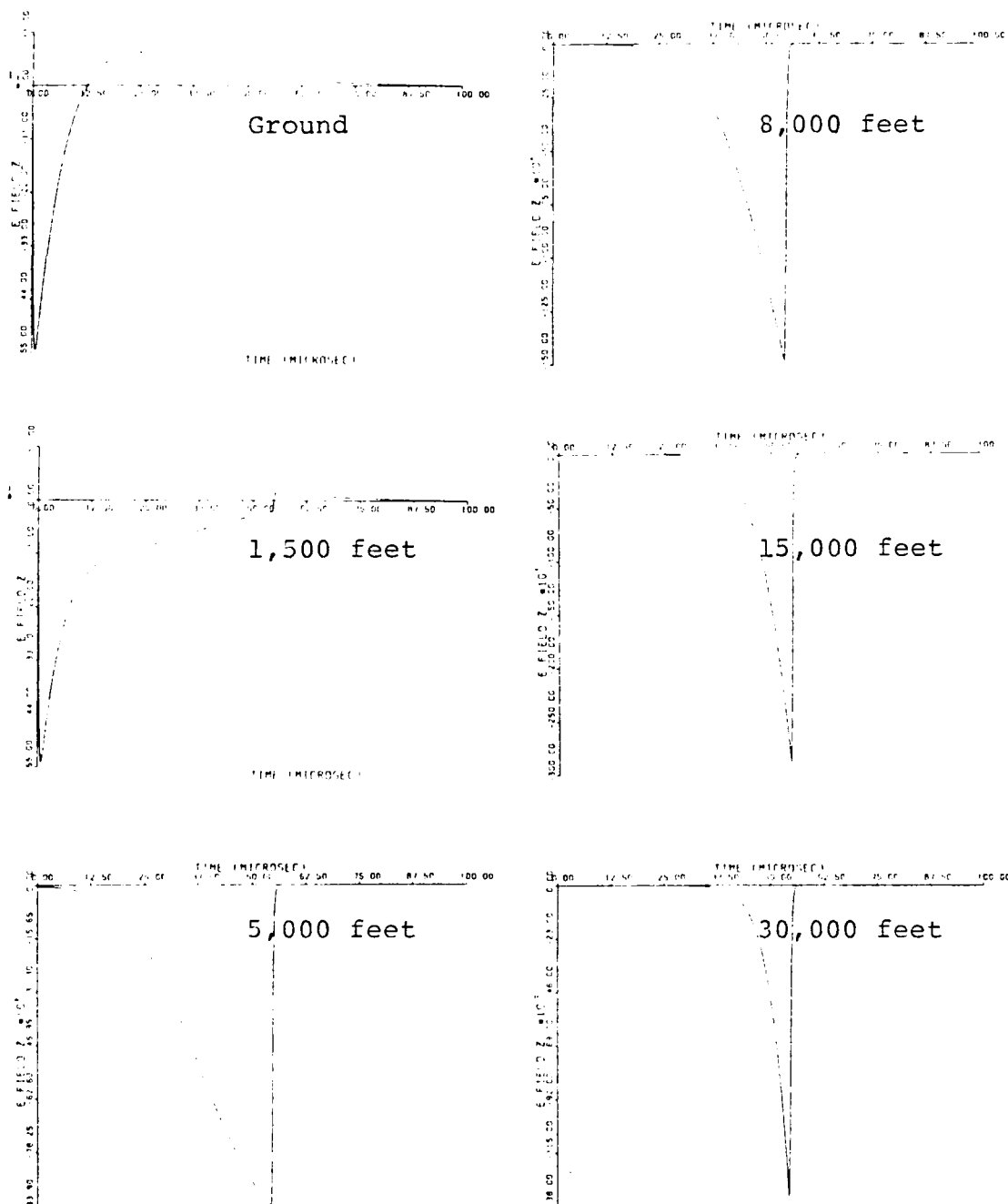


Fig. 5.26. Computer Solutions to Equation (39), The Electric Field, According to Model 3 at a Distance of 5 km, 500 nsec Rise Time, and 10 μ sec Fall Time, for the Ground and at Five Altitudes.

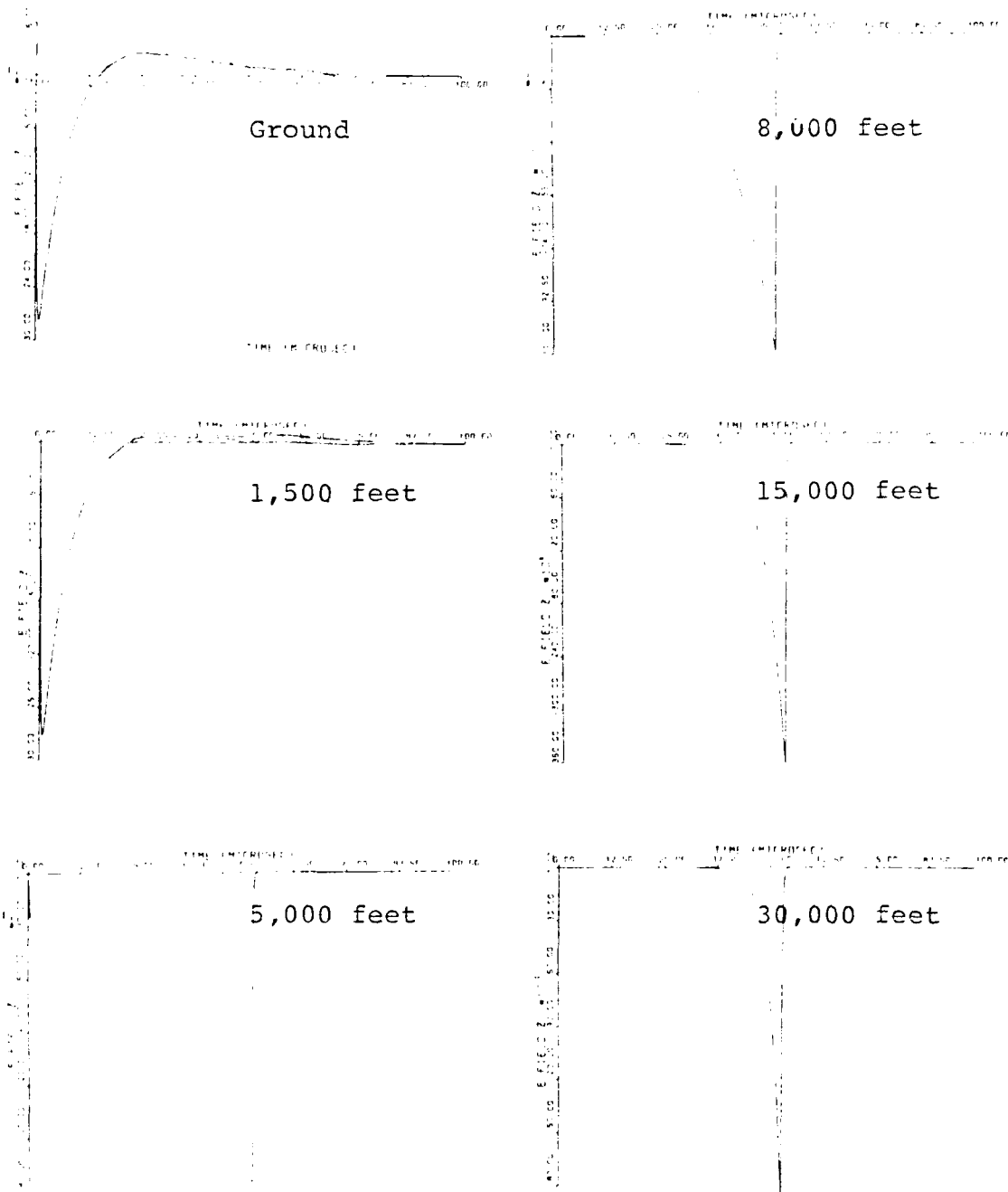


Fig. 5.27. Computer Solutions to Equation (39), the Electric Field, According to Model 3 at a Distance of 10 km, 500 nsec Rise Time, and 10 usec Fall Time, for the Ground and at Five Altitudes.

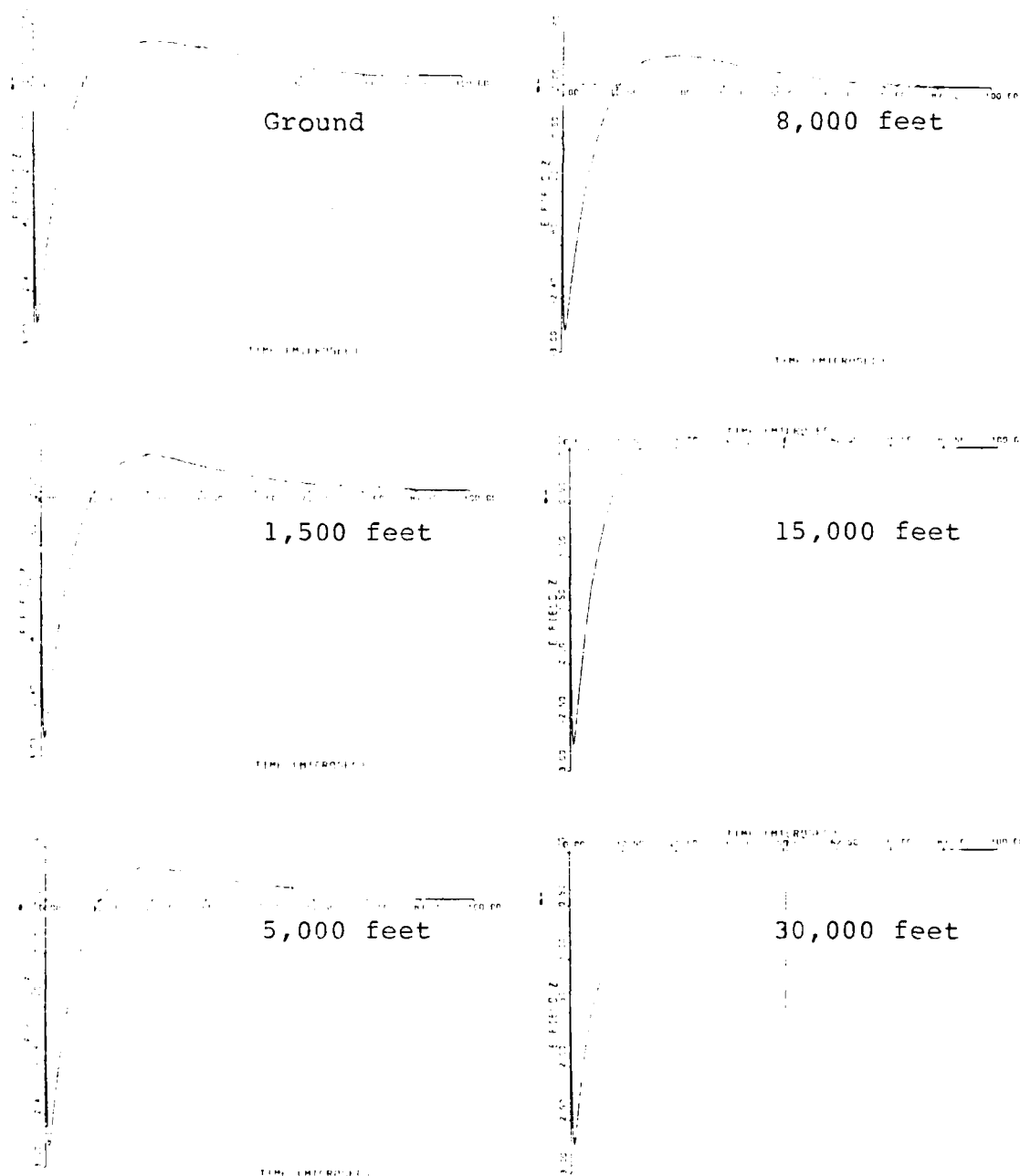


Fig. 5.28. Computer Solutions to Equation (39), the Electric Field, According to Model 3 at a Distance of 100 km, 500 nsec Rise Time, and 10 nsec Fall Time, for the Ground and at Five Altitudes.

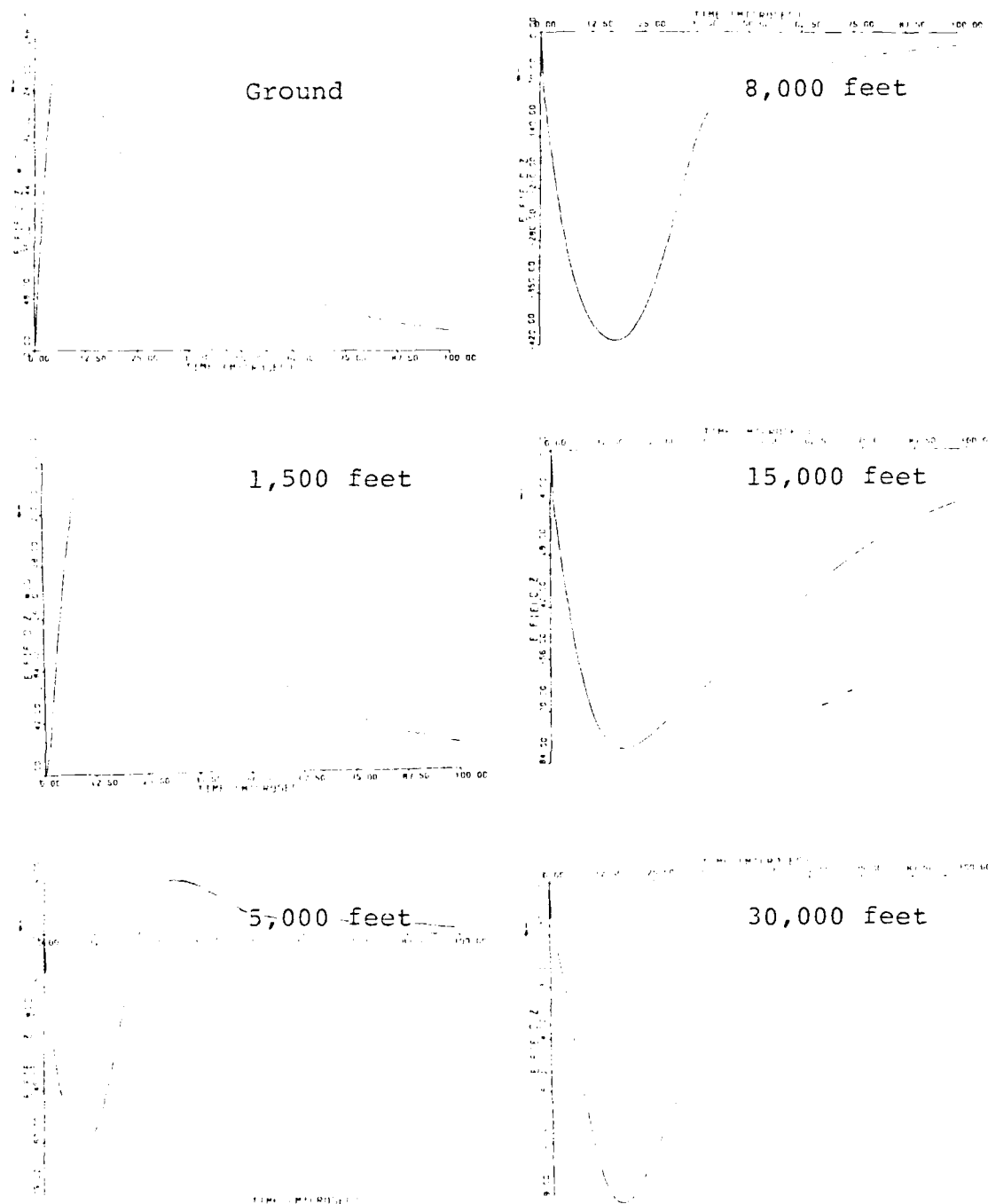


Fig. 5.29. Computer Solutions to Equation (39), the Electric Field, According to Model 3 at a Distance of 1 km, 1 μ sec Rise Time, and 25 μ sec Fall Time, for the Ground and at Five Altitudes.

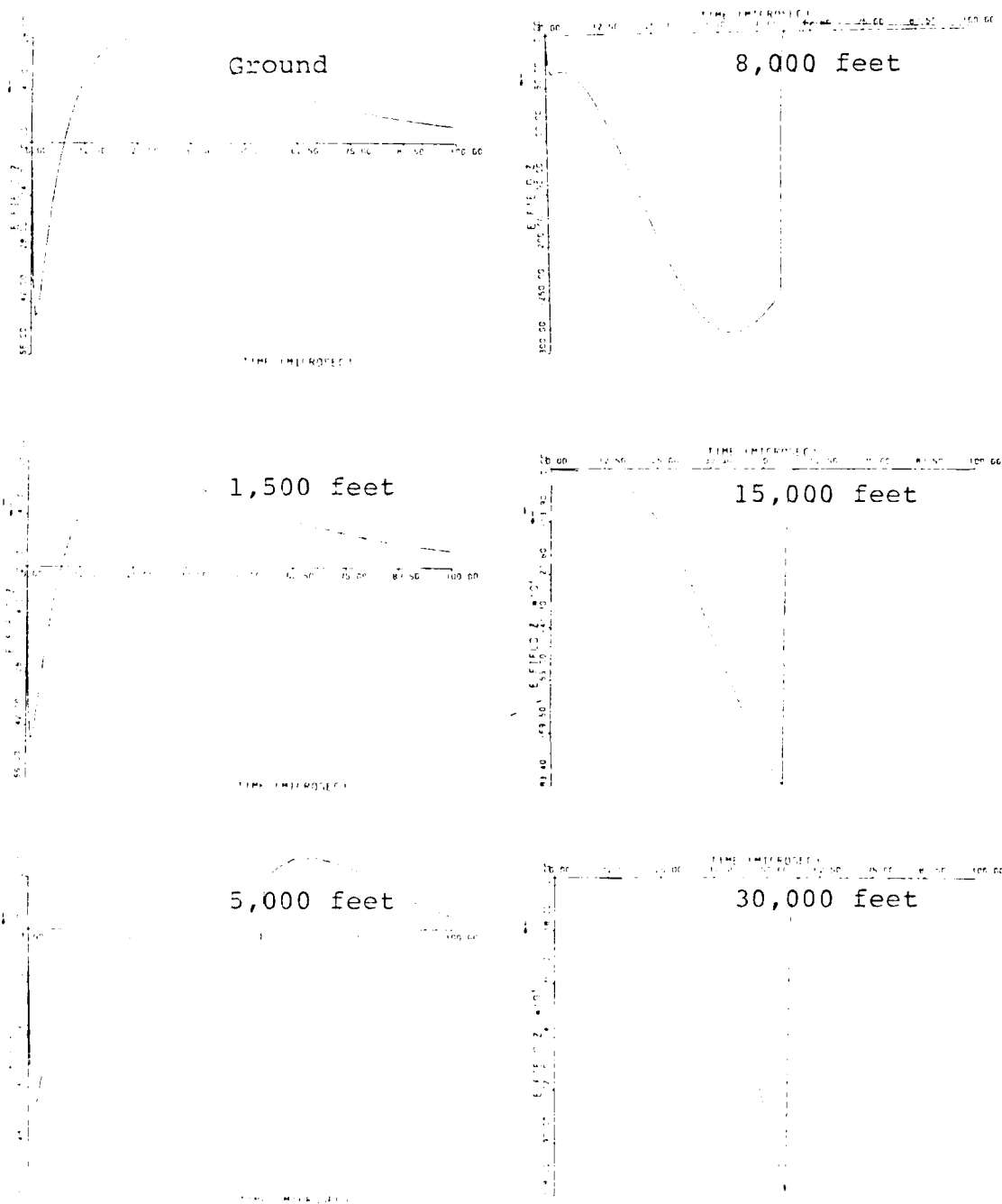


Fig. 5.30. Computer Solutions to Equation (39), the Electric Field, According to Model 3 at a Distance of 5 km, 1 μ sec Rise Time, and 25 μ sec Fall Time, for the Ground and at Five Altitudes.

AD-A151 841

AN ANALYSIS AND COMPARISON OF LIGHTNING RETURN STROKE 2/2

MODELS AT ALTITUDE(U) AIR FORCE INST OF TECH

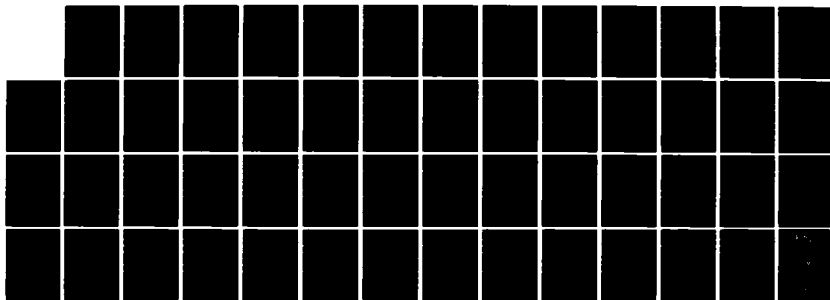
WRIGHT-PATTERSON AFB OH SCHOOL OF ENGINEERING J M CUKR

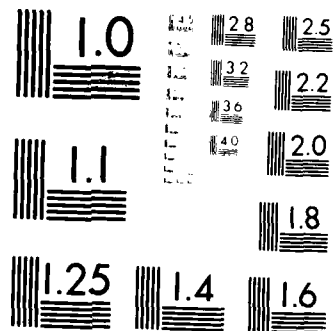
UNCLASSIFIED

DEC 81 AFIT/GE/EE/81D-15

F/G 4/2

NL





MICROCOPY RESOLUTION TEST CHART
 NATIONAL BUREAU OF STANDARDS-1963-A

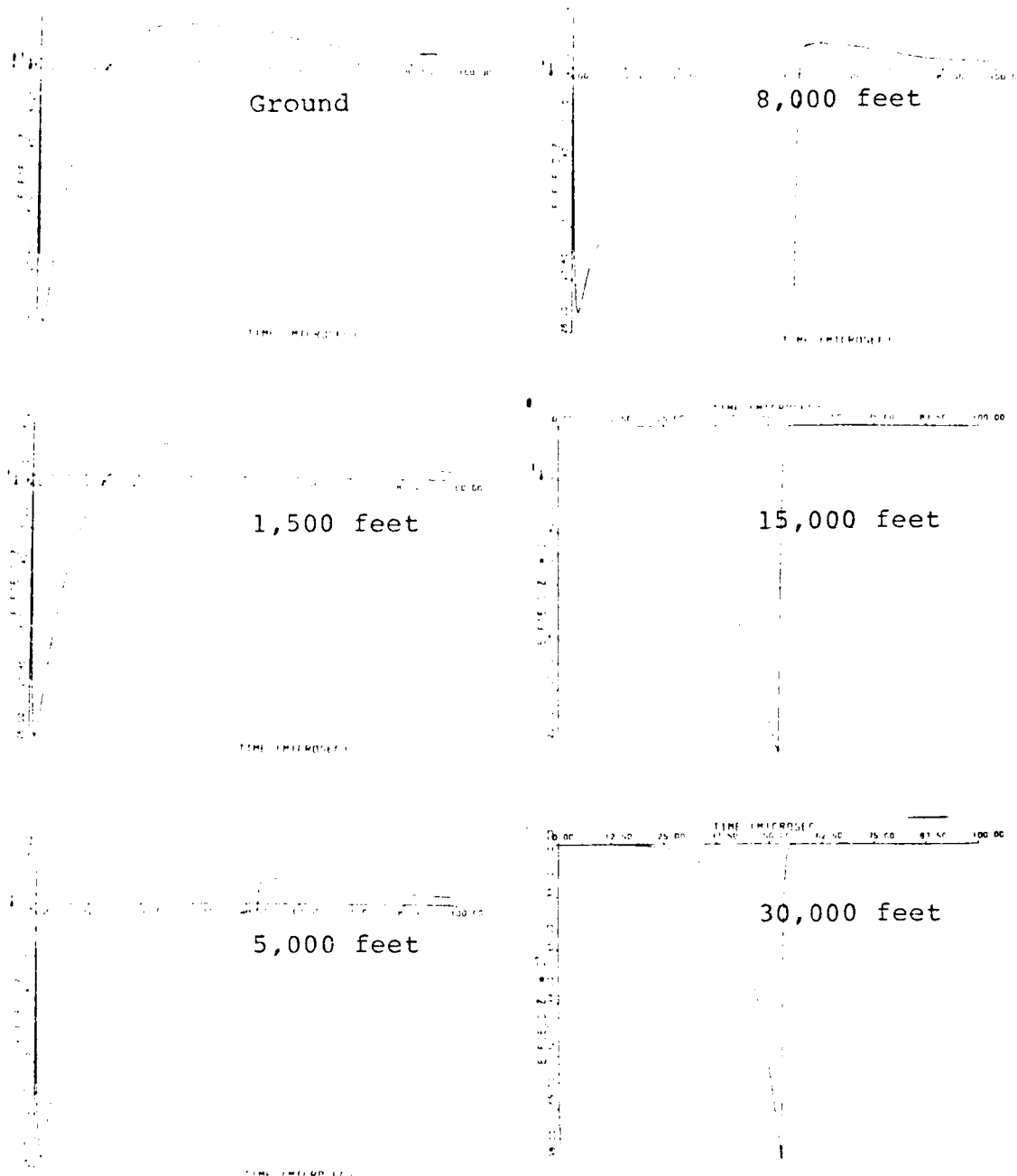


Fig. 5.31. Computer Solutions to Equation (39), the Electric Field, According to Model 3 at a Distance of 10 km, 1 μ sec Rise Time, and 25 μ sec Fall Time, for the Ground and at Five Altitudes.

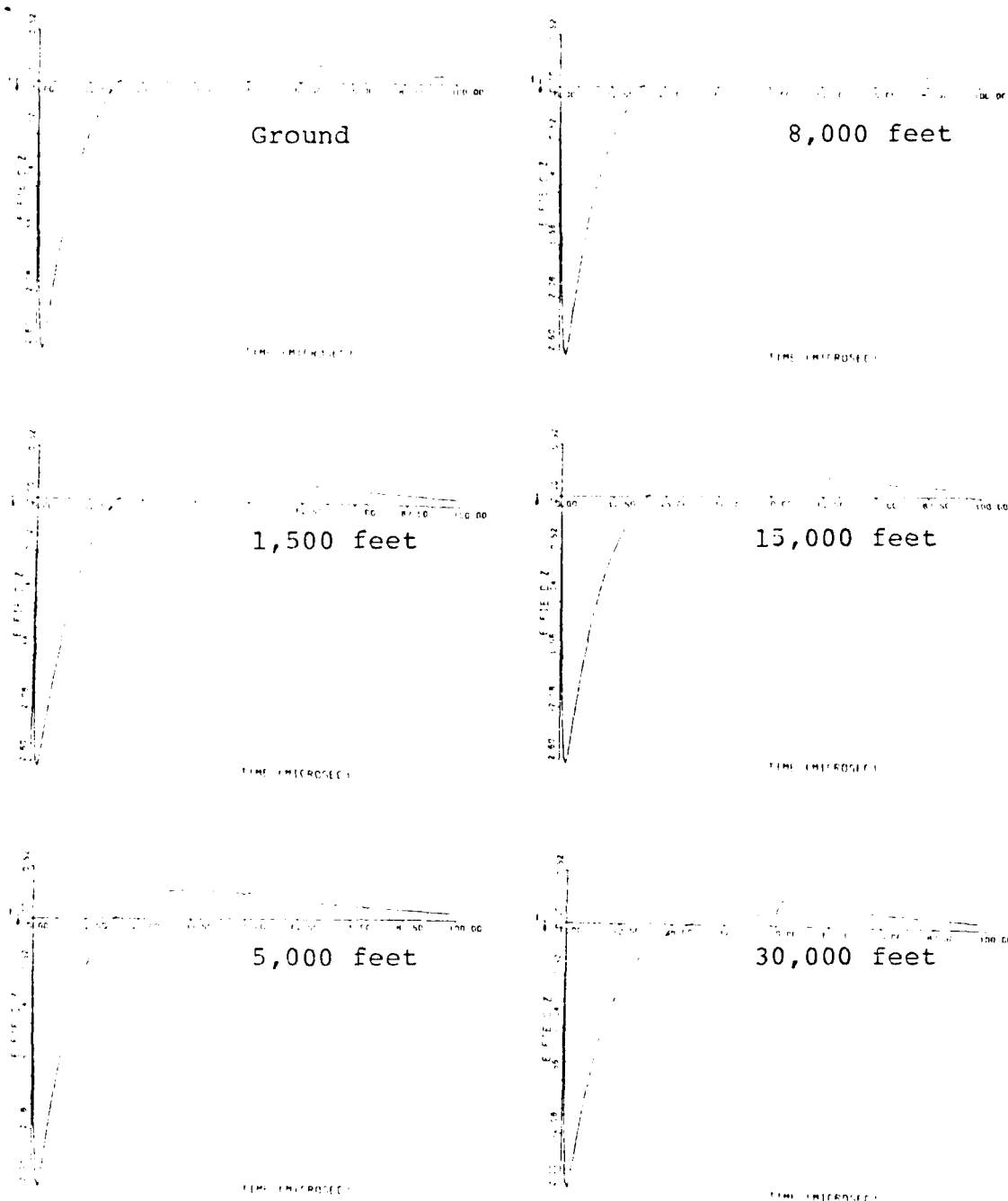


Fig. 5.32. Computer Solutions to Equation (39), the Electric Field, According to Model 3 at a Distance of 100 km, 1 μ sec Rise Time, and 25 μ sec Fall Time, for the Ground and at Five Altitudes.

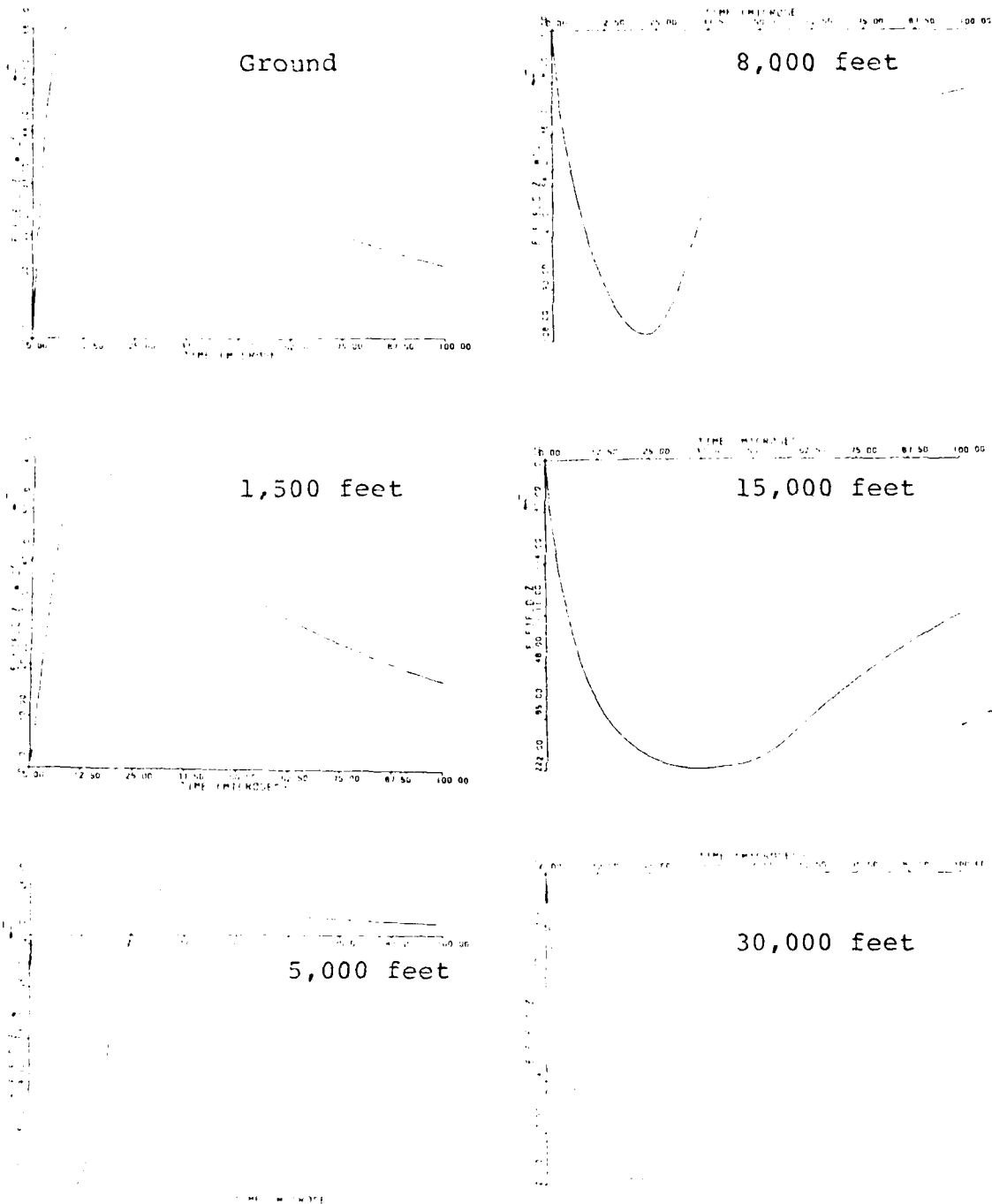


Fig. 5.33. Computer Solutions to Equation (39), the Electric Field, According to Model 3 at a Distance of 1 km, 2 μsec Rise Time, and 25 μsec Fall Time for the Ground and at Five Altitudes.

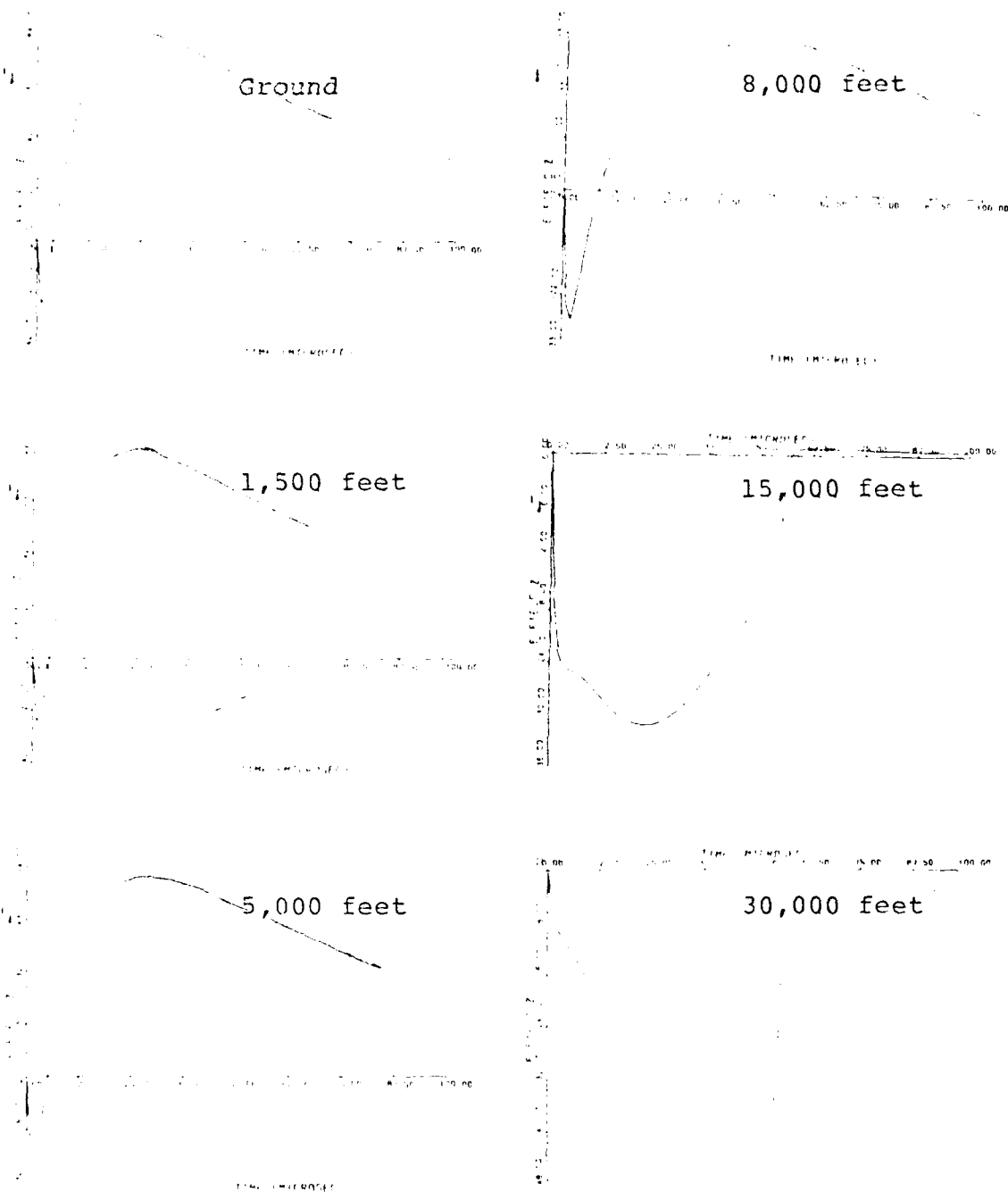


Fig. 5.34. Computer Solutions to Equation (39), the Electric Field, According to Model 3 at a Distance of 5 km, 2 μ sec Rise Time, and 25 μ sec Fall Time for the Ground and at Five Altitudes.

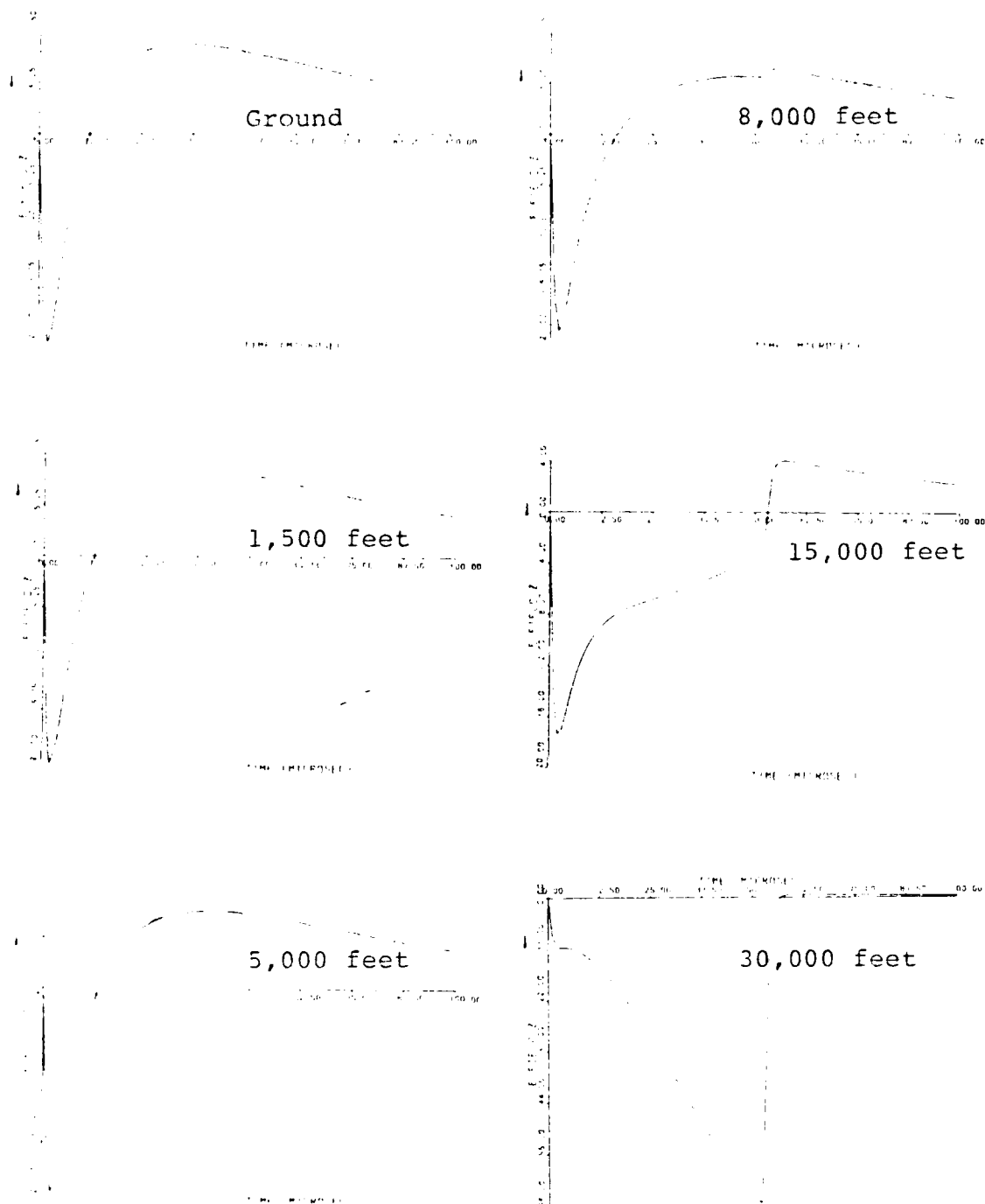


Fig. 5.35. Computer Solutions to Equation (39), the Electric Field, According to Model 3 at a Distance of 10 km, 2 μ sec Rise Time, and 25 μ sec Fall Time for the Ground and at Five Altitudes.

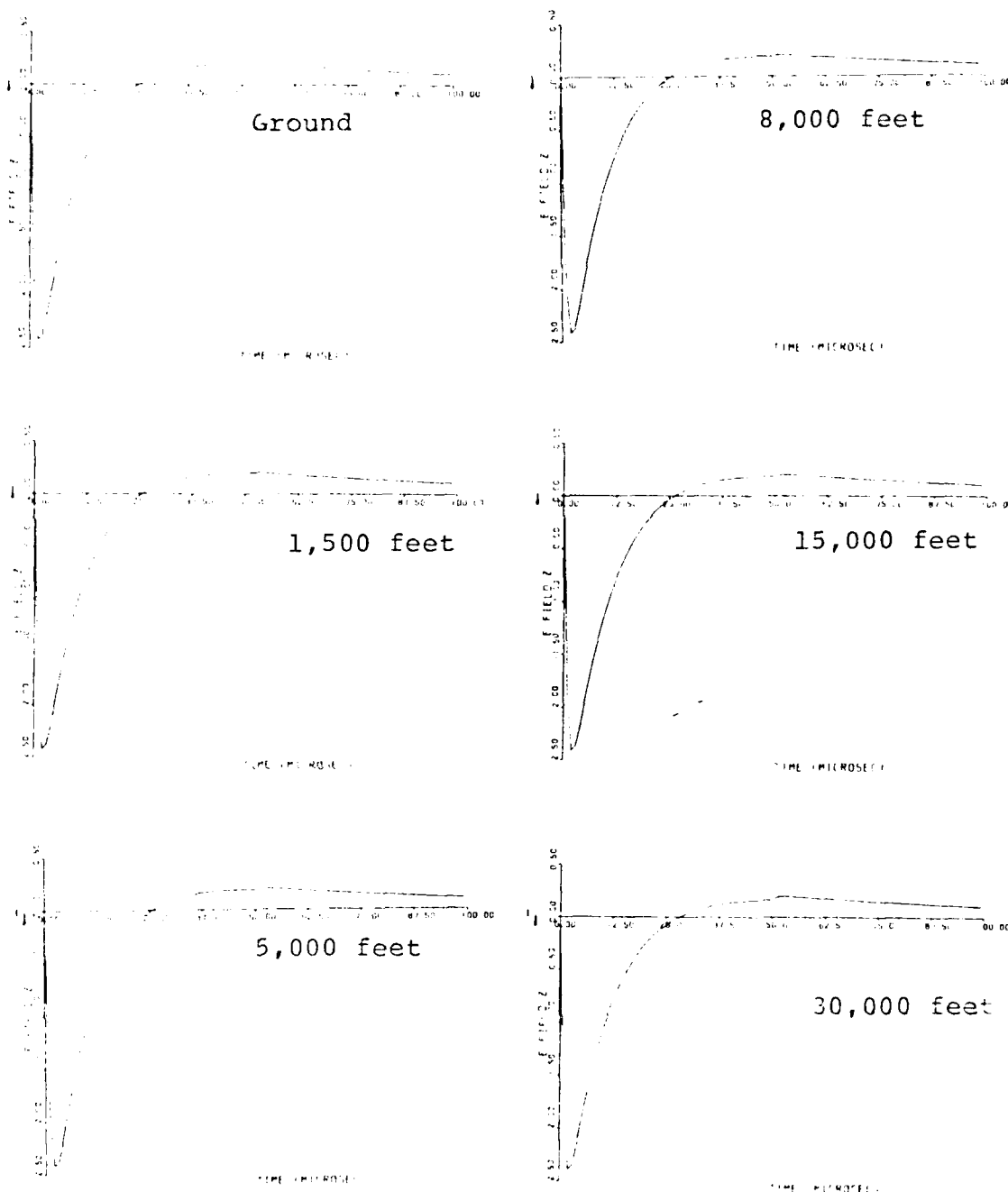


Fig. 5.36. Computer Solutions to Equation (39), the Electric Field, According to Model 3 at a Distance of 100 km, 2 μ sec Rise Time, and 25 μ sec Fall Time for the Ground and at Five Altitudes.

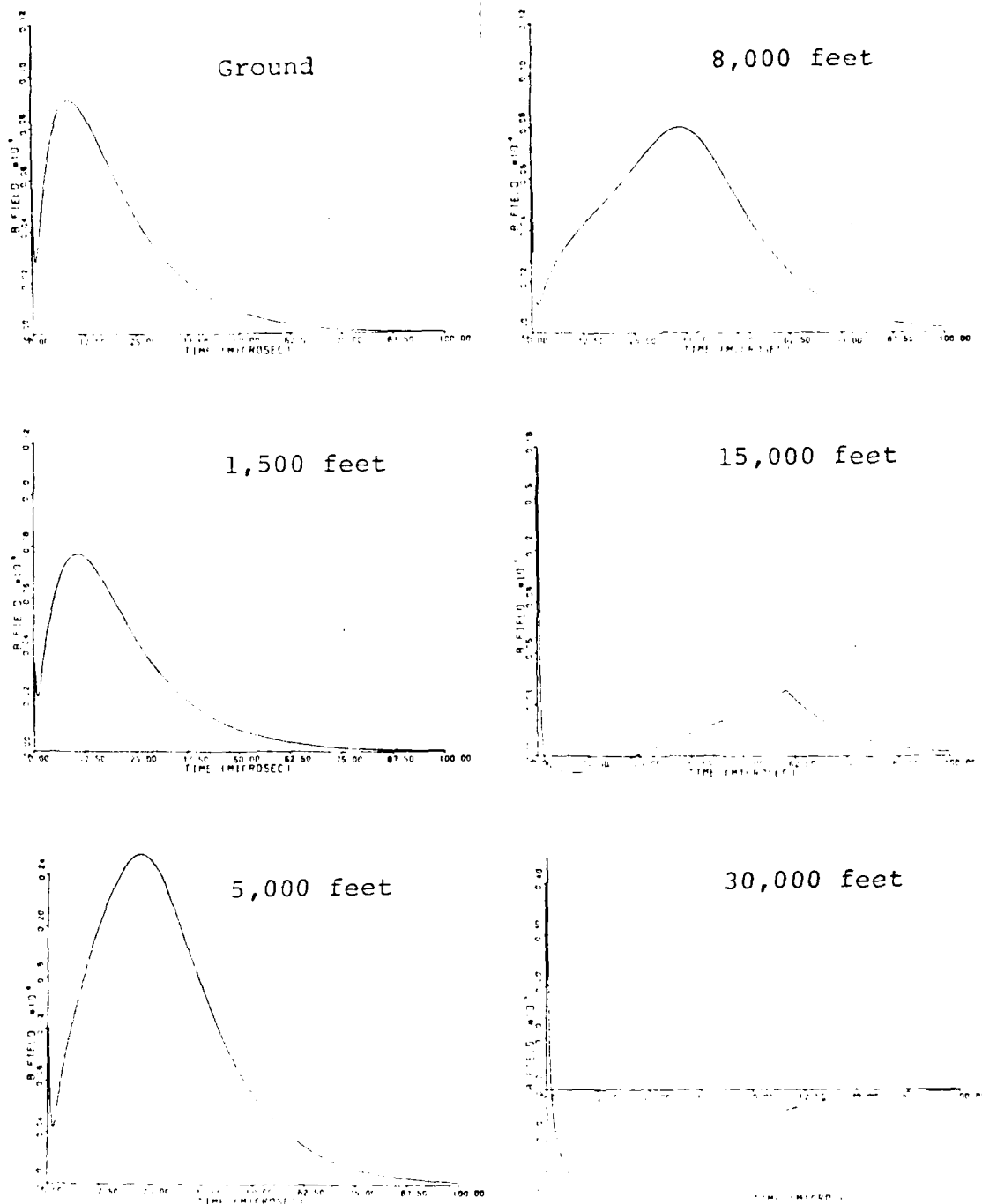


Fig. 5.37. Computer Solutions to Equation (40), the Magnetic Field, According to Model 1 at a Distance of 1 km, 500 μ sec Rise Time, and 10 μ sec Fall Time for the Ground and at Five Altitudes.

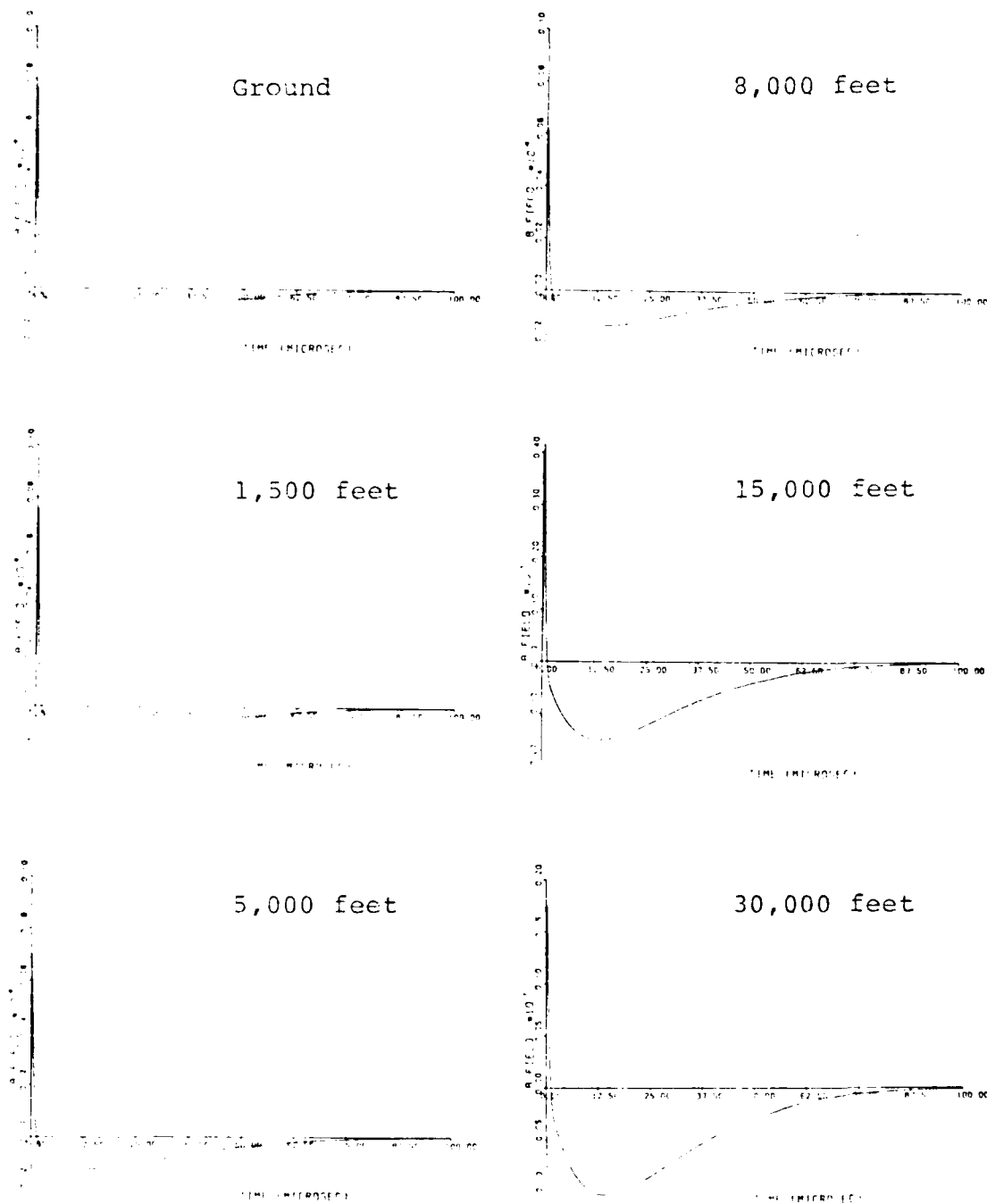


Fig. 5.38. Computer Solutions to Equation (40), the Magnetic Field, According to Model 1 at a Distance of 5 km, 500 μ sec Rise Time, and 10 μ sec Fall Time for the Ground and at Five Altitudes.

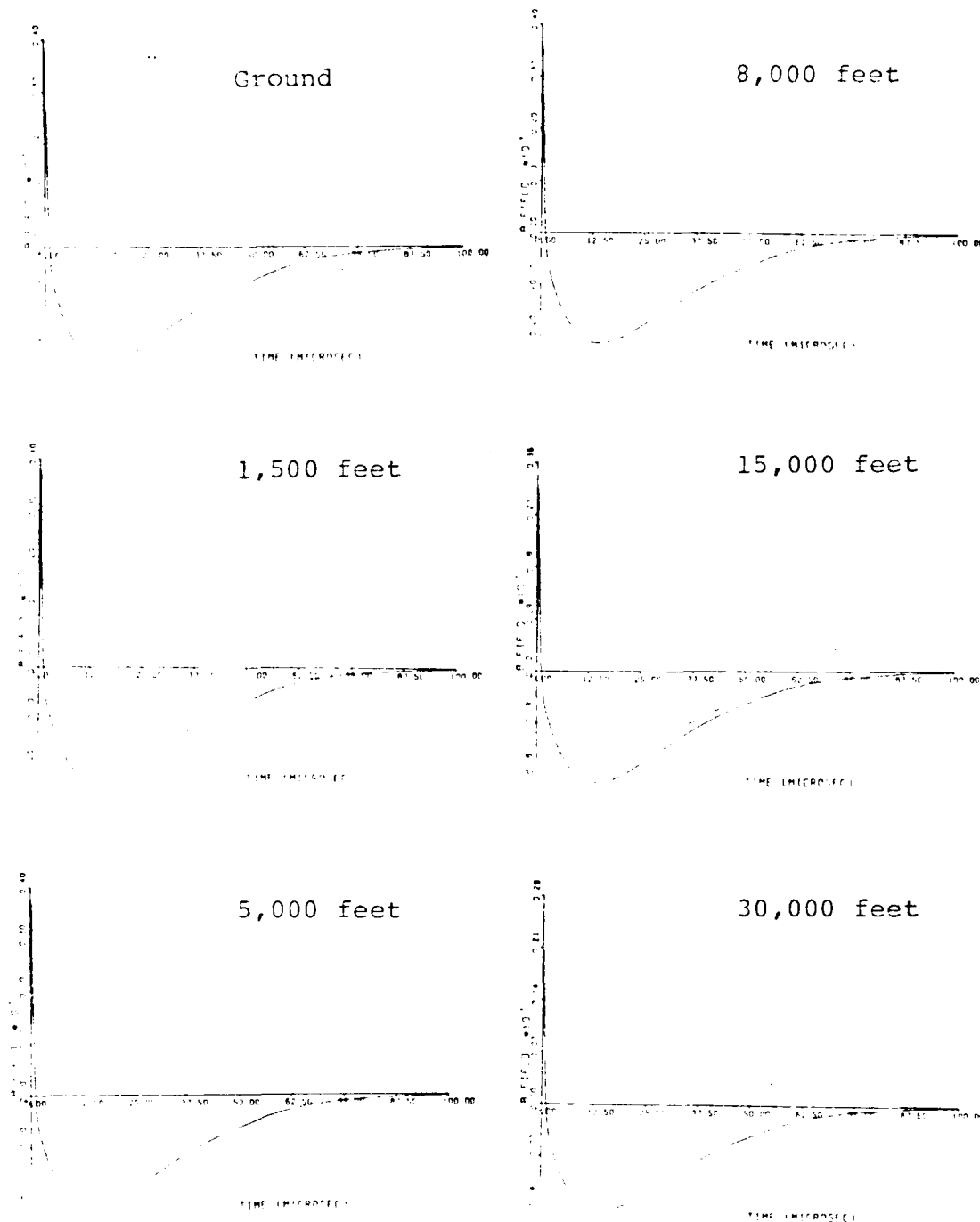


Fig. 5.39. Computer Solutions to Equation (40), the Magnetic Field, According to Model 1 at a Distance of 10 km, 500 μ sec Rise Time, and 10 μ sec Fall Time for the Ground and at Five Altitudes.

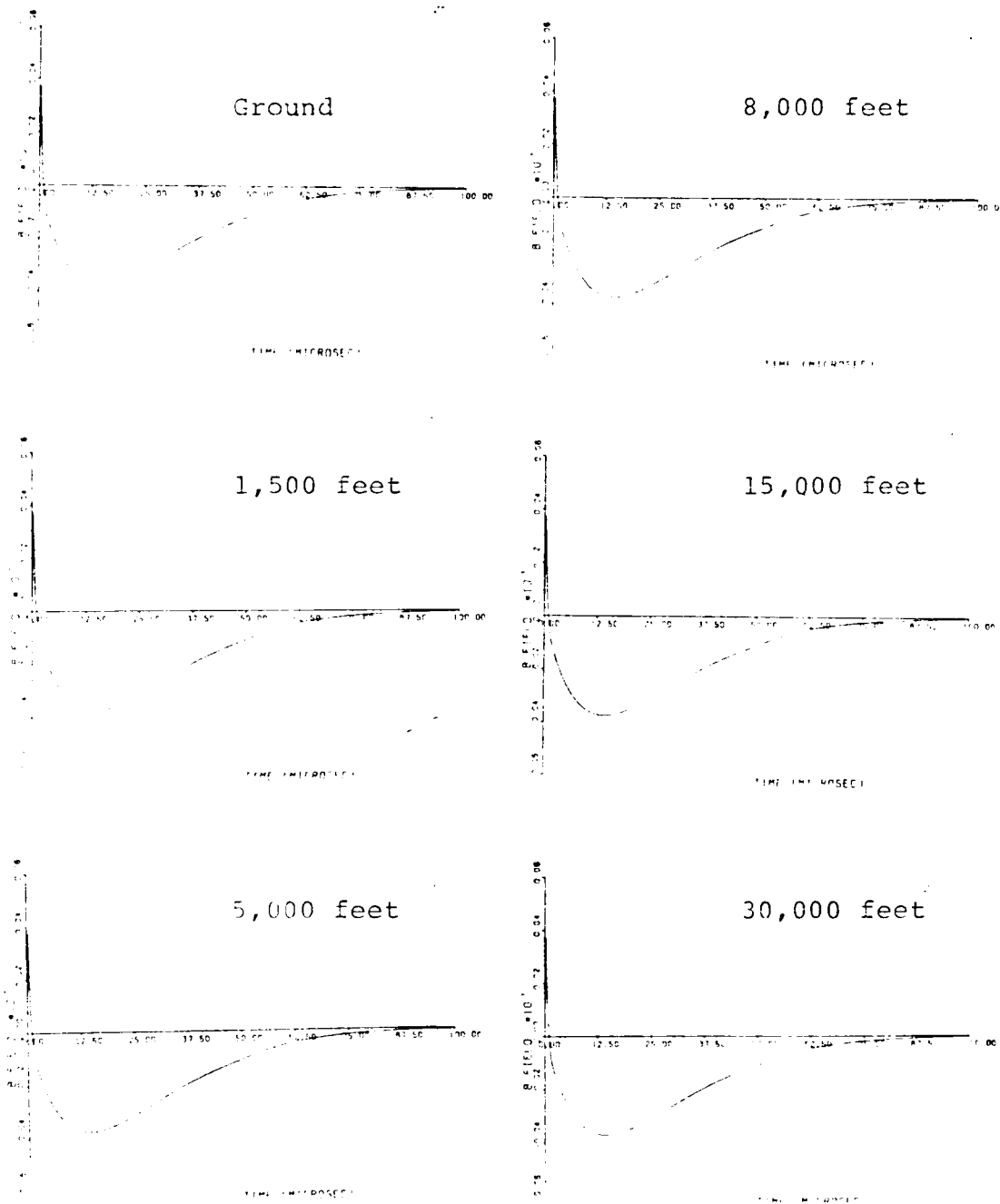


Fig. 5.40. Computer Solutions to Equation (40), the Magnetic Field, According to Model 1 at a Distance of 100 km, 500 μ sec Rise Time, and 10 μ sec Fall Time for the Ground and at Five Altitudes.

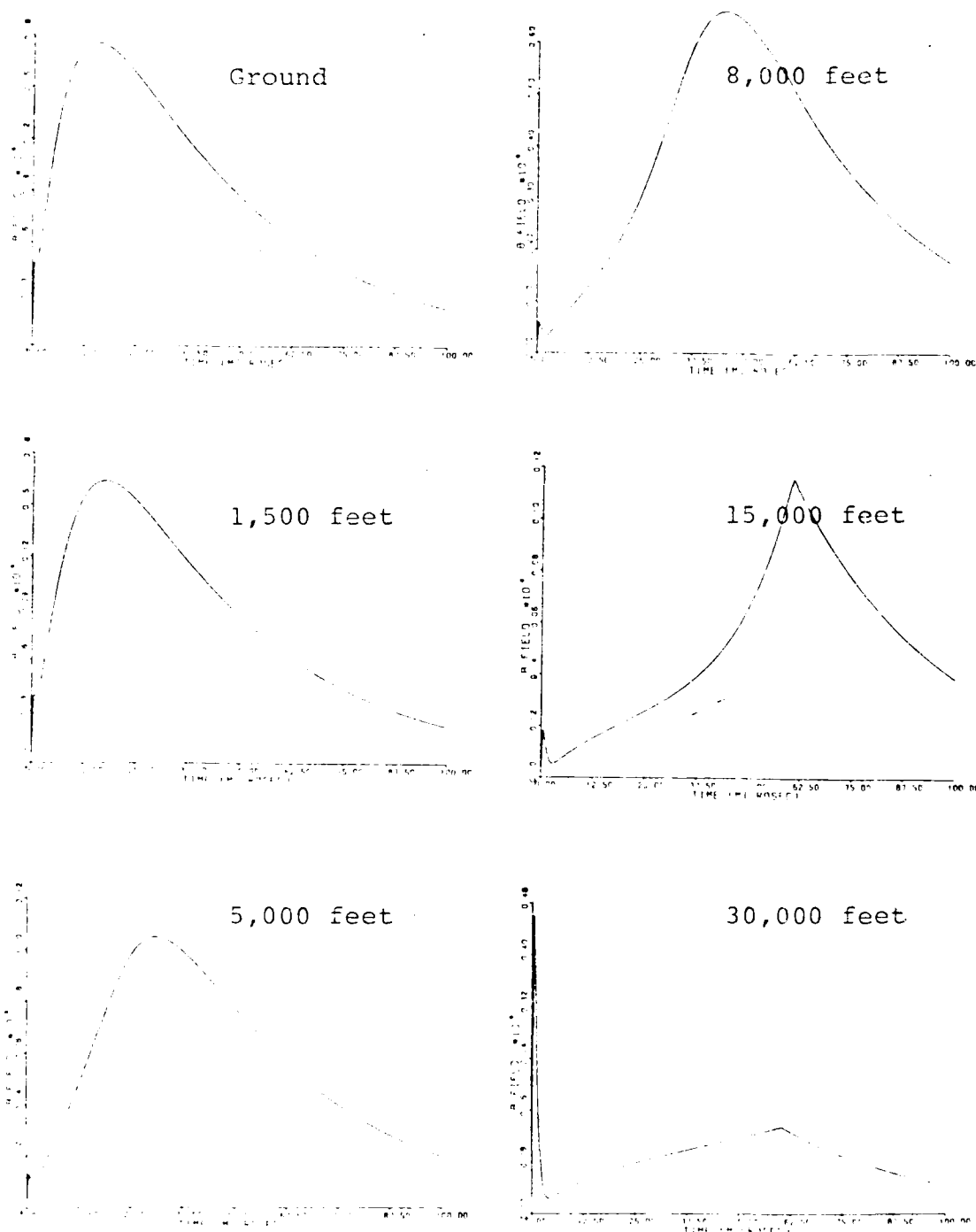


Fig. 5.41. Computer Solutions to Equation (40), the Magnetic Field, According to Model 1 at a Distance of 1 km, 1 μ sec Rise Time, and 25 μ sec Fall Time for the Ground and at Five Altitudes.

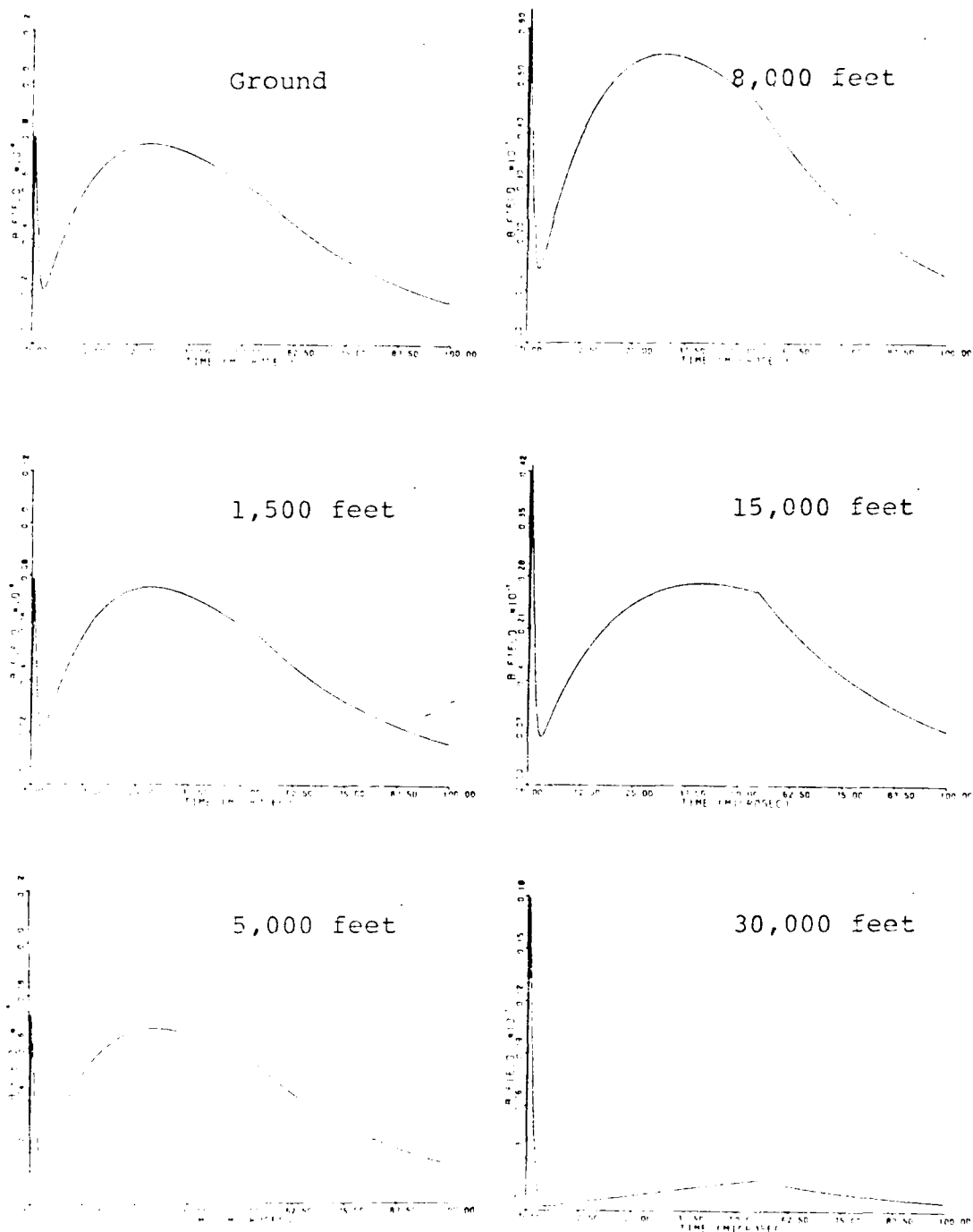


Fig. 5.42. Computer Solutions to Equation (40), the Magnetic Field, According to Model 1 at a Distance of 5 km, 1 μ sec Rise Time, and 25 μ sec Fall Time for the Ground and at Five Altitudes.

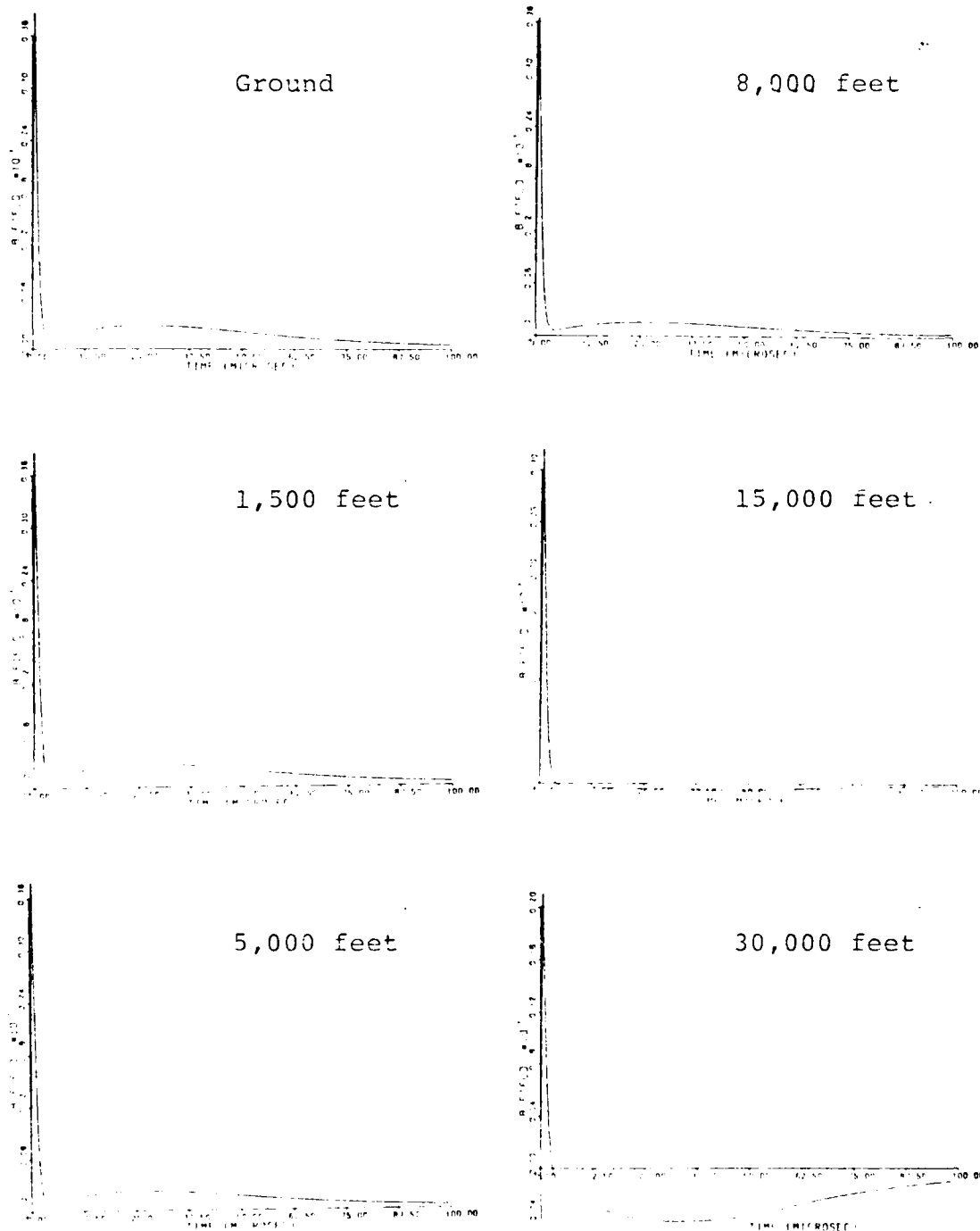


Fig. 5.43. Computer Solutions to Equation (40), the Magnetic Field, According to Model 1 at a Distance of 10 km, 1 μ sec Rise Time, and 25 μ sec Fall Time for the Ground and at Five Altitudes.

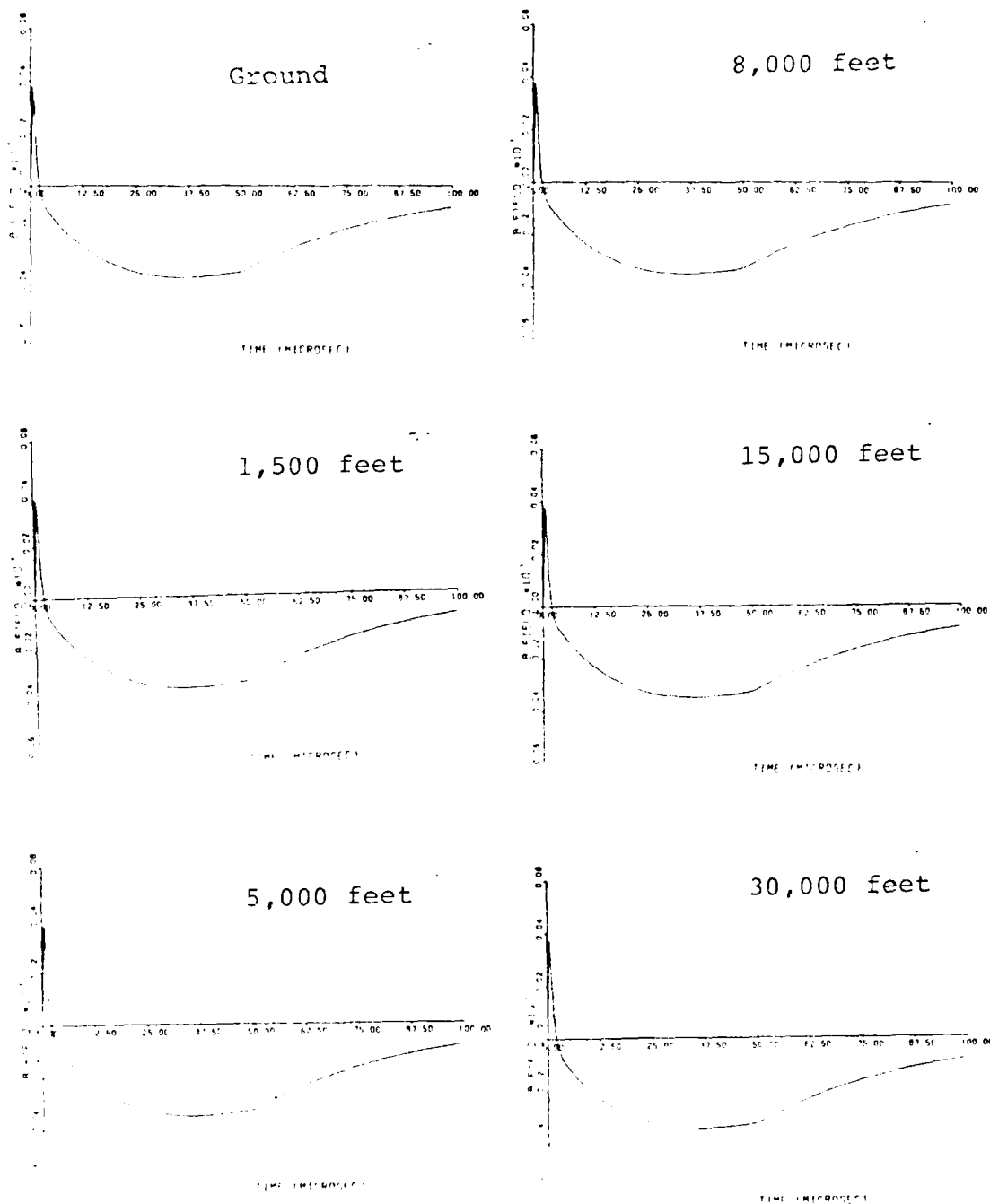


Fig. 5.44. Computer Solutions to Equation (40), the Magnetic Field, According to Model 1 at a Distance of 100 km, 1 μ sec Rise Time, and 25 μ sec Fall Time for the Ground and at Five Altitudes.

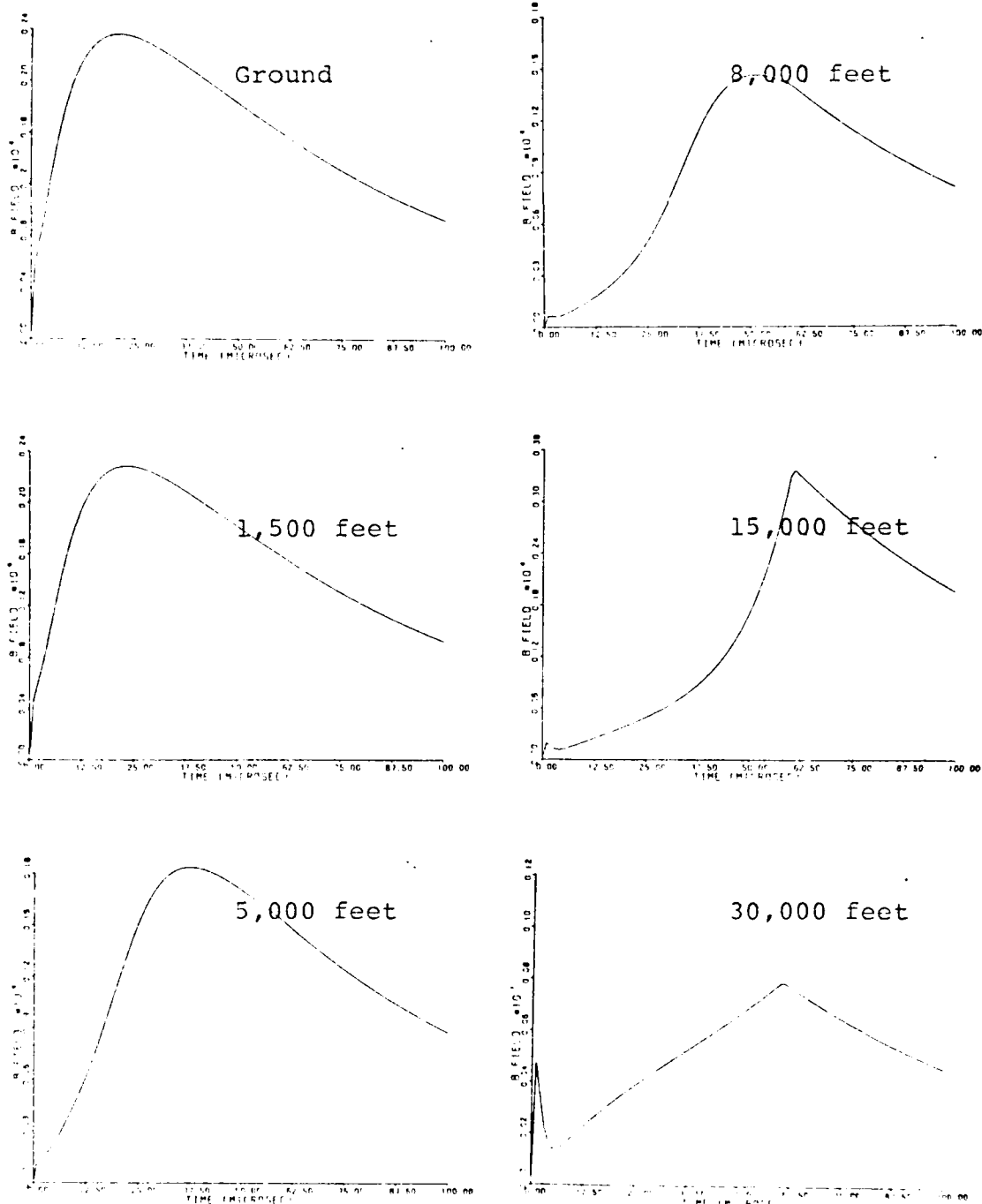


Fig. 5.45. Computer Solutions to Equation (40), the Magnetic Field, According to Model 1 at a Distance of 1 km, 2 μ sec Rise Time, and 50 μ sec Fall Time for the Ground and at Five Altitudes.

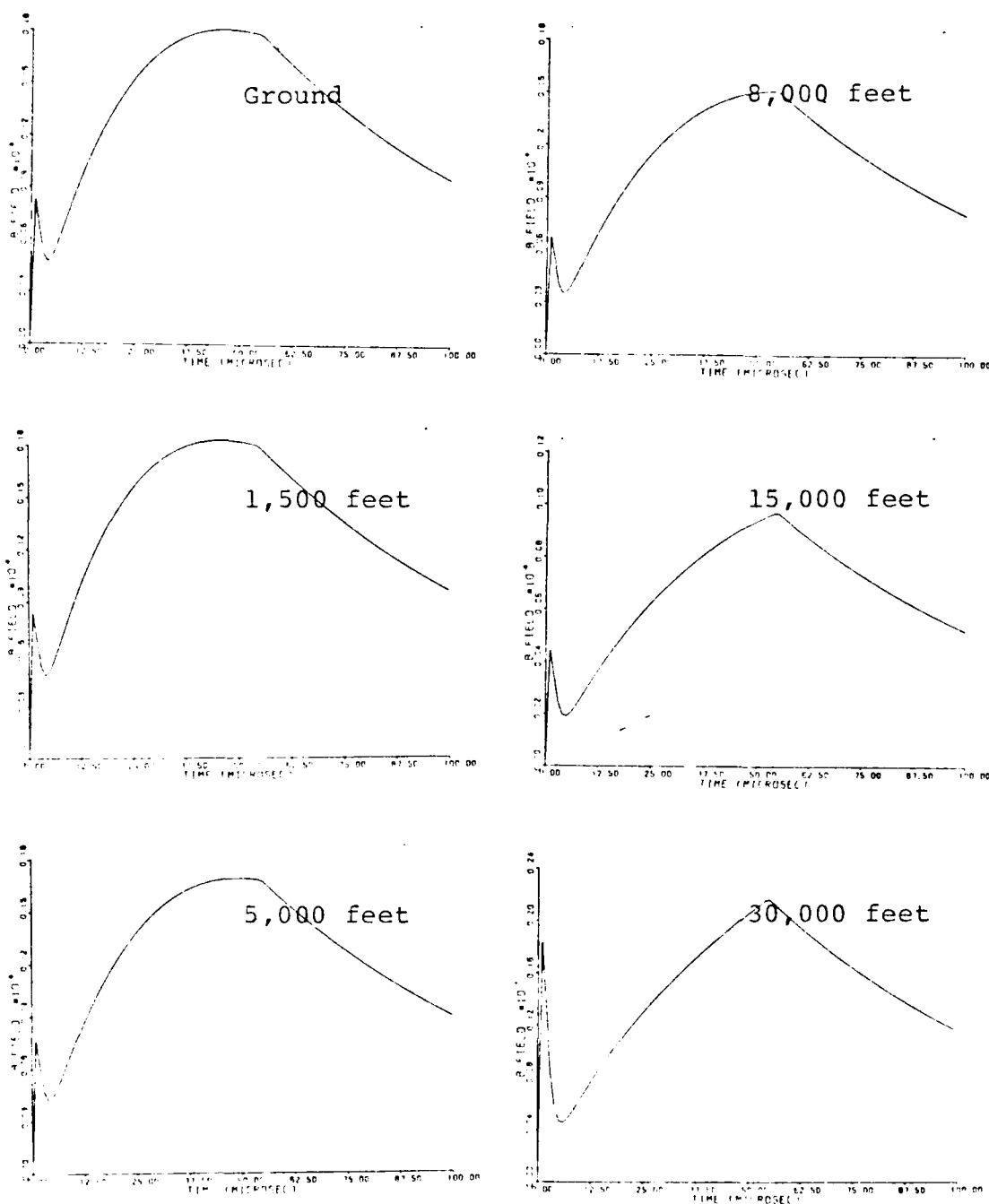


Fig. 5.46. Computer Solutions to Equation (40), the Magnetic Field, According to Model 1 at a Distance of 5 km, 2 μ sec Rise Time, and 50 μ sec Fall Time for the Ground and at Five Altitudes.

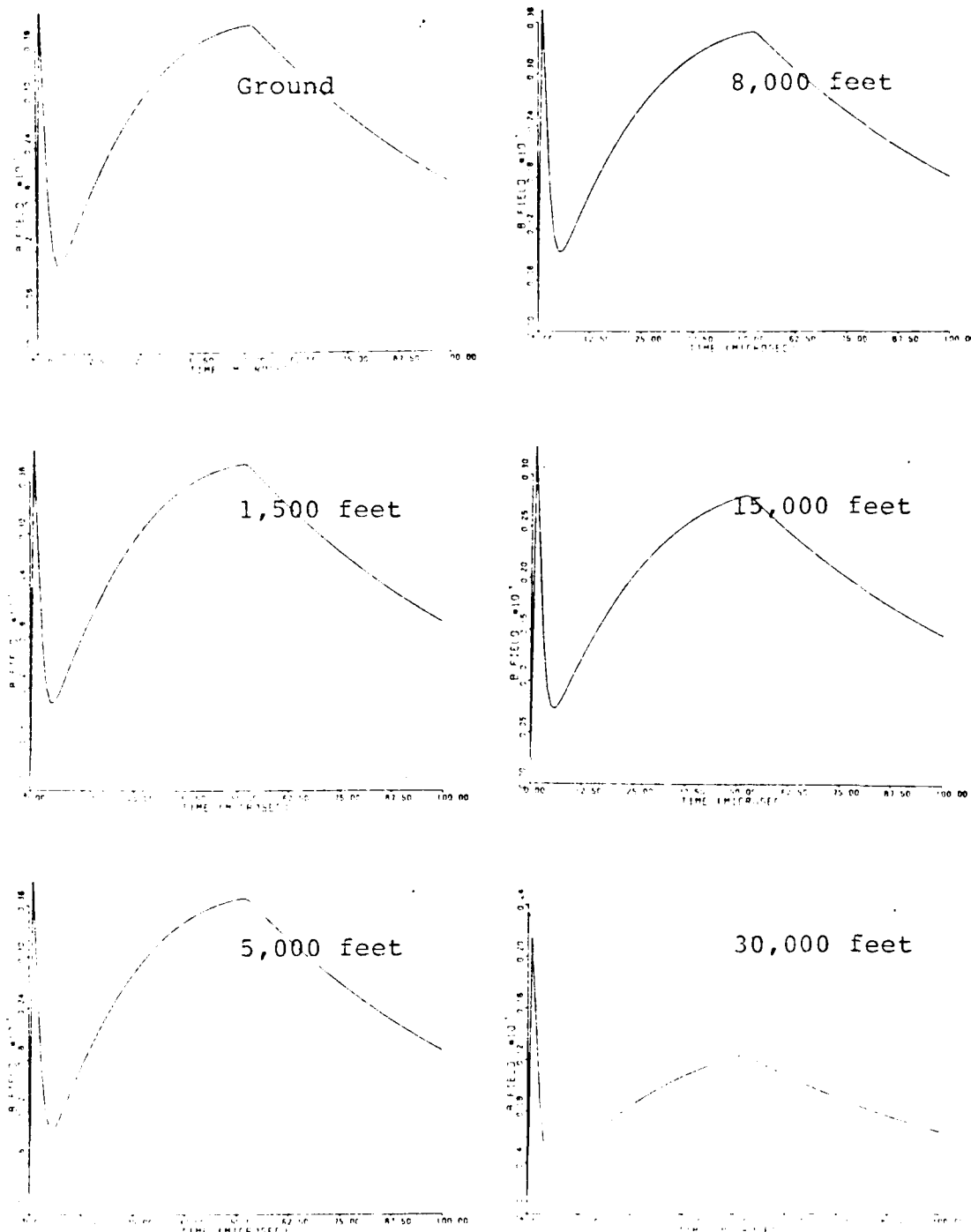


Fig. 5.47. Computer Solutions to Equation (40), the Magnetic Field, According to Model 1 at a Distance of 10 km, 2 μ sec Rise Time, and 50 μ sec Fall Time for the Ground and at Five Altitudes.

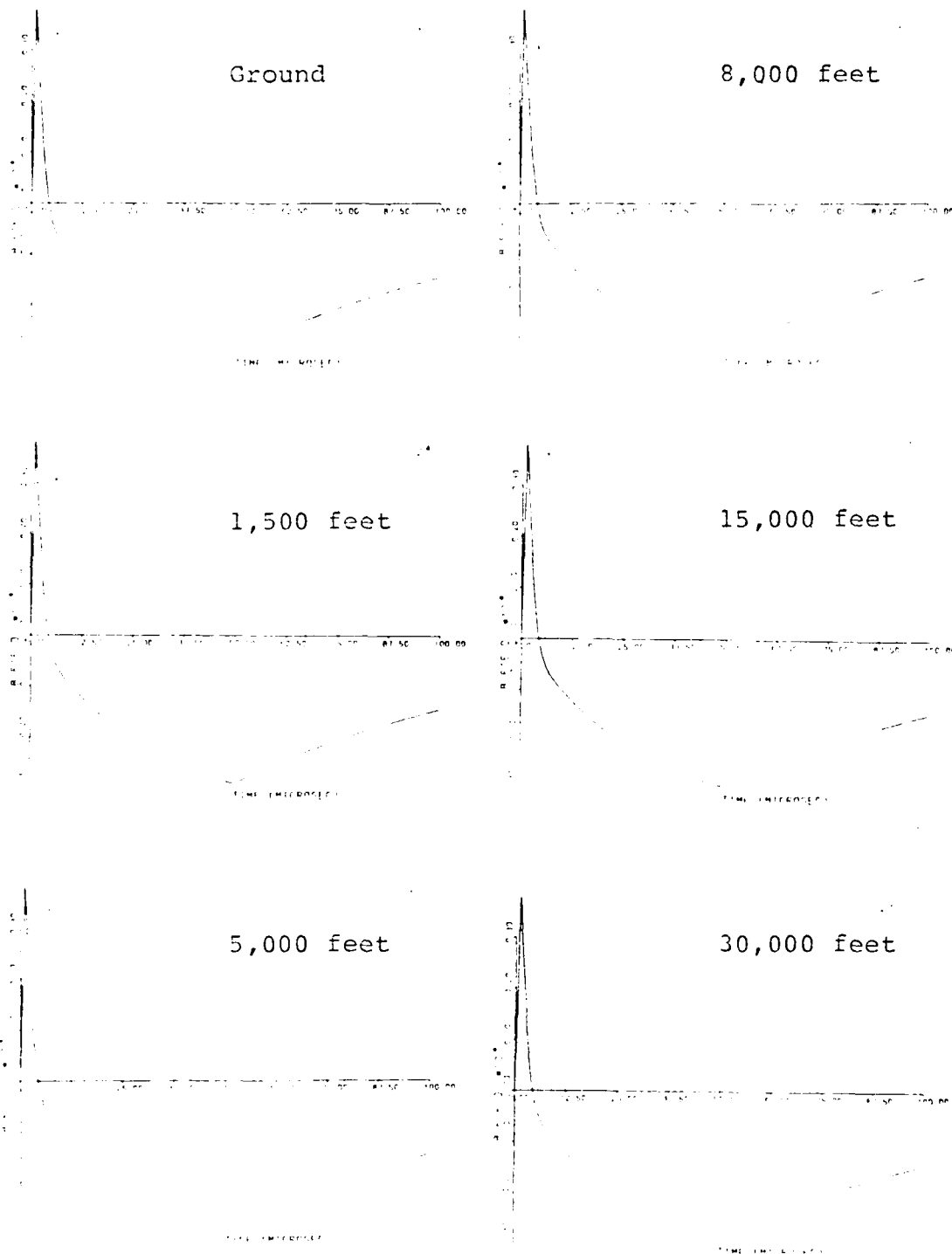


Fig. 5.48. Computer Solutions to Equation (40), the Magnetic Field, According to Model 1 at a Distance of 100 km, 2 usec Rise Time, and 50 usec Fall Time for the Ground and at Five Altitudes.

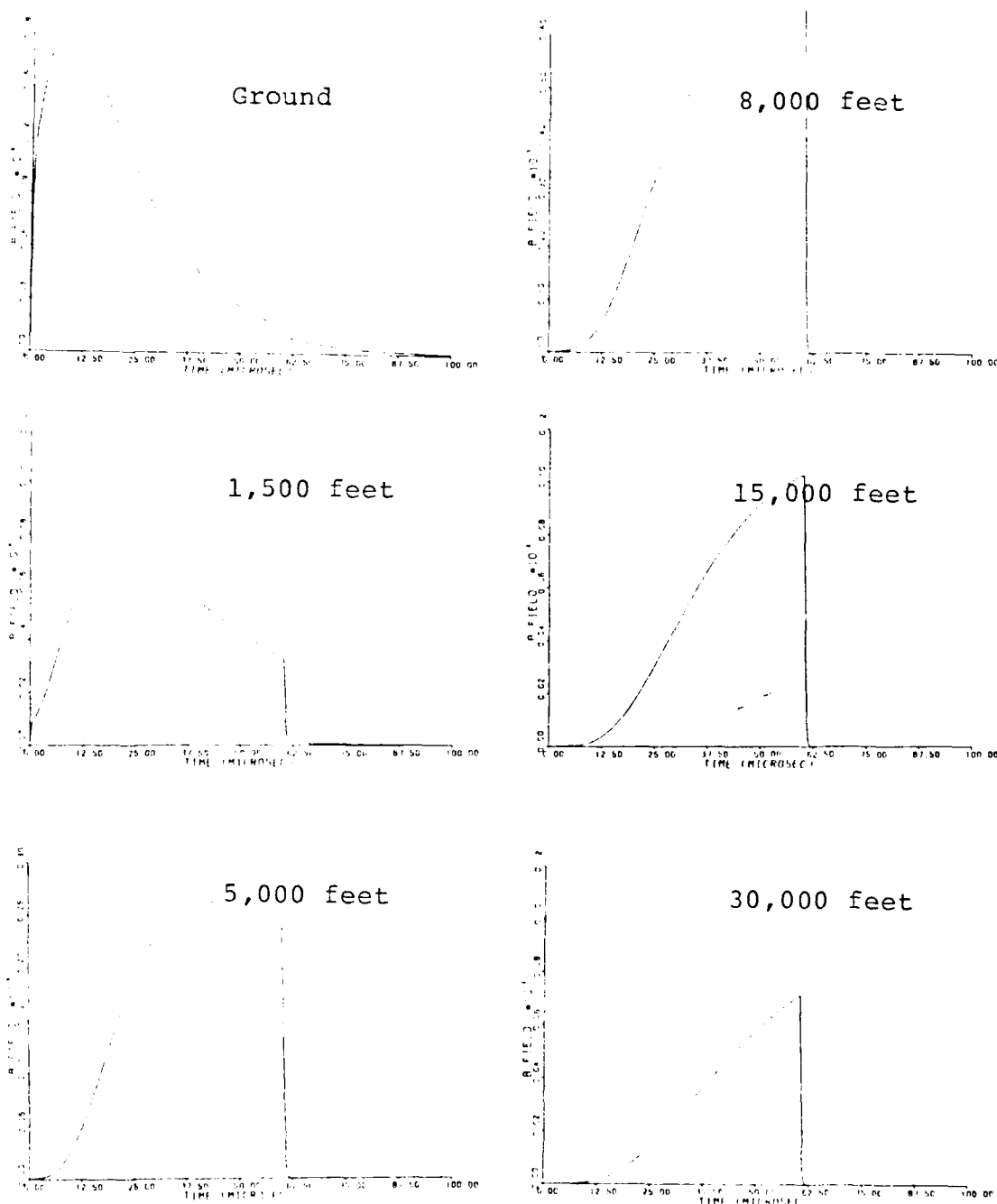


Fig. 5.49. Computer Solutions to Equation (40), the Magnetic Field, According to Model 2 at a Distance of 1 km, 500 nsec Rise Time, and 10 nsec Fall Time for the Ground and at Five Altitudes.

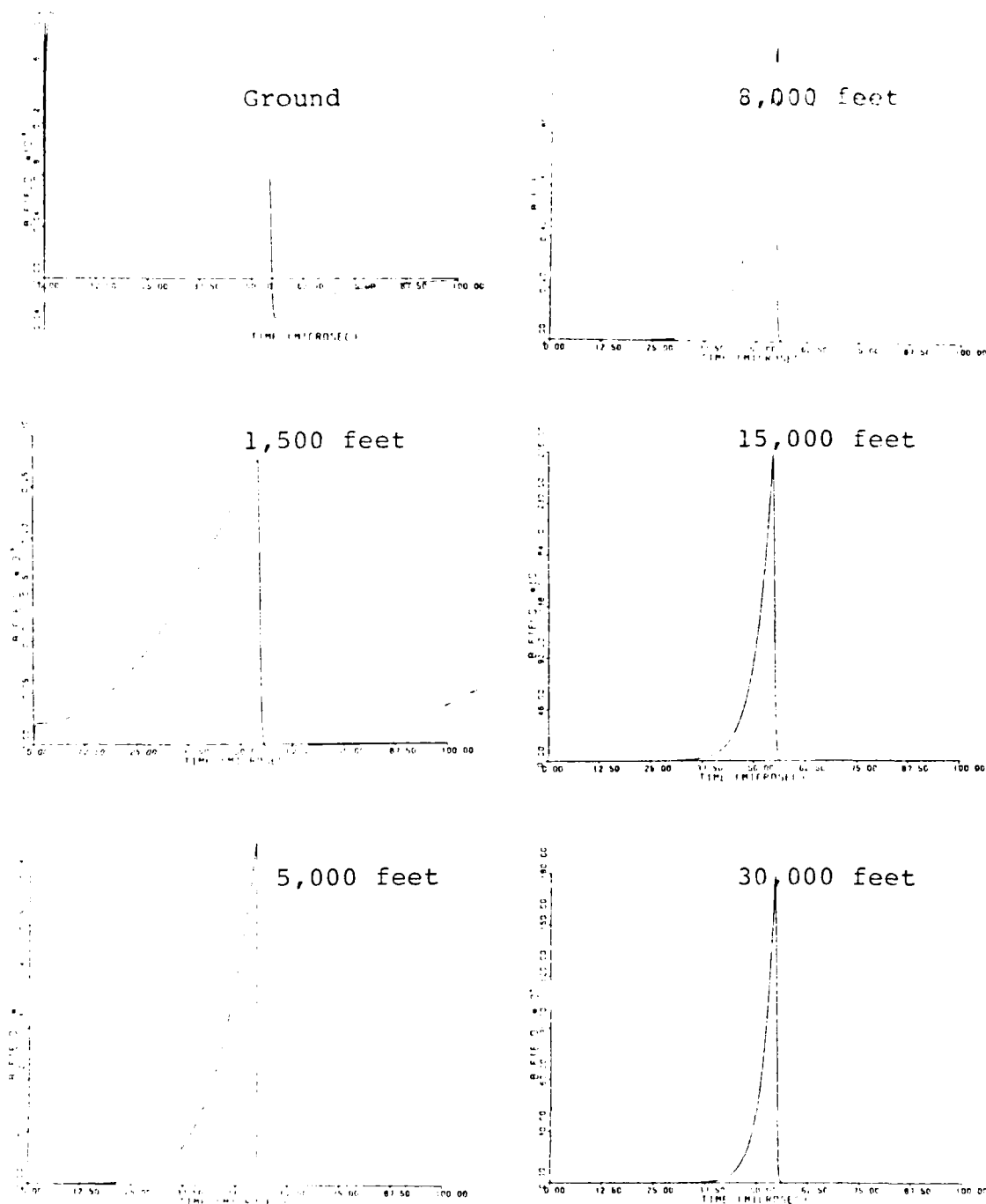


Fig. 5.50. Computer Solutions to Equation (40), the Magnetic Field, According to Model 2 at a Distance of 5 km, 500 nsec Rise Time, and 10 μ sec Fall Time for the Ground and at Five Altitudes.

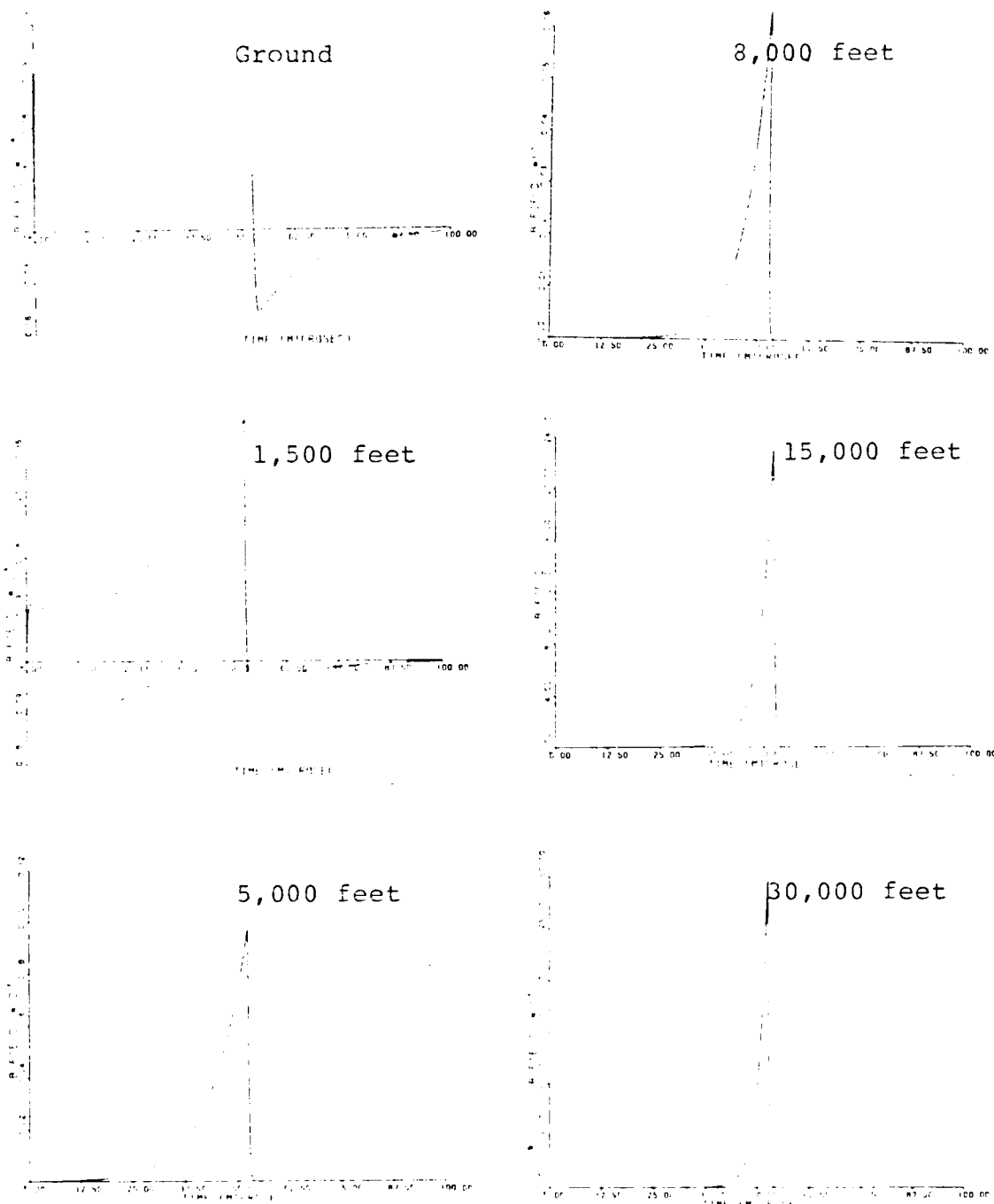


Fig. 5.51. Computer Solutions to Equation (40), the Magnetic Field, According to Model 2 at a Distance of 10 km, 500 nsec Rise Time, and 10 μ sec Fall Time for the Ground and at Five Altitudes.

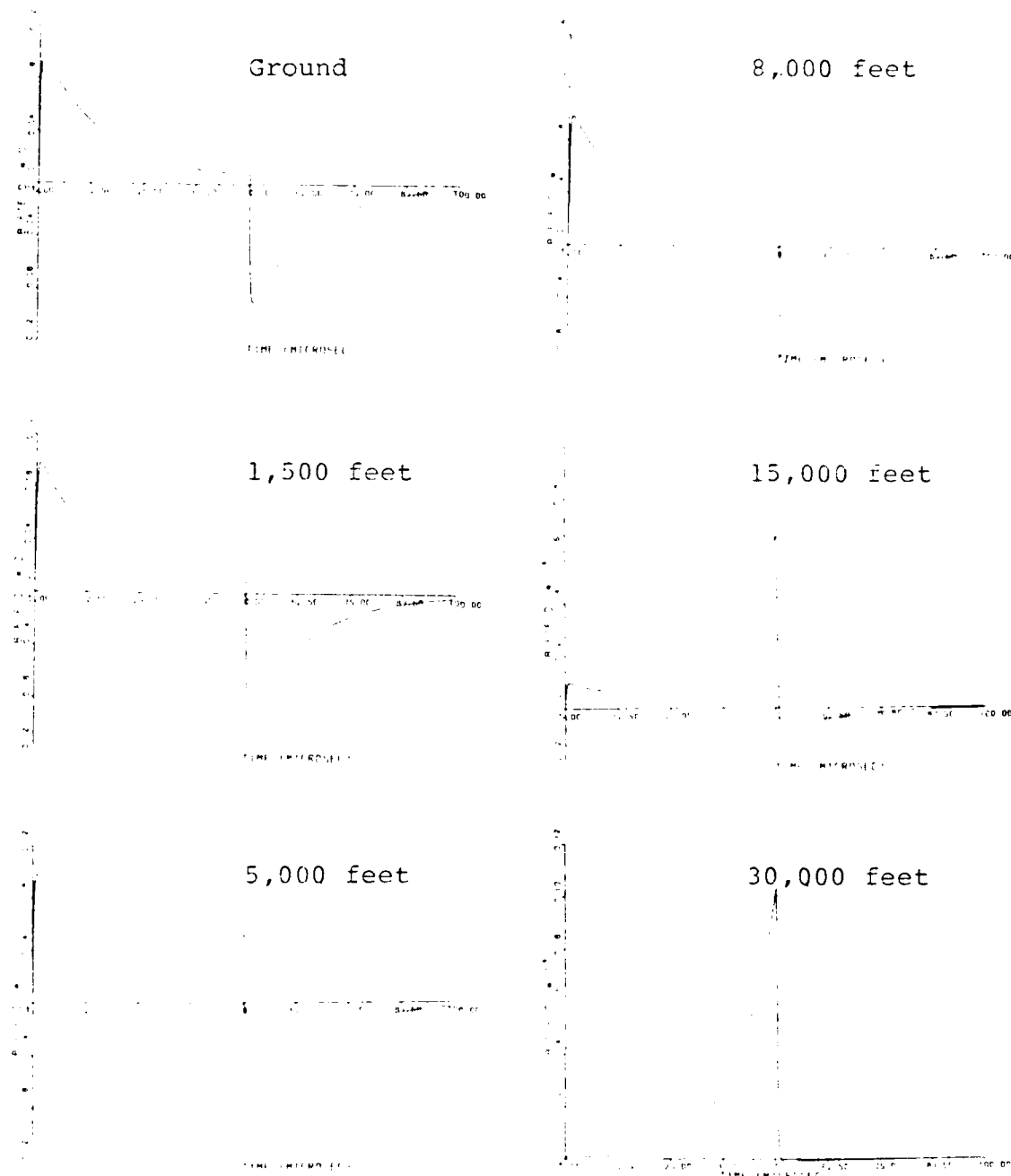


Fig. 5.52. Computer Solutions to Equation (40), the Magnetic Field, According to Model 2 at a Distance of 100 km, 500 nsec Rise Time, and 10 μ sec Fall Time for the Ground and at Five Altitudes.

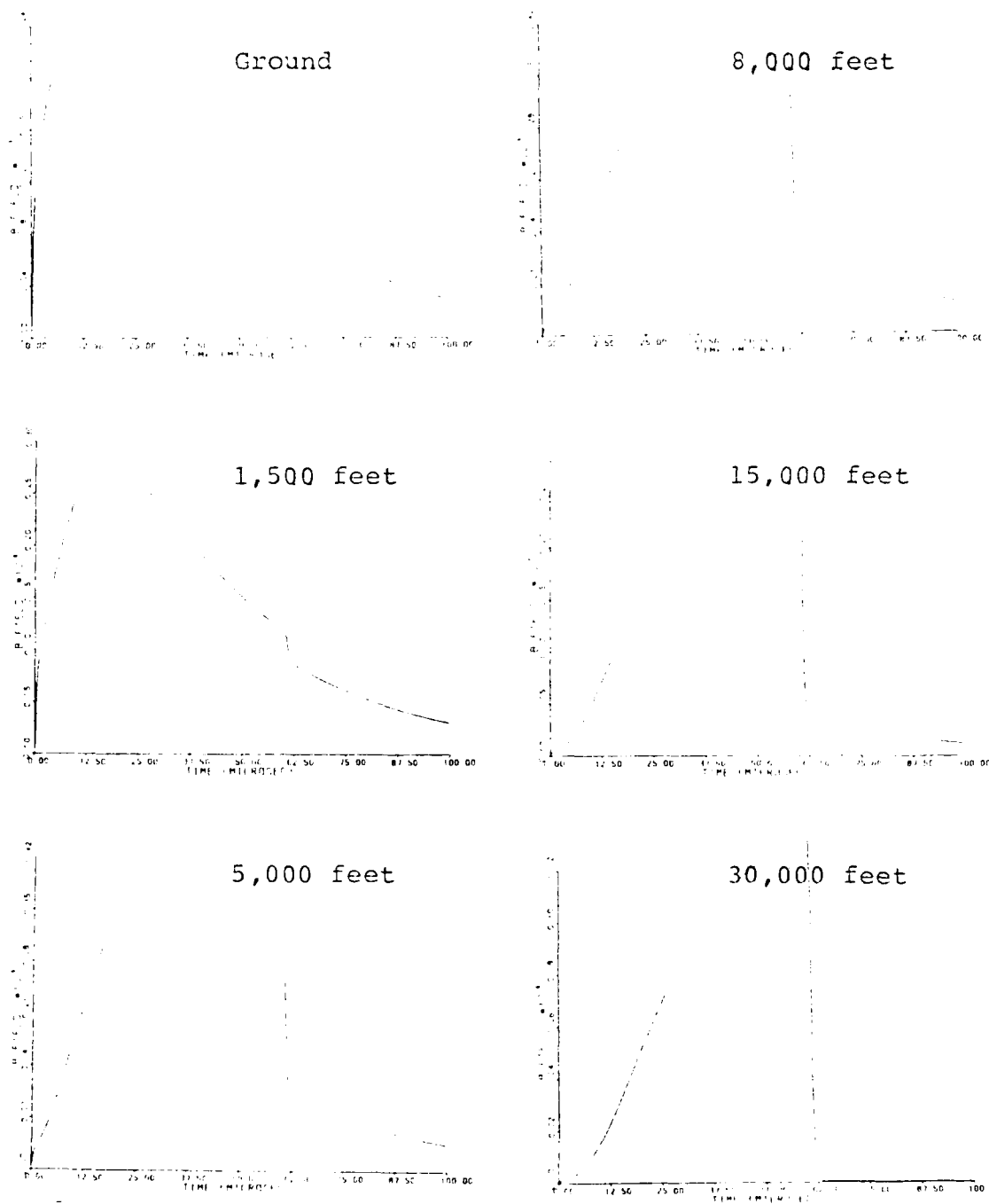


Fig. 5.53. Computer Solutions to Equation (40), the Magnetic Field, According to Model 2 at a Distance of 1 km. 1 μ sec Rise Time, and 25 μ sec Fall Time for the Ground and at Five Altitudes.

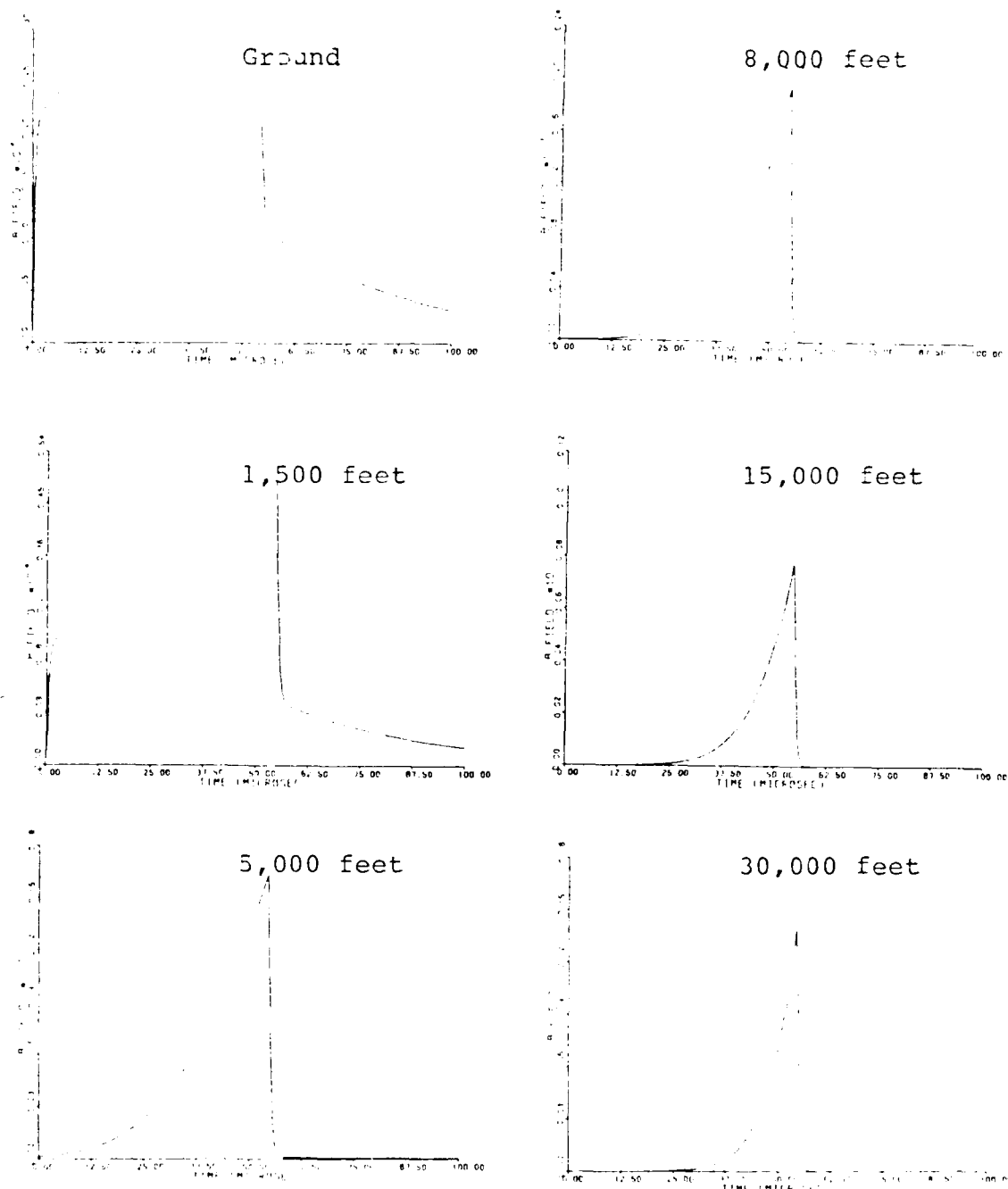


Fig. 5.54. Computer Solutions to Equation (40), the Magnetic Field, According to Model 2 at a Distance of 5 km, 1 μ sec Rise Time, and 25 μ sec Fall Time for the Ground and at Five Altitudes.

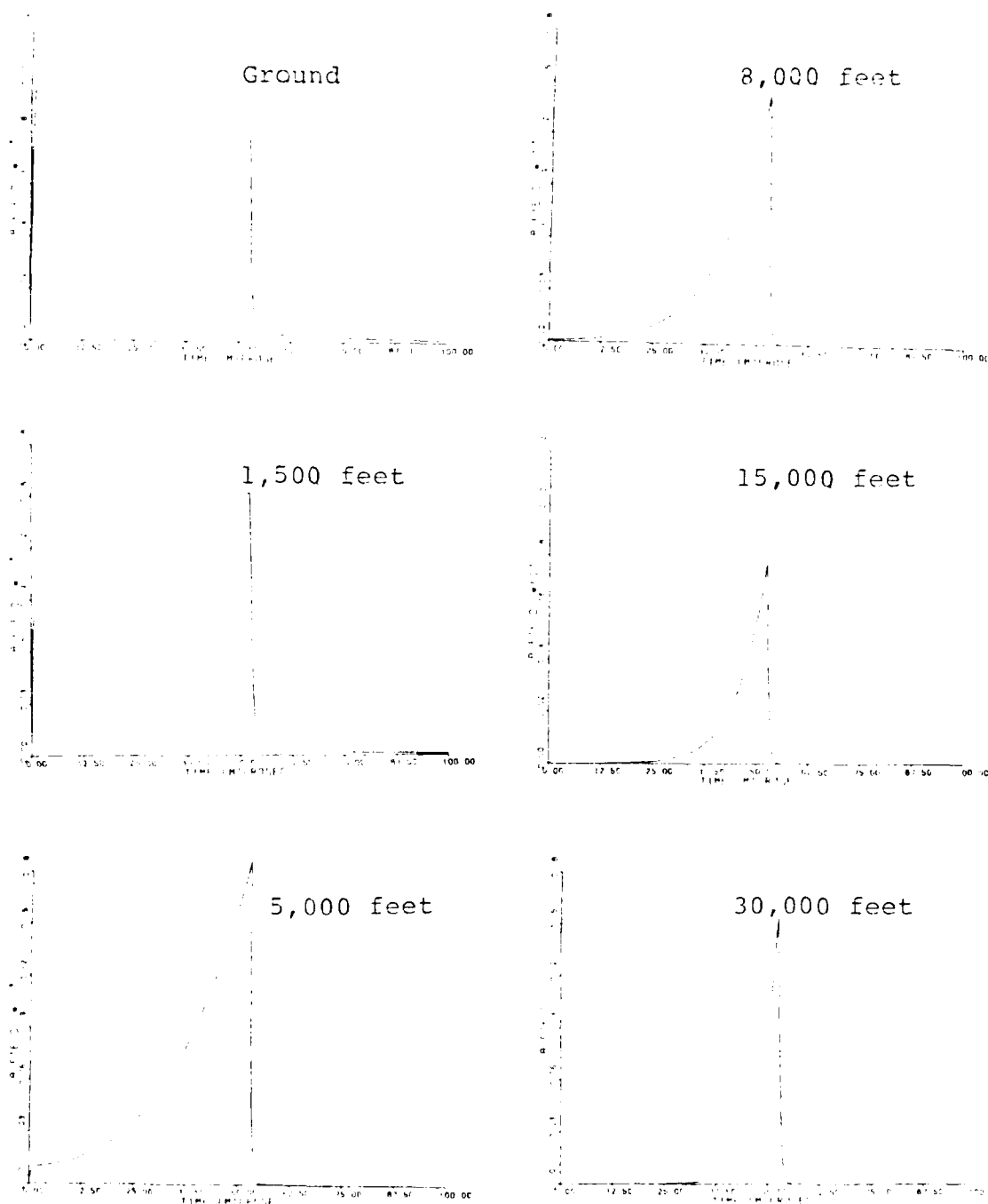


Fig. 5.55. Computer Solutions to Equation (40), the Magnetic Field, According to Model 2 at a Distance of 10 km, 1 μ sec Rise Time, and 25 μ sec Fall Time for the Ground and at Five Altitudes.

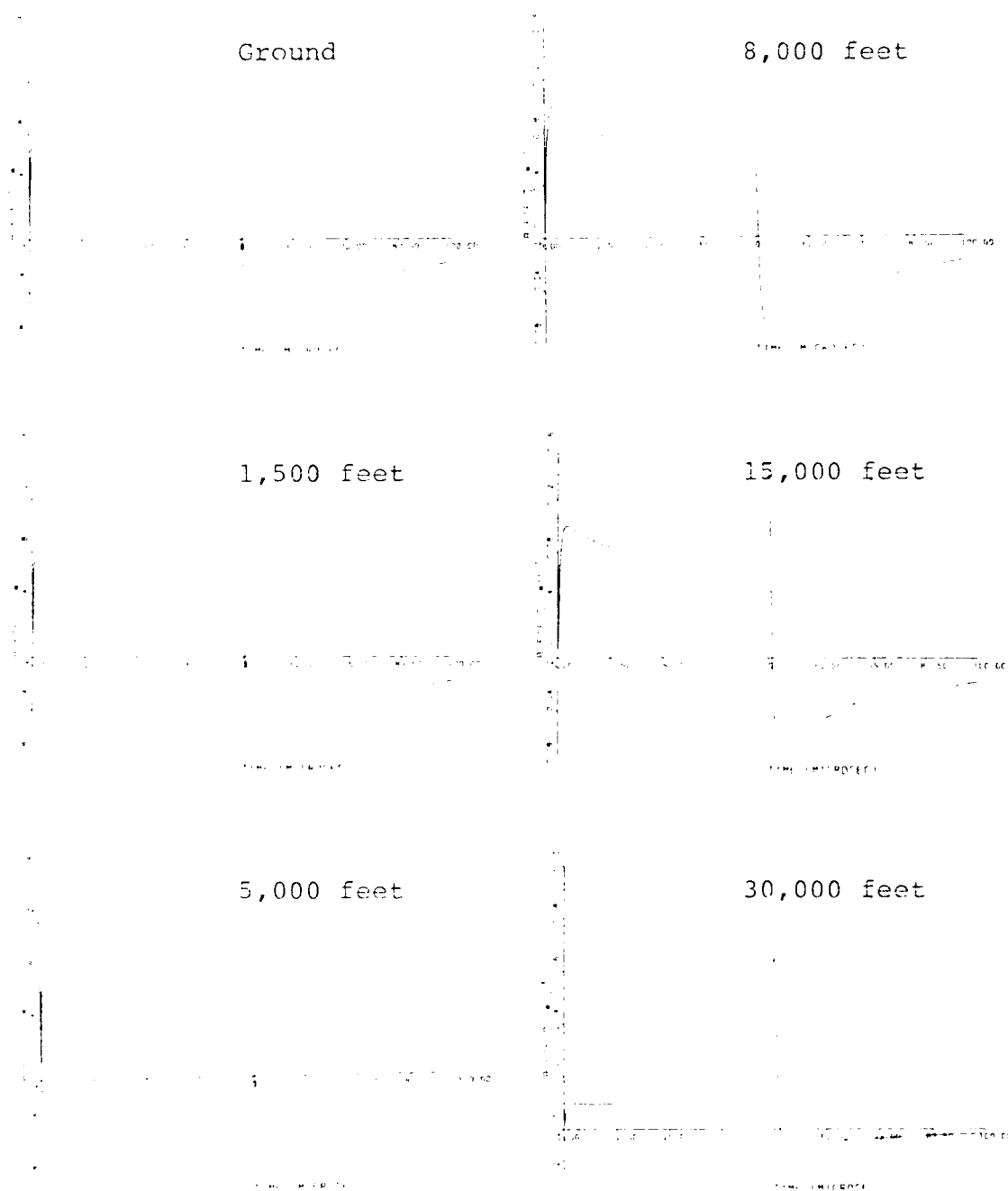


Fig. 5.56. Computer Solutions to Equation (40), the Magnetic Field, According to Model 2 at a Distance of 100 km, 1 μsec Rise Time, and 25 μsec Fall Time for the Ground and at Five Altitudes.

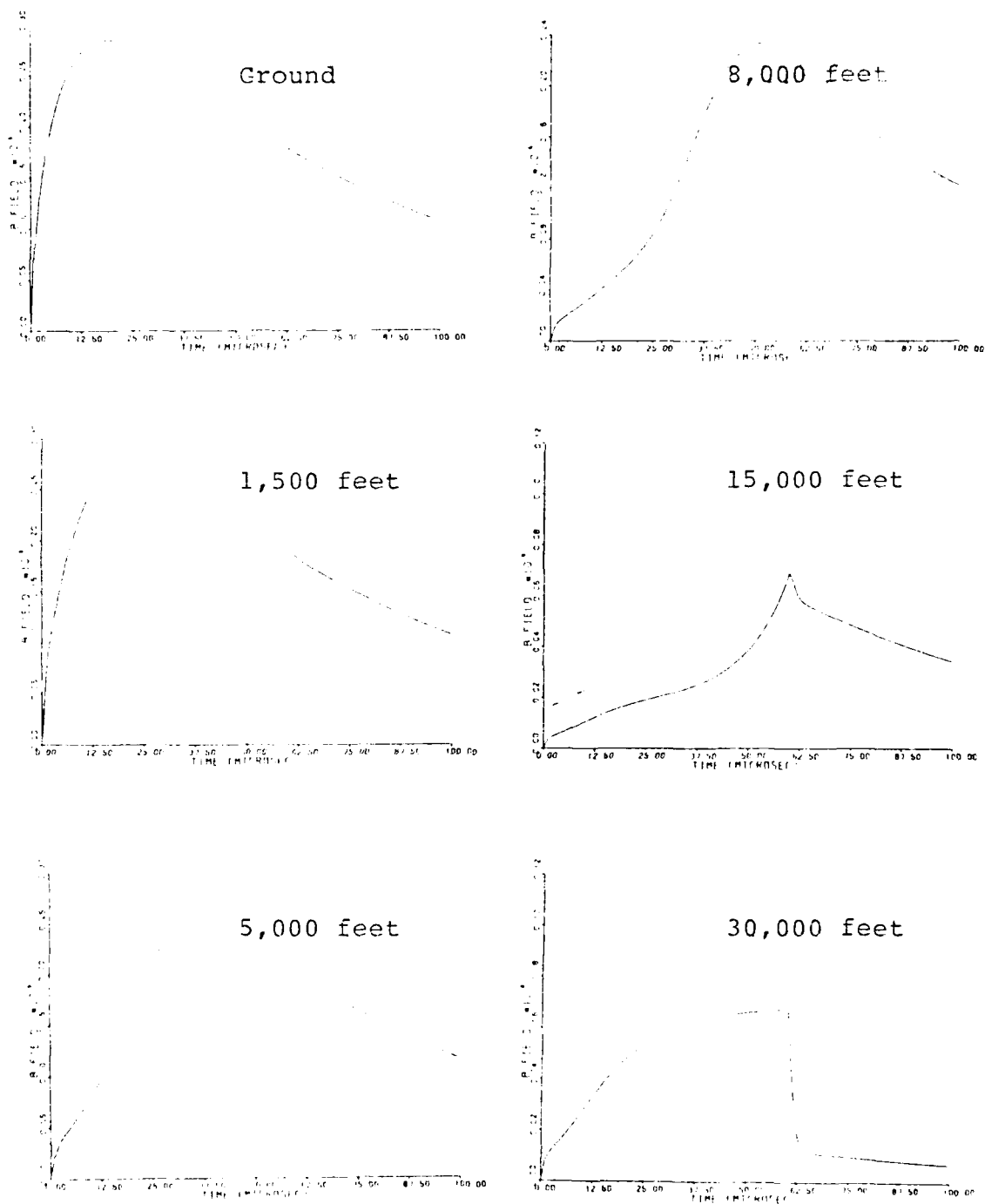


Fig. 5.57. Computer Solutions to Equation (40), the Magnetic Field, According to Model 2 at a Distance of 1 km, 2 μ sec Rise Time, and 50 μ sec Fall Time for the Ground and at Five Altitudes.

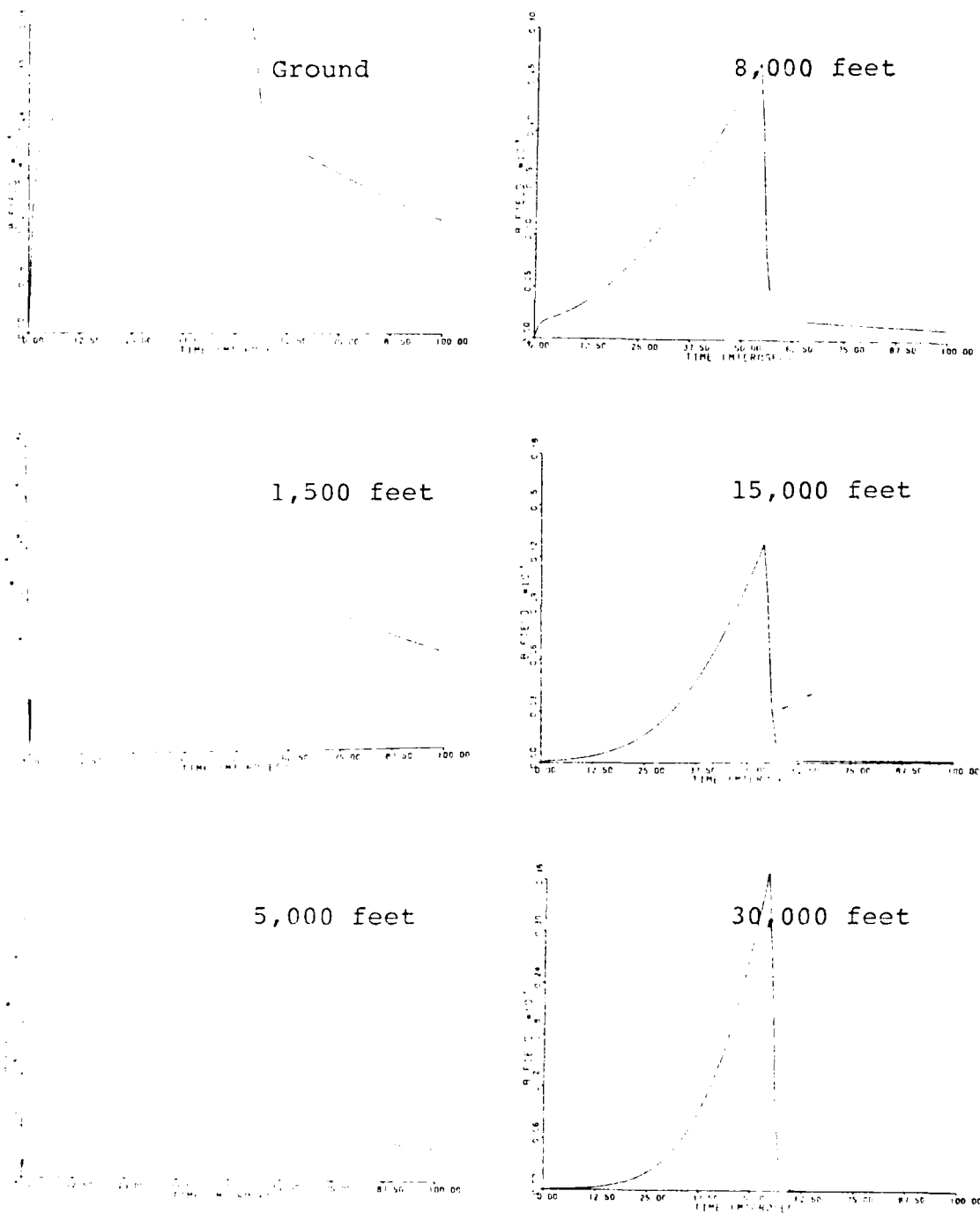


Fig. 5.58. Computer Solutions to Equation (40), the Magnetic Field, According to Model 2 at a Distance of 5 km, 2 μ sec Rise Time, and 50 μ sec Fall Time for the Ground and at Five Altitudes.

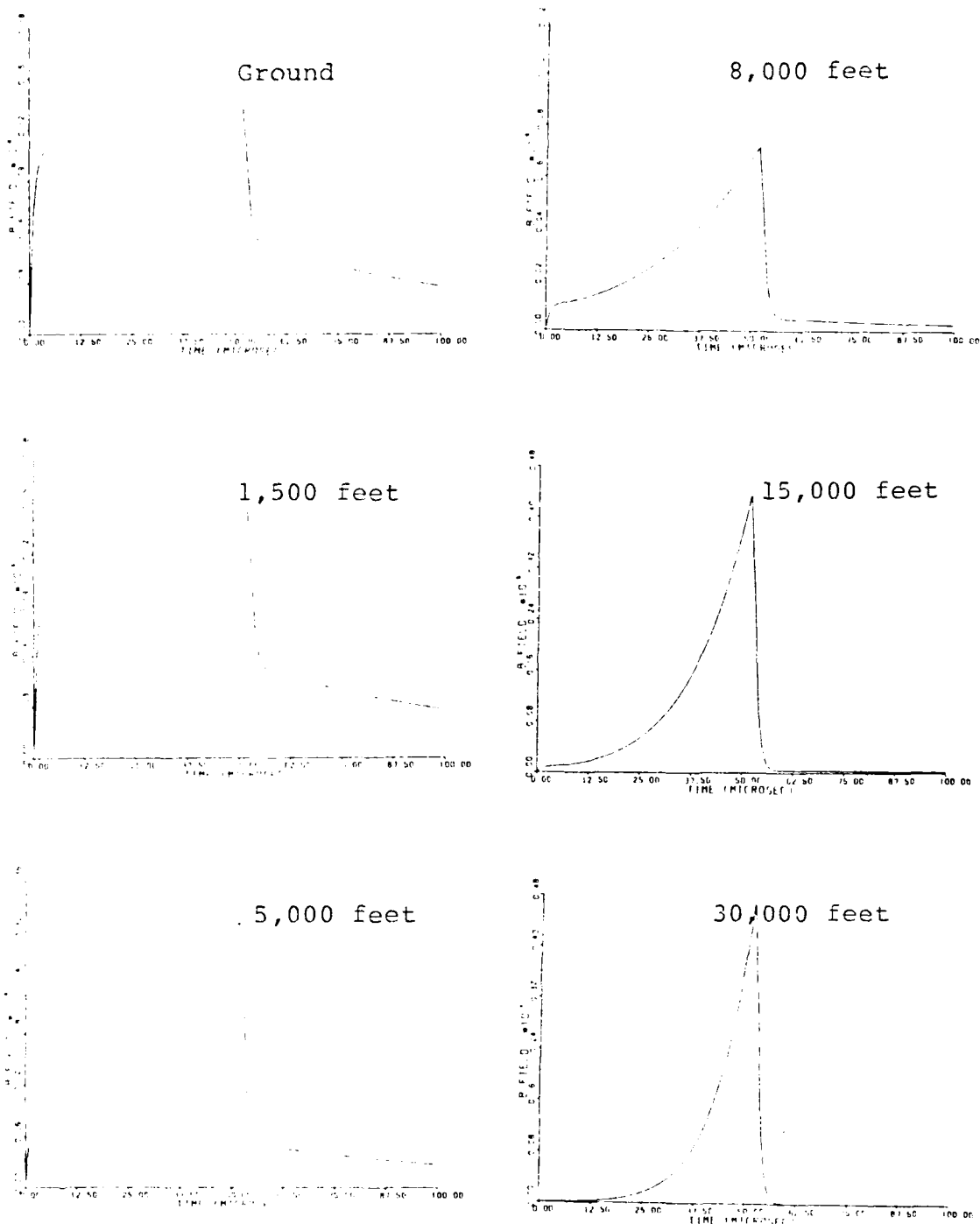


Fig. 5.59. Computer Solutions to Equation (40), the Magnetic Field, According to Model 2 at a Distance of 10 km, 2 μ sec Rise Time, and 50 μ sec Fall Time for the Ground and at Five Altitudes.

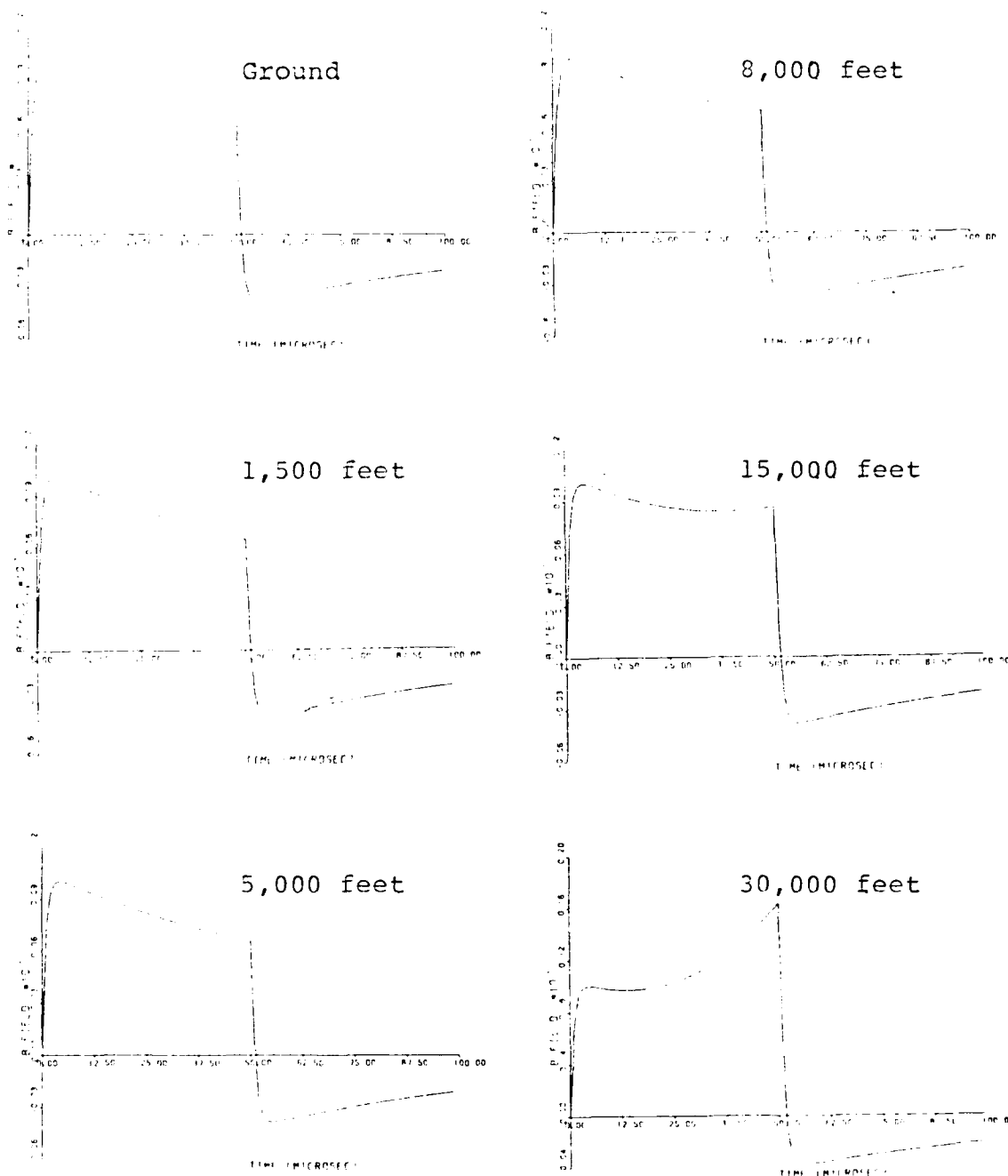


Fig. 5.60. Computer Solutions to Equation (40), the Magnetic Field, According to Model 2 at a Distance of 100 km, 2 μ sec Rise Time, and 50 μ sec Fall Time for the Ground and at Five Altitudes.

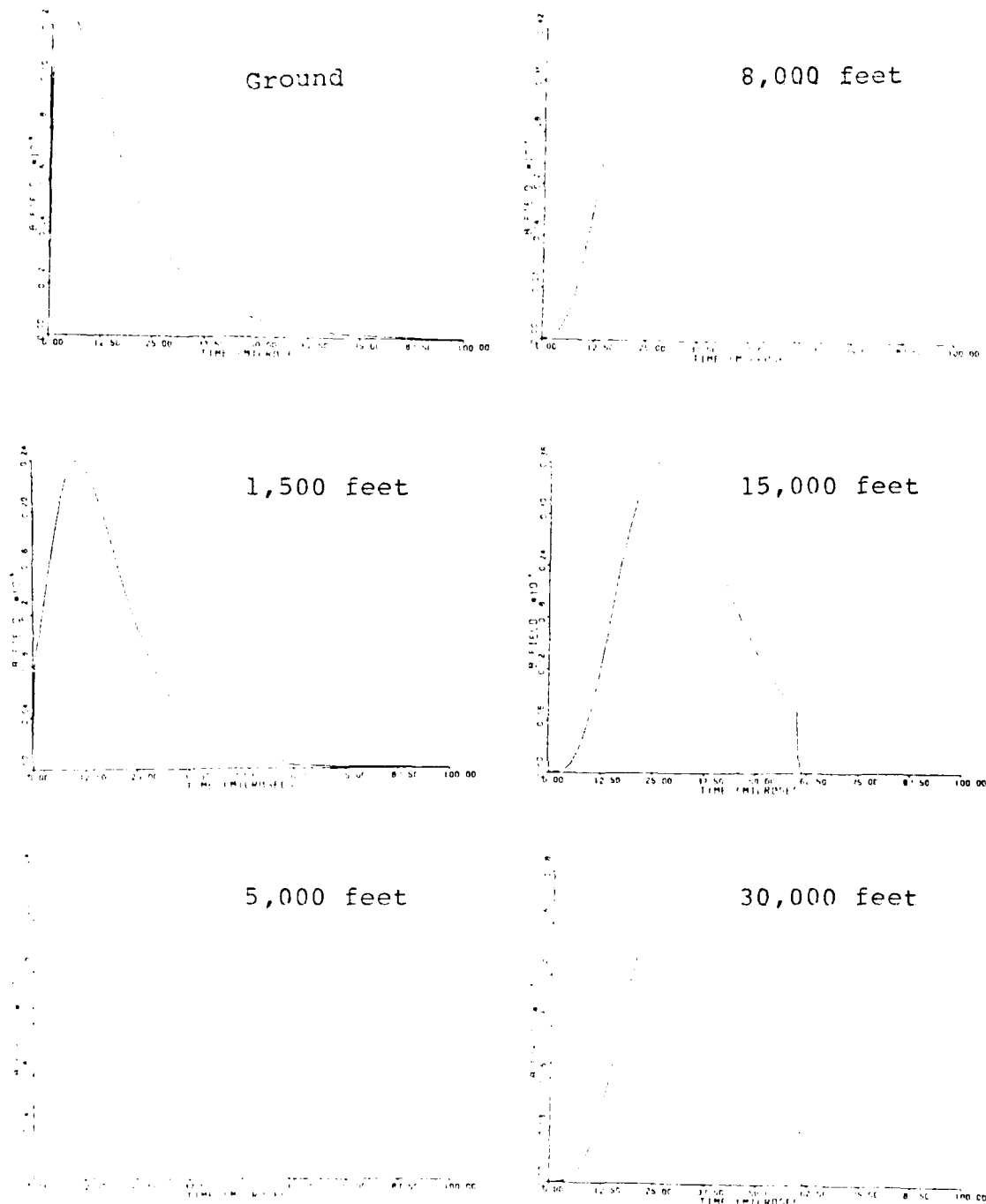


Fig. 5.61. Computer Solutions to Equation (40), the Magnetic Field, According to Model 3 at a Distance of 1 km, 500 nsec Rise Time, and 10 μ sec Fall Time for the Ground and at Five Altitudes.

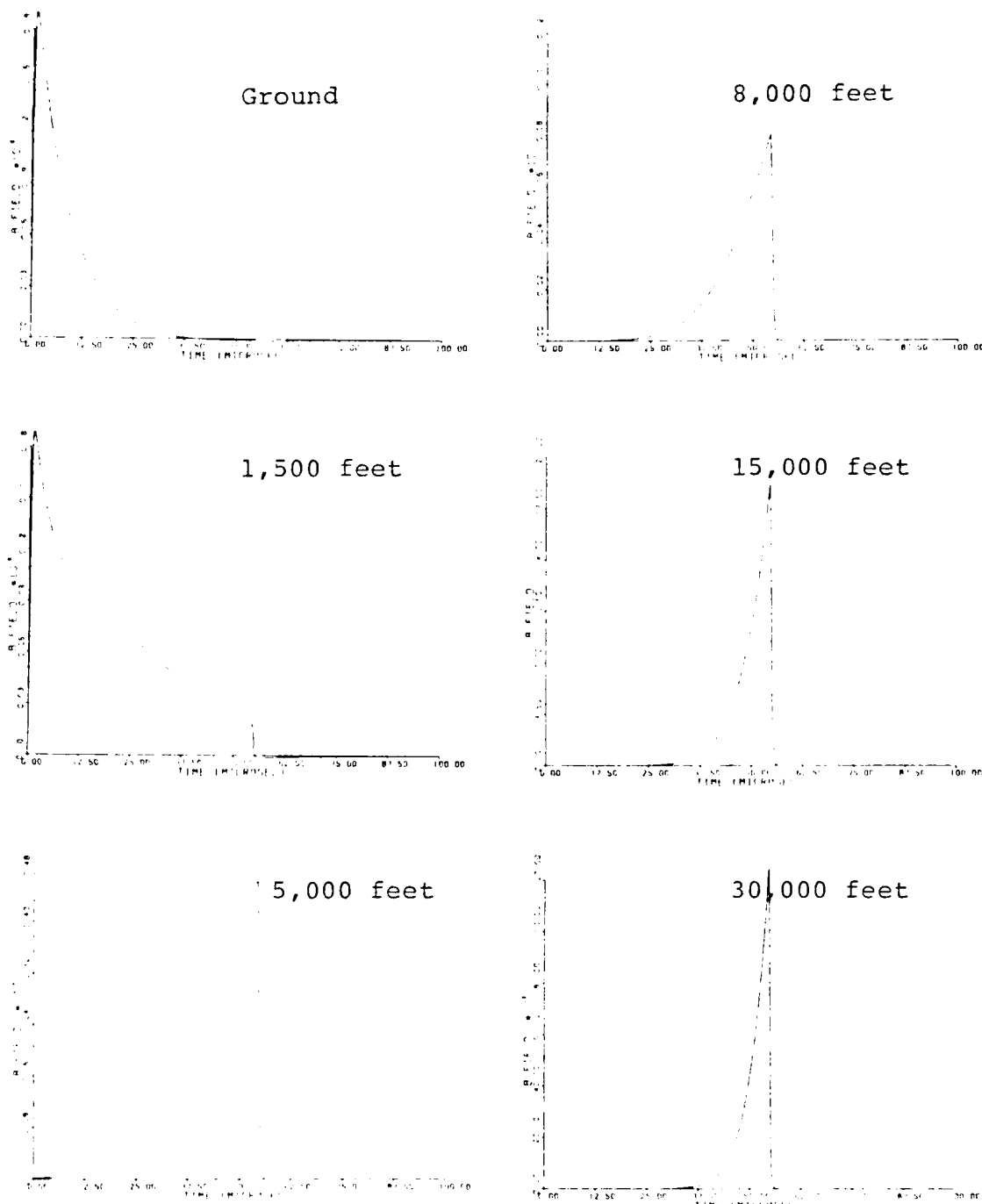


Fig. 5.62. Computer Solutions to Equation (40), the Magnetic Field, According to Model 3 at a Distance of 5 km, 500 nsec Rise Time, and 10 nsec Fall Time for the Ground and at Five Altitudes.

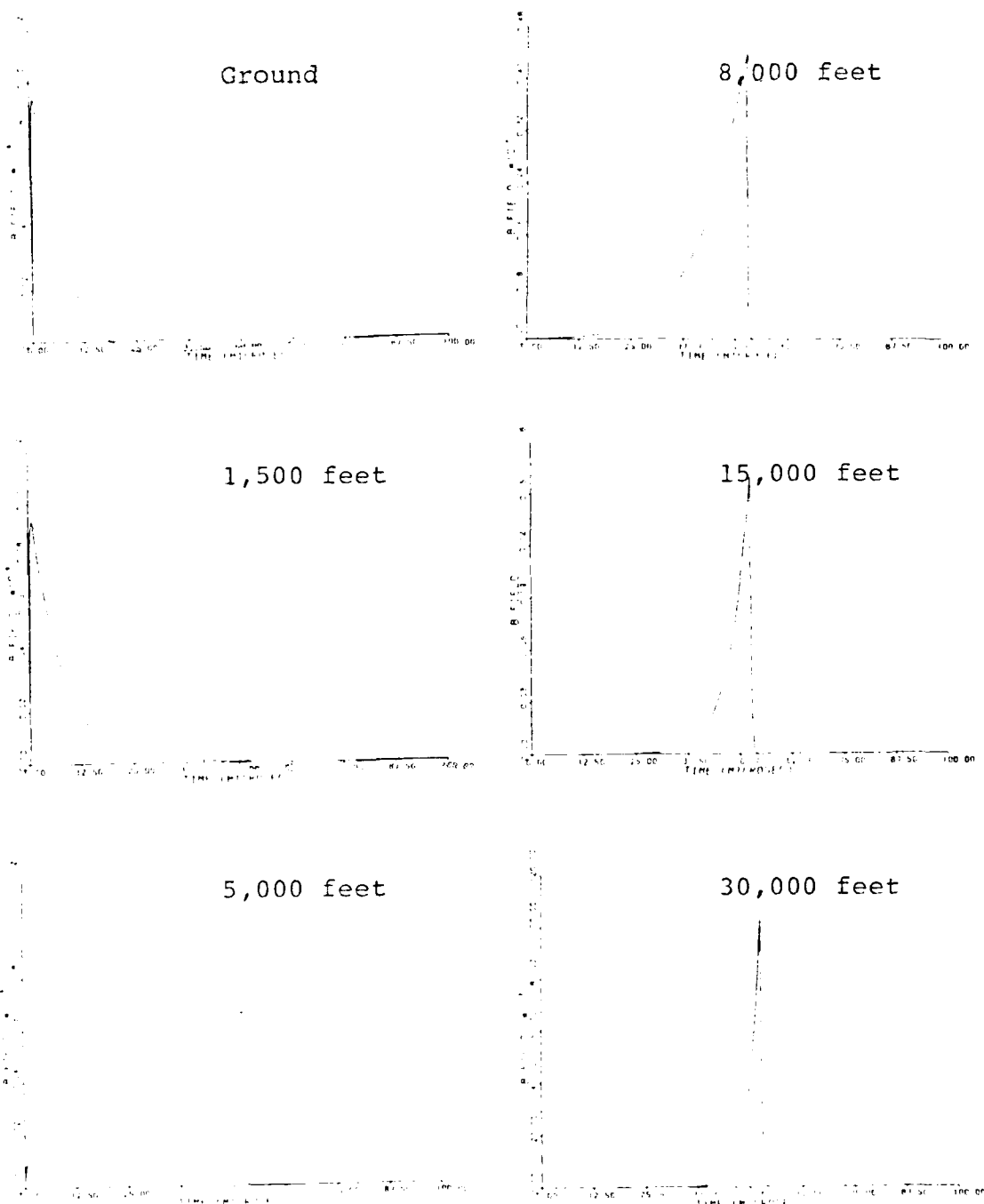


Fig. 5.63. Computer Solutions to Equation (40), the Magnetic Field, According to Model 3 at a Distance of 10 km, 500 nsec Rise Time, and 10 μ sec Fall Time for the Ground and at Five Altitudes.

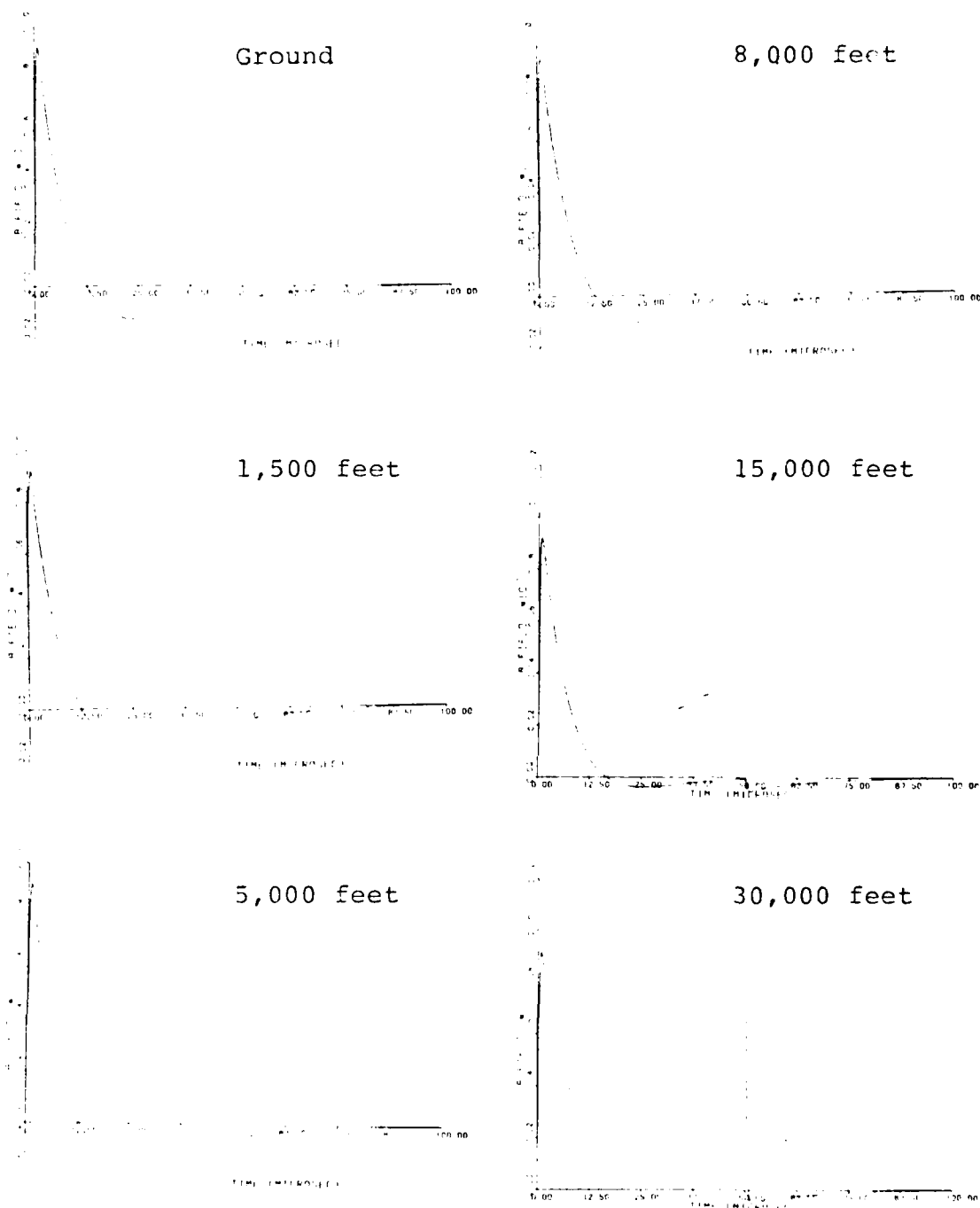


Fig. 5.64. Computer Solutions to Equation (40), the Magnetic Field, According to Model 3 at a Distance of 100 km, 500 nsec Rise Time, and 10 usec Fall Time for the Ground and at Five Altitudes,

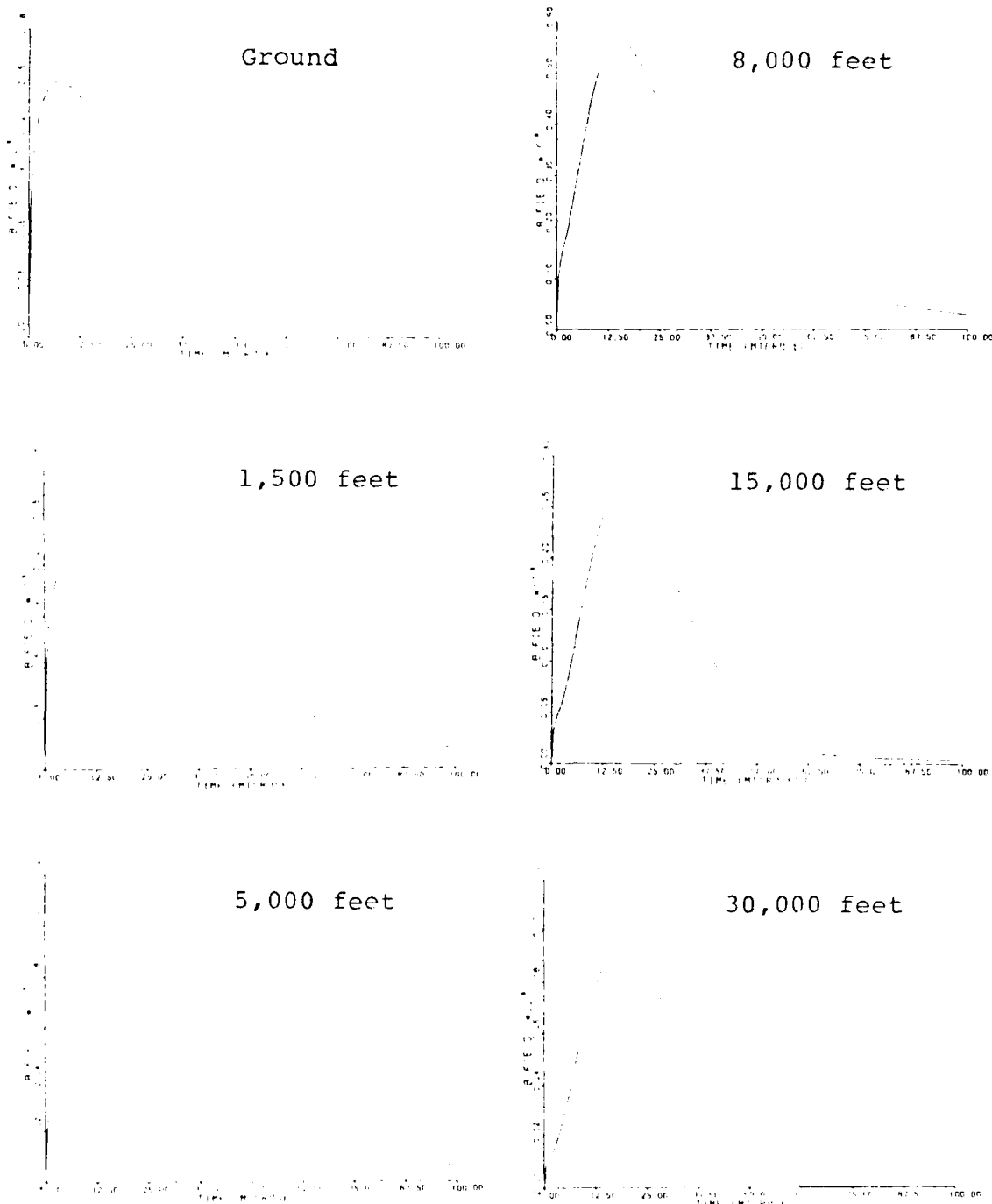


Fig. 5.65. Computer Solutions to Equation (40), the Magnetic Field, According to Model 3 at a Distance of 1 km, 1 μ sec Rise Time, and 25 μ sec Fall Time for the Ground and at Five Altitudes.

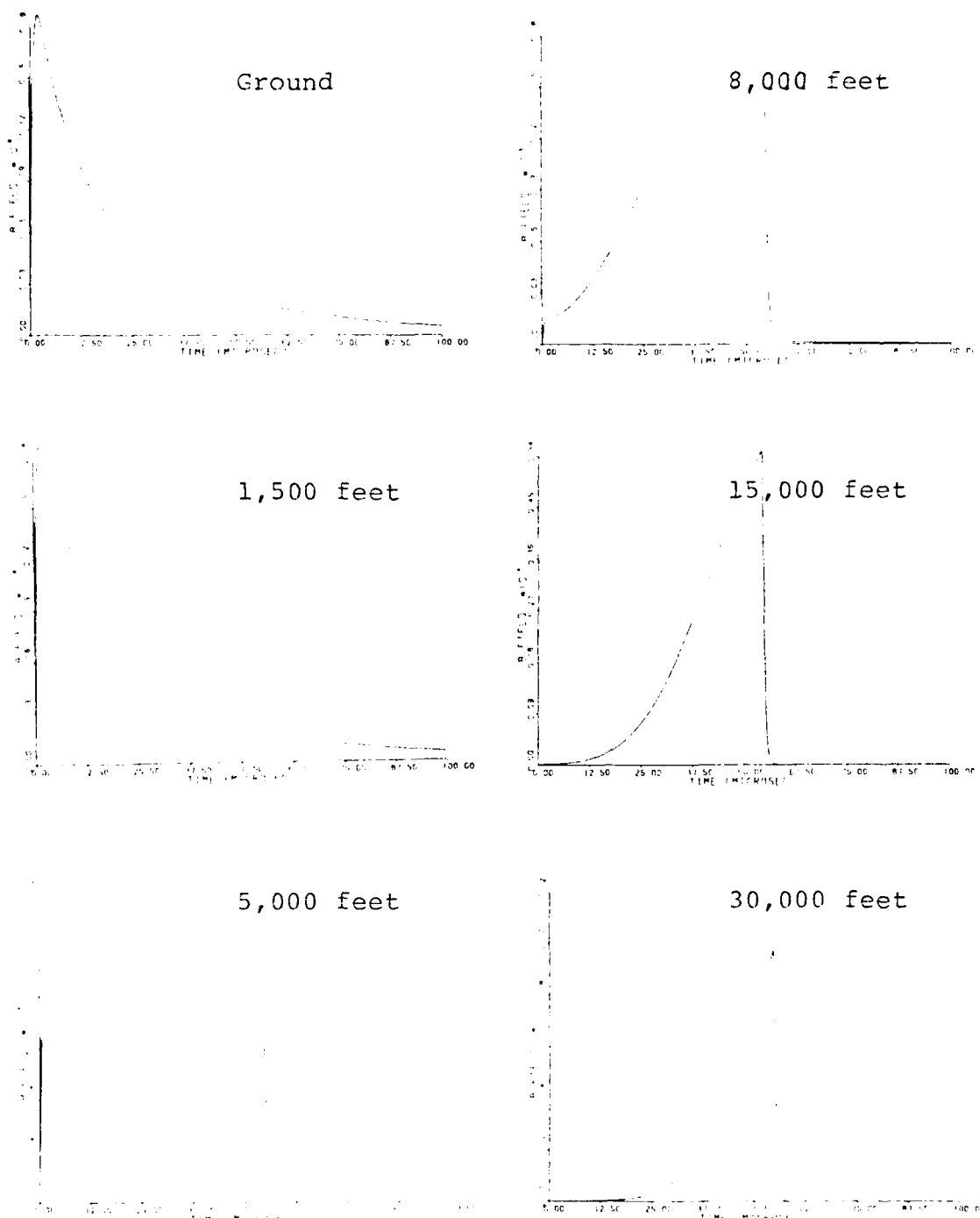


Fig. 5.66. Computer Solutions to Equation (40), the Magnetic Field, According to Model 3 at a Distance of 5 km, 1 μ sec Rise Time, and 25 μ sec Fall Time for the Ground and at Five Altitudes.

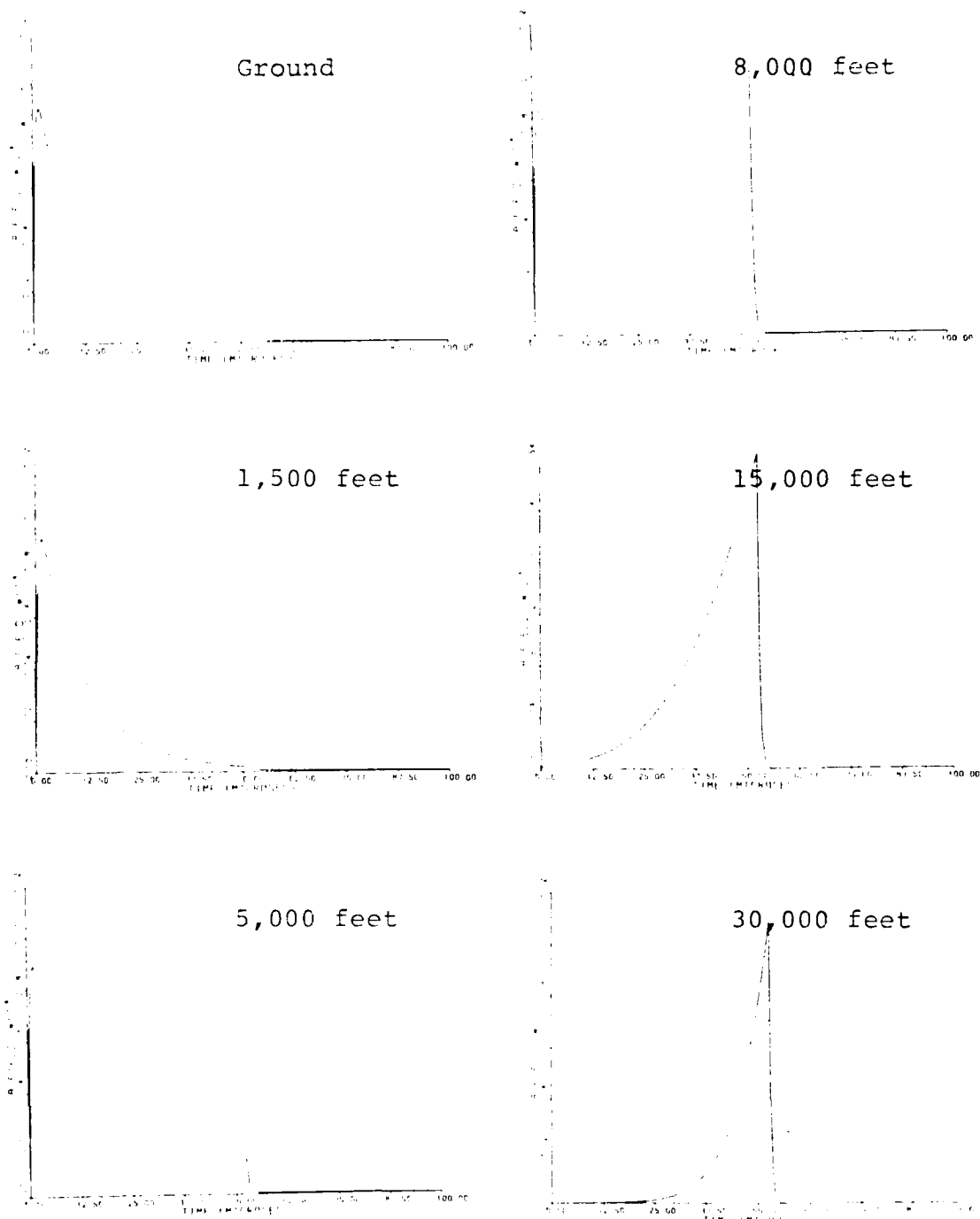


Fig. 5.67. Computer Solutions to Equation (40), the Magnetic Field, According to Model 3 at a Distance of 10 km, 1 μ sec Rise Time, and 25 μ sec Fall Time for the Ground and at Five Altitudes.

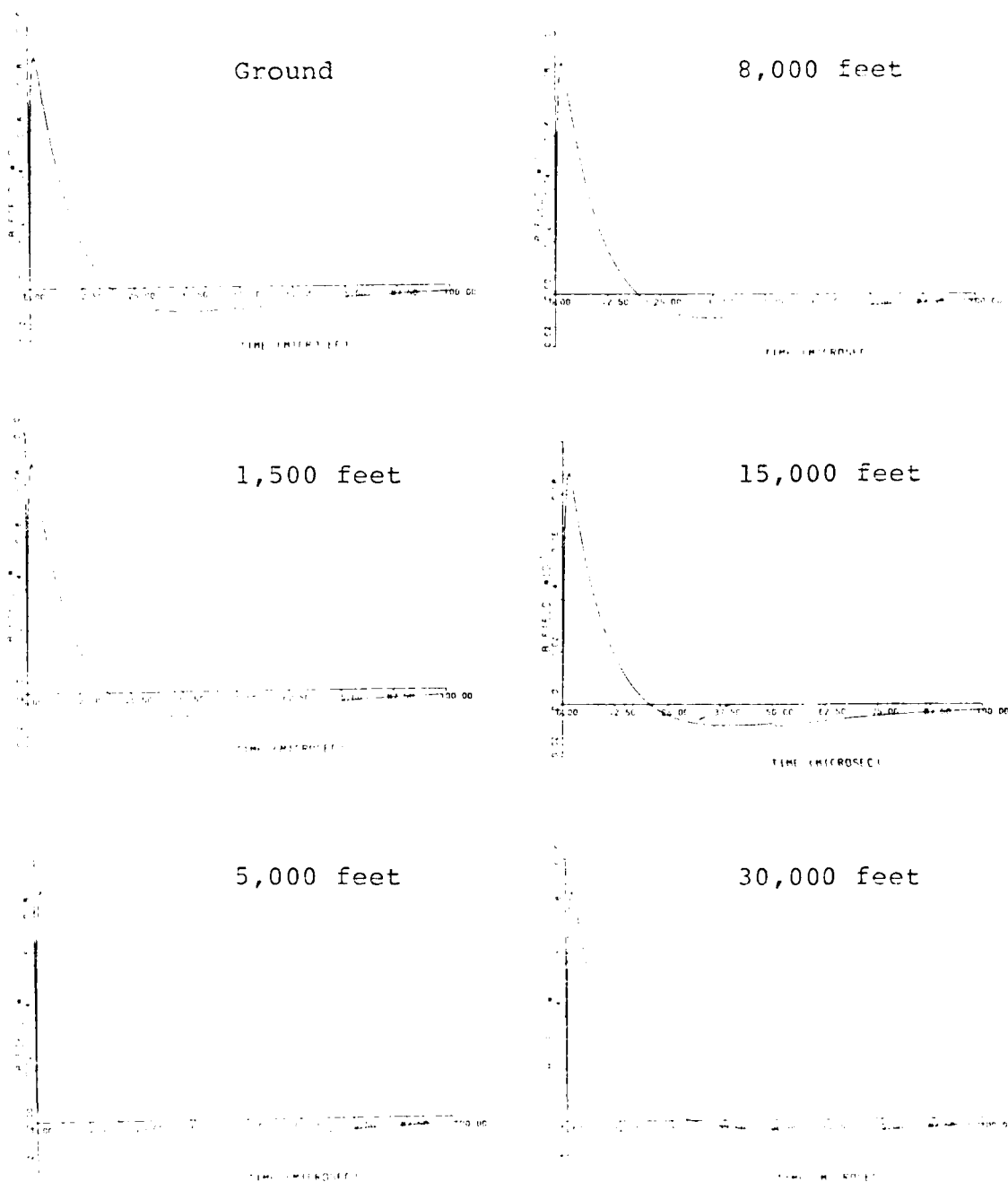


Fig. 5.68. Computer Solutions to Equation (40), the Magnetic Field, According to Model 3 at a Distance of 100 km, 1 μ sec Rise Time, and 25 μ sec Fall Time for the Ground and at Five Altitudes.

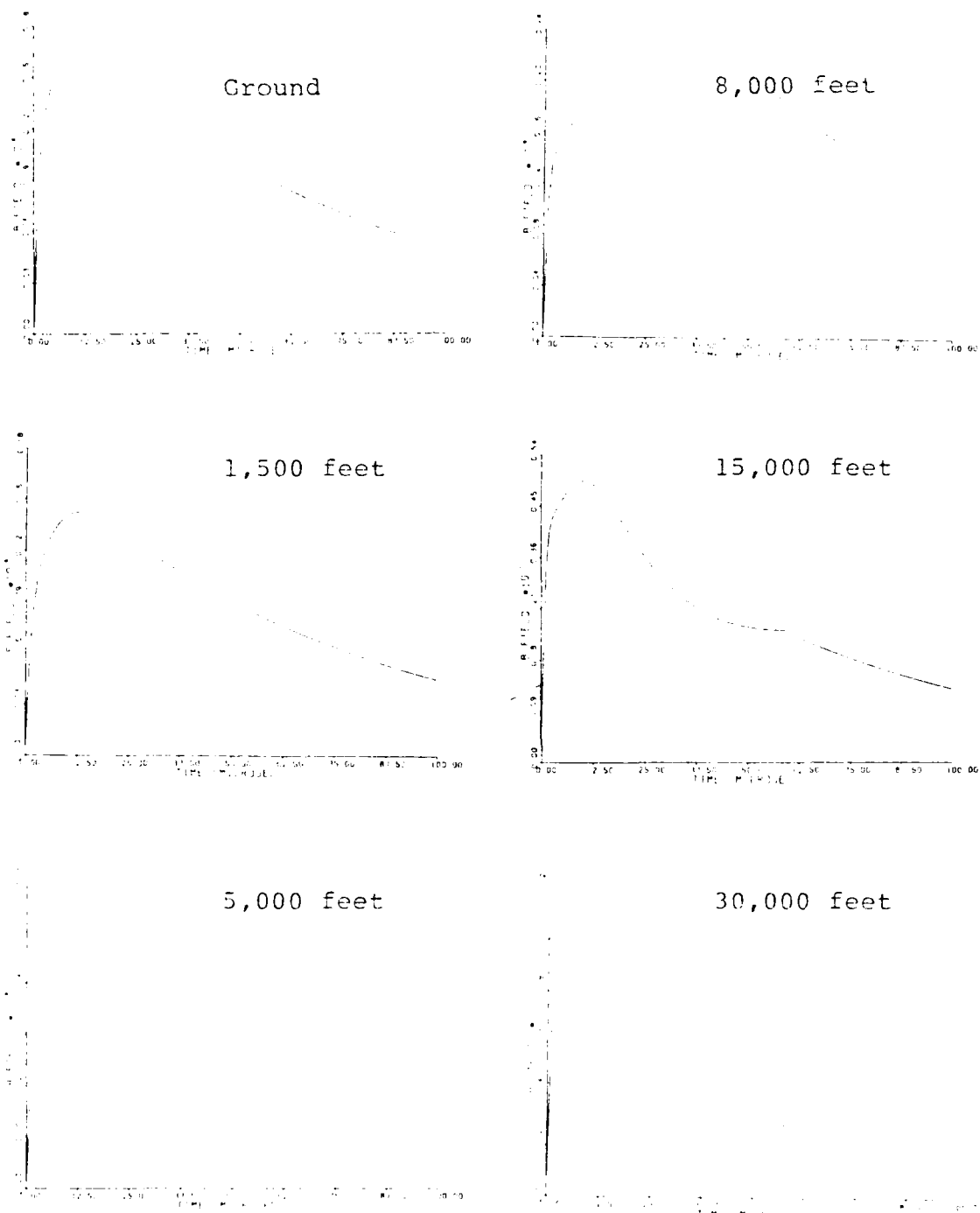


Fig. 5.69. Computer Solutions to Equation (40), the Magnetic Field, According to Model 3 at a Distance of 1 km, 2 μ sec Rise Time, and 50 μ sec Fall Time for the Ground and at Five Altitudes.

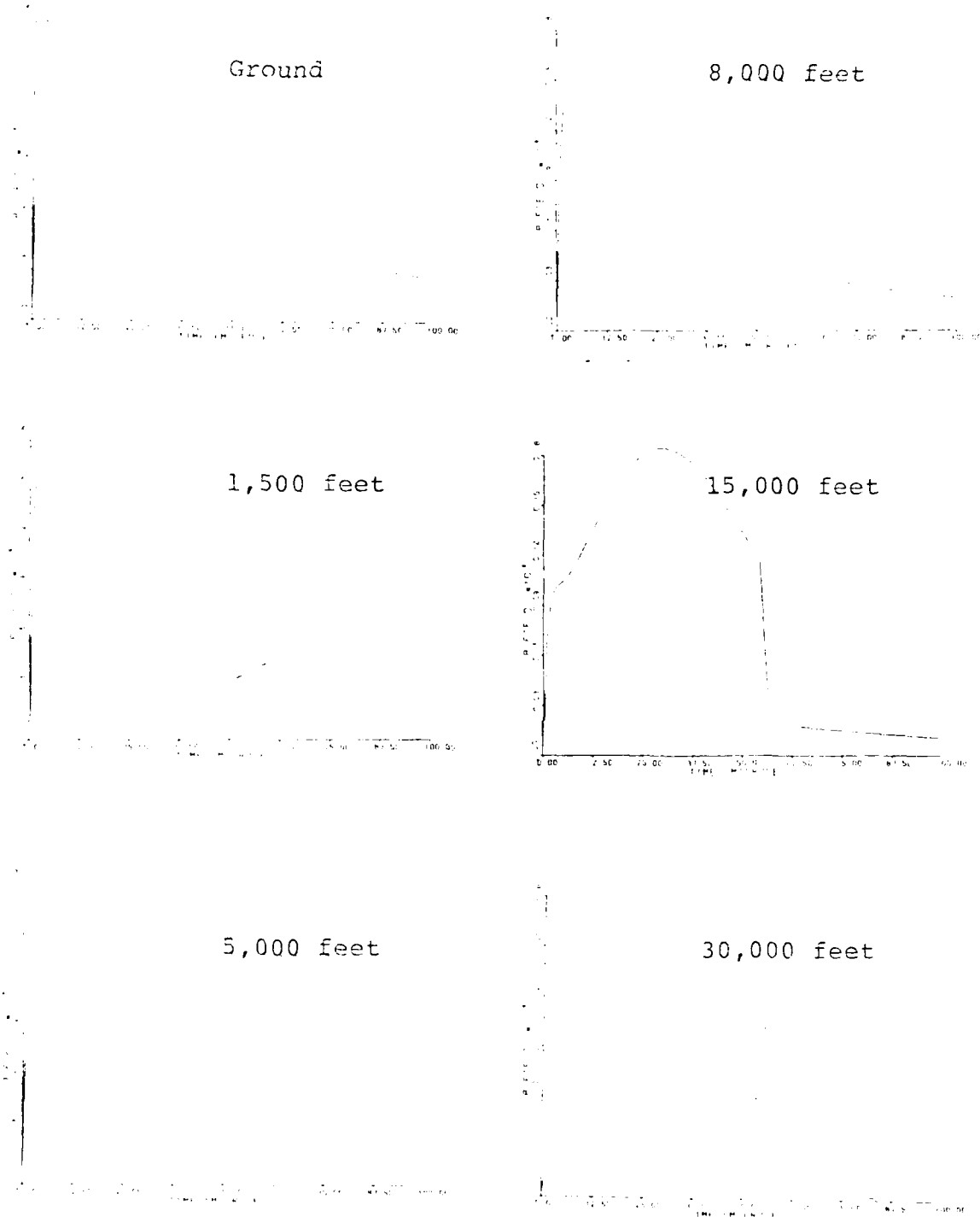


Fig. 5.70. Computer Solutions to Equation (40), the Magnetic Field, According to Model 3 at a Distance of 5 km, 2 μ sec Rise Time, and 50 μ sec Fall Time for the Ground and at Five Altitudes.

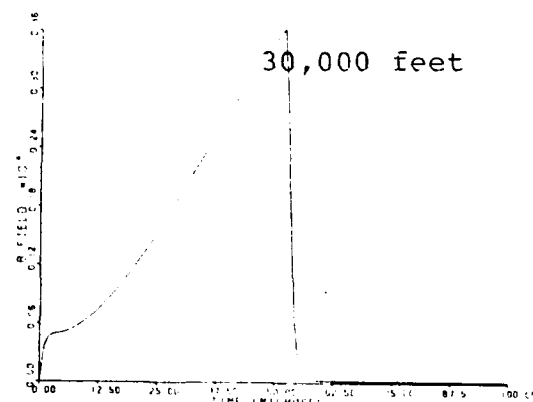
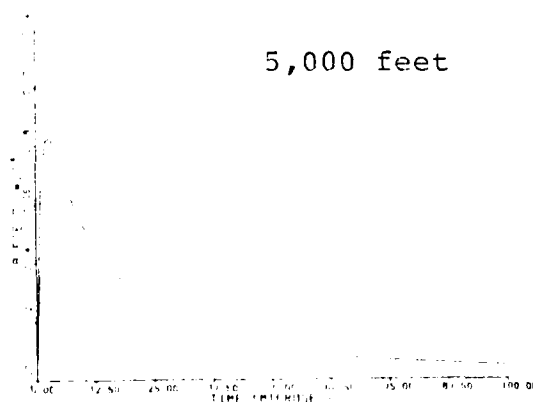
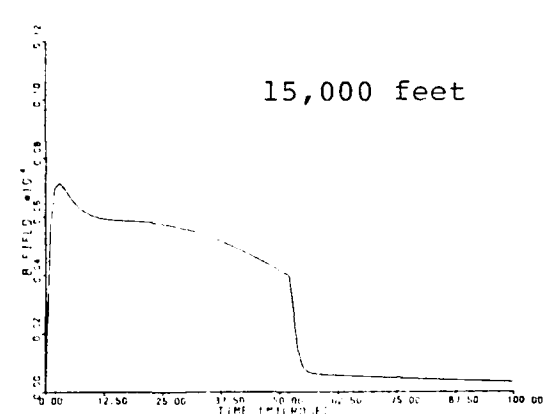
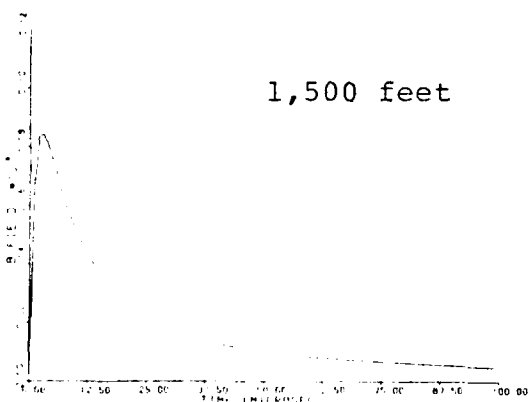
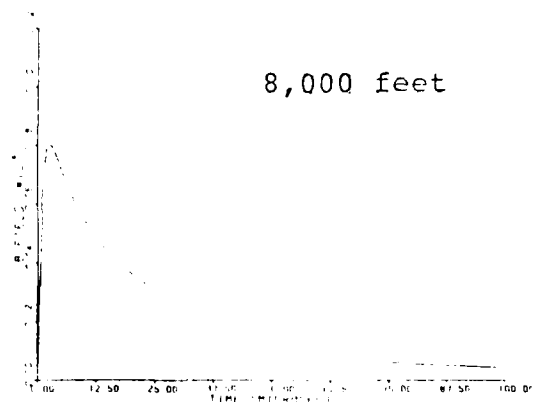
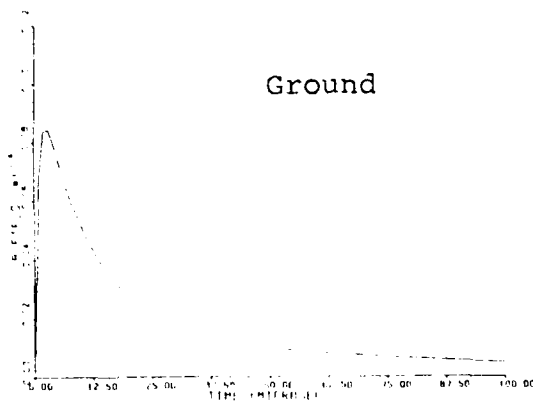


Fig. 5.71. Computer Solutions to Equation (40), the Magnetic Field, According to Model 3 at a Distance of 10 km, 2 μ sec Rise Time, and 50 μ sec Fall Time for the Ground and at Five Altitudes.

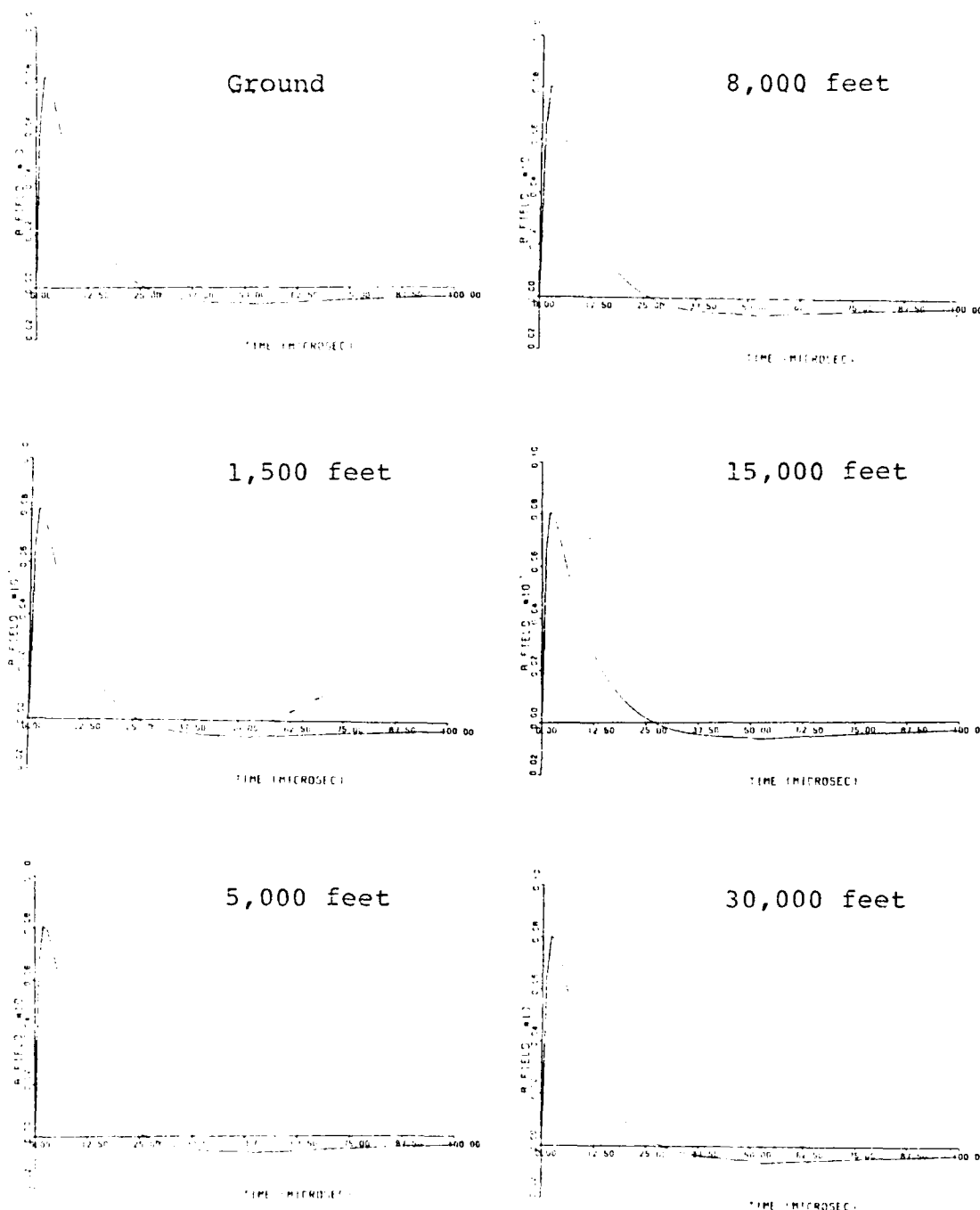


Fig. 5.72. Computer Solutions to Equation (40), the Magnetic Field, According to Model 3 at a Distance of 100 km, 2 μ sec Rise Time, and 50 μ sec Fall Time for the Ground and at Five Altitudes.

derivative gains to zero after thirty to forty microseconds; therefore, the induction term tends to predominate during the impulse period.

Experimental

In comparing the theoretical data to experimental data, what was looked for was similarity in the general waveshape. The overall magnitude was not considered important since the peak current, I_0 , is a multiplying constant that can be pulled out of the integrals of Equations (39) and (40). This means that if a model predicts a field with a shape closely corresponding to experimental data, but whose overall magnitude is off, the predicted field can be easily amended by simply increasing or decreasing I_0 accordingly. The value of I_0 needed to predict both the shape and magnitude of experimental data does become important when the I_0 necessary to closely approximate data falls outside the range of typical values--ten to twenty kiloamps--as is the case in the second model (Lin et al., 1980).

Data from the measurements of the electric and magnetic fields of two return strokes (not of the same flash) are used in this thesis. The data for the first event includes simultaneous electric field measurements on the ground (Figure 5.73) and at 1500 feet (Figure 5.74) at a distance of ten kilometers from the channel. Data for

the second event consists of only an electric field measurement at 8300 feet (Figure 5.75). All data used in this thesis was measured in an analog FM channel with 500 kHz bandwidth in either a ground station or an Air Force WC-130 aircraft sponsored by the Flight Dynamics Laboratory at Wright-Patterson AFB, Ohio.

Other data at this writing is still being processed. Also, other data was processed and available but did not closely fit the points at which the fields were theoretically predicted. Data was also taken with a VHF system; this data was preferred over the FM data but was unavailable for use in this thesis.

Looking at Figures 5.73, 5.74, and 5.75 and taking into account and accepting the possibility of data inversion, the modified Lin model used by Master et al. is clearly the best fit. However, the only conclusion that could be drawn from this comparison is that Lin's modified model as presented in Master et al., 1981 best fits experimentally measured data at ten kilometers for ground level, fifteen hundred feet, and eight thousand feet; the question of model performance for other distances and altitudes still remains unanswerable at this time. Even at that, a conclusion of this nature is not well supported due to the limited amount of experimental data. Clearly, more data for comparison purposes is needed to draw a valid conclusion of the performance of these four models.

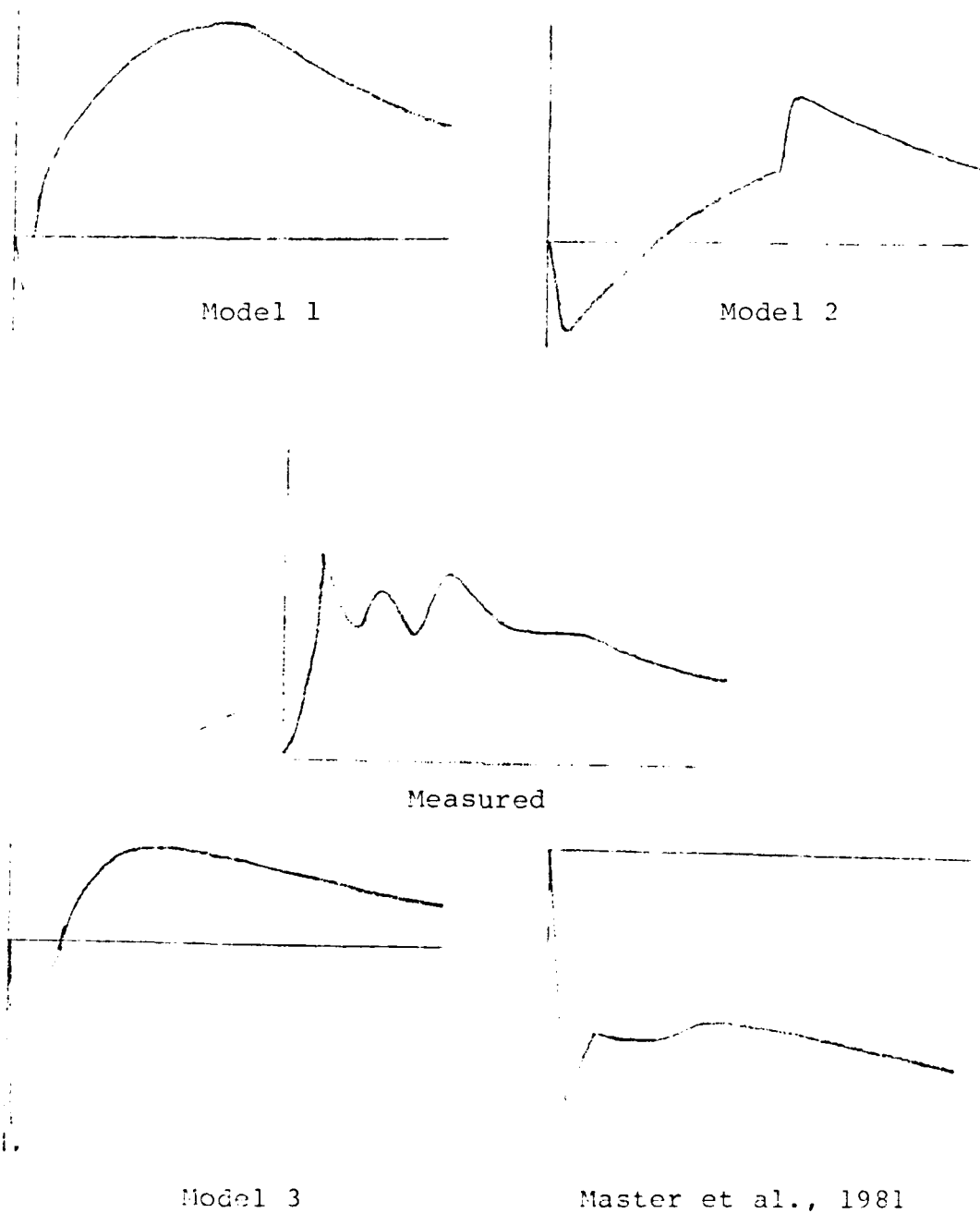


Fig. 5.73. Comparison of the Electric Field Predicted by the Three Models and Lin's Modified Model (Master et al., 1981) with Experimental Data Taken on the Ground at a Distance of 10 kilometers. Estimated Rise Time of 2 μ sec.

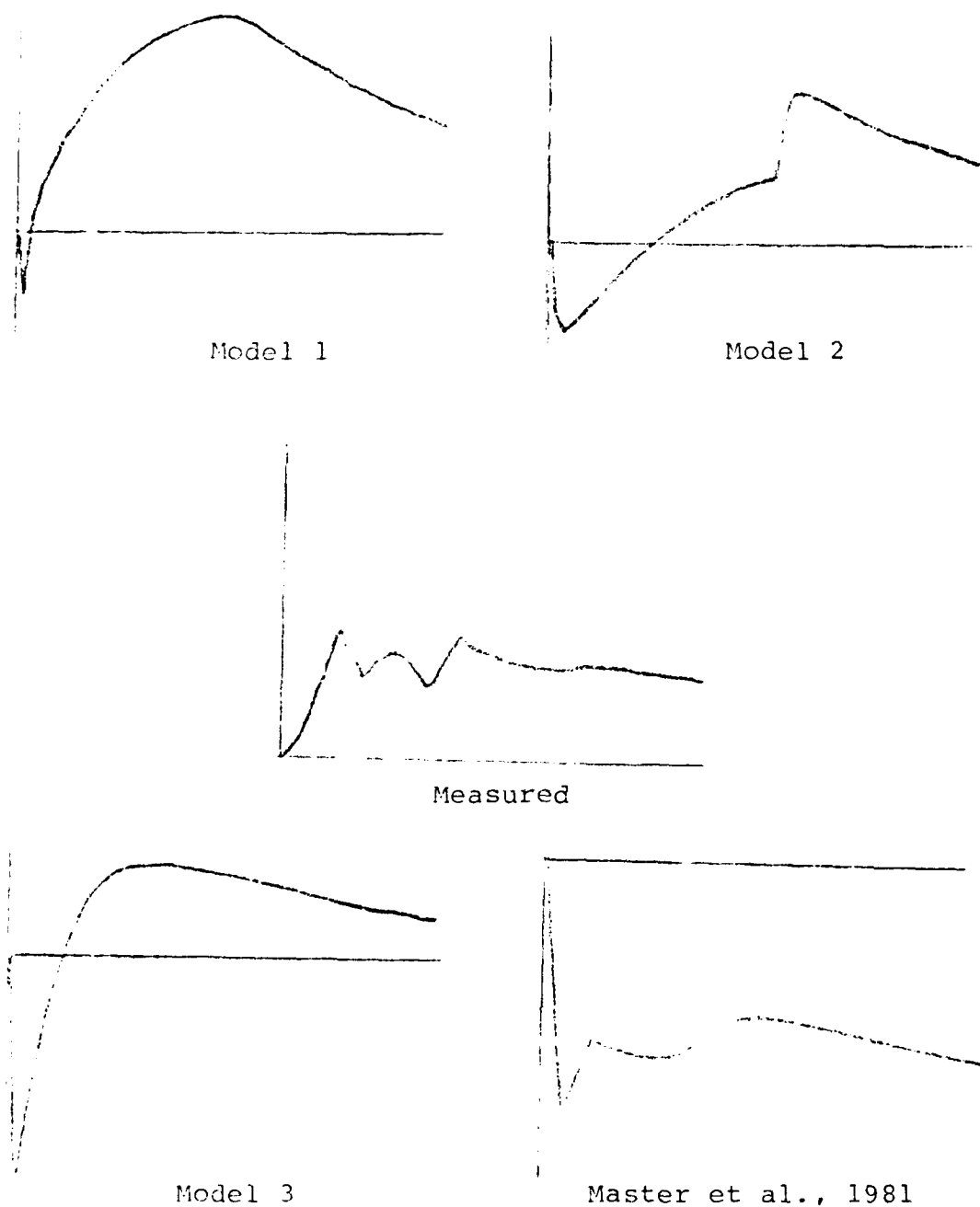


Fig. 5.74. Comparison of the Electric Field Predicted by the Three Models and Lin's Modified Model (Master et al., 1981) with Experimental Data Taken at 1500 Feet at a Distance of 10 kilometers. Estimated Rise Time of 2 μ sec.

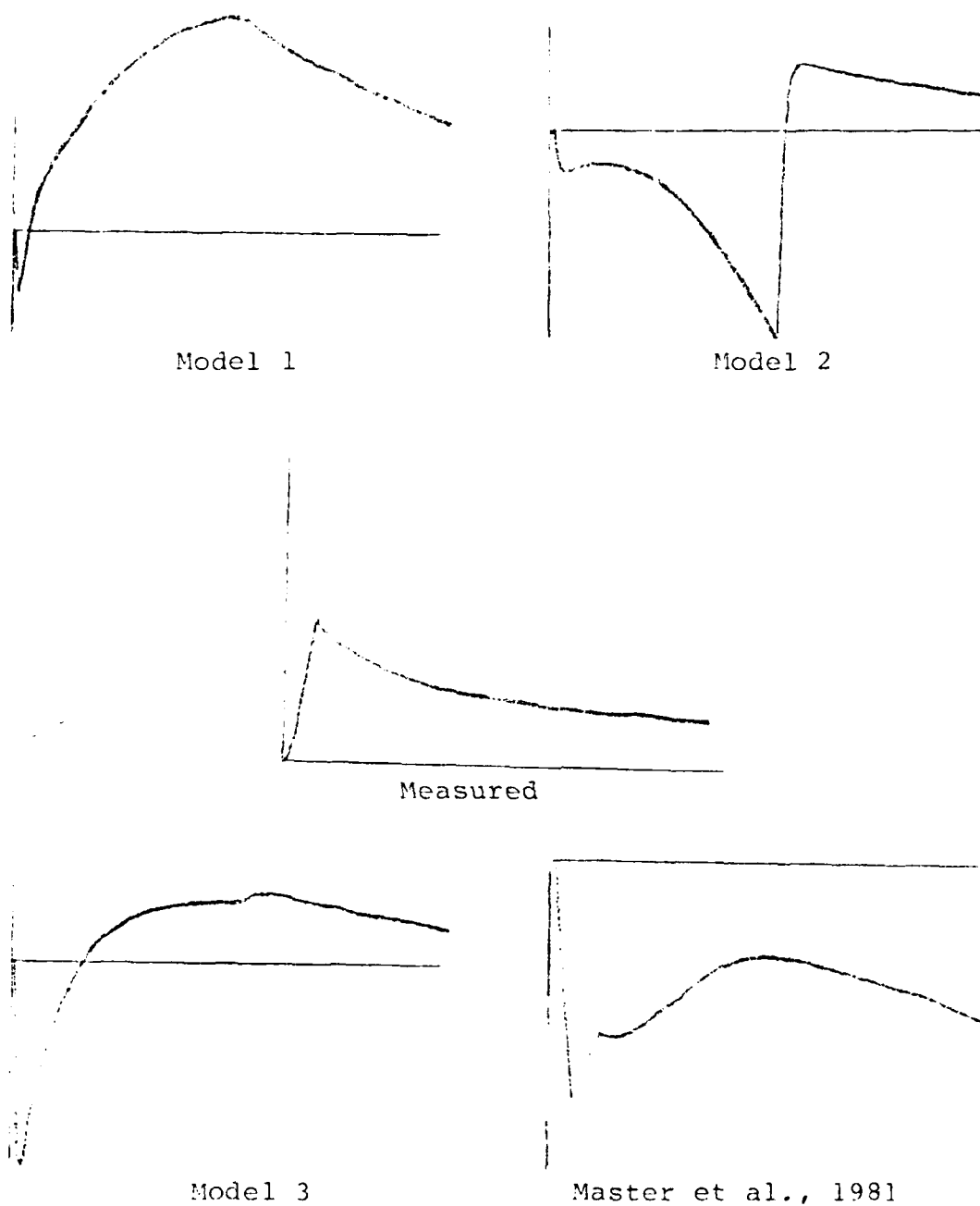


Fig. 5.75. Comparison of the Electric Field Predicted by the Three Models and Lin's Modified Model (Master et al., 1981) with Experimental Data Taken at 8300 Feet at a Distance of 10 kilometers. Estimated Rise Time of 2 μ sec.

VI. Conclusions and Recommendations

Conclusions

The only conclusion that can be drawn at this time is that the modified version of Lin's model (Master et al., 1981) best predicts the measured data at a distance of ten kilometers at ground level, fifteen hundred feet, and eight thousand feet. For other distances and other altitudes more data is needed.

Recommendations

The first recommendation is to obtain more of the data that the Flight Dynamics Laboratory of Wright-Patterson AFB, Ohio collected in Florida in August 1981. At this writing, much of the data was unavailable for use in this thesis due to incomplete processing, not fitting the theoretically predicted data points, or poor resolution. Clearly, more data is needed in order to draw a good, valid conclusion as to which model performs best under various conditions.

Another recommendation is to analyze the three currents of Lin's model separately. This would give more conclusive evidence as to which currents predominate at various times in the calculations. Along those same lines, it may prove fruitful to analyze each of the currents separately

in terms of the electrostatic, induction, and radiation fields they produce.

A third recommendation is to theoretically analyze these models at distances closer than one kilometer and at distances between ten and one hundred kilometers. This would not only allow the use of more of the experimental data but provide more insight to the more affecting (to the aircraft) closer lightning flashes.

Another recommendation is to do some analysis of the models for faster rise times. Recent data has shown that some return strokes may have rise times as fast as one hundred nanoseconds (private conversation with Dr. Pete Rustan, Fall 1981).

Final recommendations are to put some sort of decay or attenuation on the leader current in Lin's model and to model the channel with an unmatched load at the top.

Bibliography

Baum, R. K., et al. "Airborne Electromagnetic Characterization of Lightning," Vith International Conference on Atmospheric Electricity, Manchester, England, July 1980.

Baum, R. K. Airborne Lightning Characterization, Lightning Technology, Proceedings of a Technical Symposium held at NASA Langley Research Center, Hampton, VA, April 1980, Supplement to NASA Conference Publication 2128, FAA-RD-80-30, pp. 1-19.

Golde, R. H., ed. Lightning, Academic Press Inc., New York, 1977 (2 Vols.).

LeVine, D. M. and Meneghini, R. "Simulation of Radiation from Lightning Return Strokes: The Effects of Tortuosity," Radio Science, 13, 5, 1978, pp. 801-809.

Little, P. F. "Transmission Line Representation of a Lightning Return Stroke," J. Phys. D, 11, 1893-1910, 1978.

Lin, Y. T. Lightning Return--Stroke Models, doctoral dissertation, University of Florida, 1978.

Lin, et al. "Lightning Return Stroke Models," JGR, Vol. 83, No. C3, pp. 1571-1583, March 20, 1980.

Master, et al. "Calculations of Lightning Return Stroke Electric and Magnetic Fields Above Ground," JGR, 1981 (in process of publication).

Pearlman, R. A. "Lightning Near Fields Generated by Return Stroke Current," IEEE Symposium on Electro-Magnetic Compatibility, 68-71 (1979).

Pitts, F. L., and M. E. Thomas. 1980 Direct Strike Lightning Data, NASA Technical Memorandum 81946, Langley Research Center, Hampton, VA, Feb. 1981.

Uman, M. A. Lightning, McGraw-Hill, Inc., New York, 1969.

Uman, M. A., et al. "The Electromagnetic Radiation from a Finite Antenna," American Journal of Physics, Vol. 43: 33-38 (1975).

Vita

Jeffrey Michael Cukr was born in Detroit, Michigan where he attended and graduated from Osborn High School in 1974. After high school he went to the United States Air Force Academy from which he graduated with a Bachelor of Science Electrical Engineering degree in 1978. His first assignment was to the Air Force Flight Test Center (AFFTC) at Edwards AFB, California. While at the AFFTC, Lt Cukr was involved in the design of flight test instrumentation for the Air Launched Cruise Missile and the B-52 Offensive Avionics systems. Lt Cukr then was assigned to the Air Force Institute of Technology (AFIT) as a resident student where he received his Master of Science Electrical Engineering degree in December 1981. Lt Cukr's follow-on assignment after graduating from AFIT was to the Boeing Aircraft Company, Seattle, Washington where he is currently working as Test Director on the AWACS aircraft.

Permanent Address: 2909 Hearthhaven Place
Route #1
Gaylord, Michigan 49735

UNCLASSIFIED

SECURITY CLASSIFICATION OF THIS PAGE (When Data Entered)

REPORT DOCUMENTATION PAGE		READ INSTRUCTIONS BEFORE COMPLETING FORM
1. REPORT NUMBER	2. GOVT ACCESSION NO.	3. RECIPIENT'S CATALOG NUMBER
AFIT/GE/EE/81D-15		
4. TITLE (and Subtitle)		5. TYPE OF REPORT & PERIOD COVERED
AN ANALYSIS AND COMPARISON OF LIGHTNING RETURN STROKE MODELS AT ALTITUDE		Master's Thesis
7. AUTHOR(s)		6. PERFORMING ORG. REPORT NUMBER
Jeffrey M. Cukr		
9. PERFORMING ORGANIZATION NAME AND ADDRESS		8. CONTRACT OR GRANT NUMBER(s)
Air Force Institute of Technology (AFIT/EN) Wright-Patterson AFB, Ohio 45433		
11. CONTROLLING OFFICE NAME AND ADDRESS		10. PROGRAM ELEMENT, PROJECT, TASK AREA & WORK UNIT NUMBERS
Air Force Wright Aeronautical Laboratory/ FIESL Wright-Patterson AFB, Ohio 45433		
14. MONITORING AGENCY NAME & ADDRESS (if different from Controlling Office)		12. REPORT DATE
		December 1981
		13. NUMBER OF PAGES
		132
		15. SECURITY CLASS. (of this report)
		UNCLASSIFIED
		15a. DECLASSIFICATION DOWNGRADING SCHEDULE
16. DISTRIBUTION STATEMENT (of this Report)		
Approved for public release; distribution unlimited		
17. DISTRIBUTION STATEMENT (of the abstract entered in Block 20, if different from Report)		
<p>Approved for public release; IAW AFR 190-17.</p> <p><i>[Signature]</i> 21 FEB 85</p> <p>Director of Public Affairs</p> <p>Wright-Patterson AFB, Ohio 45433</p>		
18. SUPPLEMENTARY NOTES		
Approved for public release; IAW AFR 190-17		
FREDRIC C. LYNCH, Major, USAF Director of Public Affairs		
19. KEY WORDS (Continue on reverse side if necessary and identify by block number)		
Lightning Models Electromagnetic Fields Analysis and Comparison Altitude		
20. ABSTRACT (Continue on reverse side if necessary and identify by block number)		
<p>A comprehensive analysis and comparison of lightning return stroke models is presented. A brief description of the lightning process and deviations of the equations for calculating the electric and magnetic fields at points on the ground and at points at altitude for an arbitrary current waveform are also presented. The models analyzed are the Bruce-Golde model, Uman's transmission line model (the breakdown pulse current not attenuated), and Uman's</p>		

DD FORM 1 JAN 73 1473

EDITION OF 1 NOV 65 IS OBSOLETE

UNCLASSIFIED

SECURITY CLASSIFICATION OF THIS PAGE (When Data Entered)

85

03

13

178

model using an attenuating breakdown pulse current. Plots of the electric and magnetic fields that these three models predict for various distances and altitudes and different parameters (rise and fall time of the current) are included. The above three models along with a recently modified version of Lin's model (where the breakdown pulse is attenuated) are then compared with recently acquired lightning return stroke electromagnetic data. The data was obtained simultaneously on the ground and at various altitudes in a WC-130 aircraft in South Florida.

END

FILMED

5-85

DTIC